UNIVERSIDAD DE CHILE
FACULTAD DE CIENCIAS FÍSICAS Y MATEMÁTICAS
DEPARTAMENTO DE INGENIERÍA MECÁNICA

COUPLED MODEL OF HEAT TRANSFER AND PLASTIC DEFORMATION FOR FRICTION STIR WELDING (FSW)

MEMORIA PARA OPTAR AL TÍTULO DE INGENIERA CIVIL MECÁNICA

SOFÍA ISABEL SALAZAR TORRES

PROFESOR GUÍA:
Patricio Mendez Pinto

MIEMBROS DE LA COMISIÓN:
Rubén Fernandez Urrutia
Williams Calderón Muñoz

Este trabajo ha sido parcialmente financiado por el Gobierno Canadiense a través de la beca "Emerging Leaders in the Americas Program"

SANTIAGO DE CHILE
2022

RESUMEN DE LA MEMORIA PARA OPTAR
AL TÍTULO DE INGENIERA CIVIL
MECÁNICA
POR: SOFÍA ISABEL SALAZAR TORRES
FECHA: 2022
PROF. GUÍA: PATRICIO MENDEZ PINTO

MODELO ACOPLADO DE TRANSFERENCIA DE CALOR Y DEFORMACIÓN PLÁSTICA EN SOLDADURA POR FRICCIÓN-AGITACIÓN (FSW)

La soldadura por fricción y agitación, abreviada como FSW es un proceso de union de metales de baja densidad mediante el uso de un pin que gira a alta velocidad en medio de la unión de dos placas. Este proceso es clave para el desarollo de tecnologías que requieren de un menor peso, como naves aeroespaciales o maritimas ya que posibilita la soldadura en aleaciones de bajo peso como el aluminio. A lo largo de los años ha sido estudiado de una manera experimental, de la cual se han obtenido observaciones claves,y posibilitó la formación de una data base. No obstante, debido a la complejidad termofísica de este proceso, se han desarrollado pocos estudios en un ámbito matemático, que faciliten el desarrollo de ecuaciones que modelen este procedimiento, y aún más importante, el desarrollo de estas ecuaciones, abre paso a encontrar la ecuación que refleja la temperatura necesaria para deformar un material. Lo anterior motiva e impulsa el objetivo de esta tésis, que es optimizar las ecuaciones planteadas por el Dr.Mendez mediante la incorporación de un nuevo factor matemático que añade al modelo la pérdida de calor mediante la placa que esta siendo soldada. Este factor con anterioridad era despreciado porque se creia infimo pero su integración al modelo demuestran su relevancia. Los resultados evidencian mejoras en los gráficos de máxima temperatura y torque ya que reflejan una mayor proximidad entre lo obtenido experimentalmente y lo estimado por las ecuaciones, lo cual representa una mayor cercania entre el modelo planteado y la realidad. Para la obtención de los gráficos se trabajó con 196 datos de los cuales se pudieron hacer comparaciones entre lo estimado para el grosor de la capa de deformación, el torque, la temperatura máxima alcanzada, y las 4 simplificaciones realizadas que modelan y representan este tipo de proceso. En el caso de la temperatura y torque, aquellos que consideran la pérdida de calor tienen en promedio 55.52% y 22.41% menos error respectivamente, que aquellos que no. Sin embargo en el caso del espesor de la capa de deformación hay un 233.81% más de error.

RESUMEN DE LA MEMORIA PARA OPTAR
AL TÍTULO DE INGENIERA CIVIL
MECÁNICA
POR: SOFÍA ISABEL SALAZAR TORRES
FECHA: 2022
PROF. GUÍA: PATRICIO MENDEZ PINTO

COUPLED MODEL OF HEAT TRANSFER AND PLASTIC DEFORMATION FOR FRICTION STIR WELDING (FSW)

Friction stir welding, abbreviated as FSW is a union process of low density metals by the use of a high rotational speed pin that moves through the union of two plates. This process is key for the development of technologies that require low weights, such as space or maritime ships, because it allows the joining and welding of low density alloys, such as aluminium. Over the years, this process has being studied in an experimental way, which has lead to important observations, and also made possible the development of a database. However, because of the thermophysical complexity of this process, few studies have being conducted in a mathematical sense, that facilitate the development of equations that model this procedure, and even more important, the development of this equations open the path to found the equation that describe the initial temperature in which the metals can be deformed. This has being the inspiration and motivates the main purpose of this thesis, which is the optimization of Dr.Mendez equations that model FSW by the incorporation of a new mathematical term that describes the heat loss by the plate being welded. In the past this term was not taken in consideration, because it was believed that it was extremely small, but the incorporation to the model proves its relevance. The results demonstrate improvements in the graphs of maximum temperature and torque, because it reflects a closer proximity between what was expected by the equations and the measures from the experiments, which in other words means more contiguity among the reality and the mathematical model. In order to make the graphs, 196 samples were used, and these graphs allowed the comparison between what was expected for the shear layer thickness, the torque, and maximum reach temperature and the four simplifications that made the model and represent FSW process. In the graphs of Temperature and Torque it can be observed, that those who consider the heat lost through the plate have a 55.52% and 22.41% less error, respectively, than those that didn't. But in the case of shear layer there is 233.81% of more error considering the heat loss.

What is an ocean but a multitude of drops?

David Mitchell

Acknowledgments

For those who contributed from far or near to help me accomplish this thesis and reach where I am right now academically and personally. First I would like to thank my loving parents; Alejandro Salazar and Maria Isabel Torres, for always being there and supporting me in all the possible ways, for never letting me fall and helping me find my path in life, thanks for encouraging me to pursue this trip and the valuable gift of education that both of you gave me. I also thank my sister Paulina Salazar for literally everything, for always being at the other side of the phone, of the computer, and the street. for helping me develop myself professionally and personally. You have always been there for me, and I will always be there for you sis. I would also like to thank my sister Catalina Salazar for inspiring me to be adventurous and enjoy life and my thanks also goes to my brother Alejandro Salazar and his wife Daniela Aguirre for always receiving me at their house and making me feel one of their family.

I would also like to thank my teacher Dr. Patricio Mendez for this opportunity, for trusting me and always making time to help me solve my doubts and put me back on track to achieve more and do better with my research, for welcoming me in his Lab and be part of the activities that the team enjoys every Friday. I also thank all the teachers that participated in my academic development and helped me reach this point of my university career.

I thank my friends, for loving and accepting me as who I really am, for the laughter and tears we shared, and for the times we spent reflecting about life and guiding me. For this, I thank Nicolas Marchant, Stephany Droguett, and Natalie Tapia, for all the adventures, pasta nights and encouragement to defend myself.

I thank my roommates Marwa Khemir and Maria Guadalupe for being literally the best roomies ever, for transforming such a house in a home, for those karaokes, pancakes and studies night that we shared, for having faith and accept me. Also for making my internship experience so nice. Also I would like to thank Fransisco Basaure and Sofía Silva for also making my Canadian experience so wonderful by receiving me, by skating, by laughing and travelling with me.

Table of Content

List of Tables

List of Figures

Chapter 1

Introduction

Every means of transportation, structure components, electronic devices, metallic structures for construction requires some kind of welding, whether for the union of electric wires with chips, or for the union of different kind of automobile structures, or the beams of a building. Welding is one of the key points for the resistance and reliability of any structural element, which is why it should be one of the main focus of attention in any kind of project. A clear example of its relevance was the disaster of Alexander Kielland offshore oil platform, which collapsed due to a fatigue fissure originated by a deficient welding procedure in the base of the platform.

Throughout the human history a lot of welding technique have been created, such as diffusion welding, forge, roller welding, with inert gas welding (MIG), shielded metal arc welding (SMAW), laser or electron beam welding, even explosion welding, between other. All of this techniques have different methods and purposes. Most of them use the principle of melting the metal through high temperatures (some of them are even above the sun temperature) and pressure that allow the plastic deformation of the metal and his union with other pieces by mixing both metals. The main difference between the welding techniques lies in how to generate that union and mixing of the two metals. However the method selected depends on the kind of metal, required conditions for the piece and external conditions, like the environment in which the welding must be carried out.

This thesis is mainly focus in friction stir welding (FSW) method, which was created on 1992 in Cambridge welding center, and consists in the introduction of a high rotational speed pin, capable of generating enough heat by friction to plastically deform both metals and mix them by its own rotation, therefore joining both metals. FSW presents several advantages, such as low consumption of electricity, lack of need for filler materials, moreover it also has low risk associated because of the absence of sparks, arcs and high temperatures. Furthermore it also has the advantage over other welding methods that it can weld alloys of aluminium, without affecting their mechanical properties.

FSW represents an advance for the joining of weldable metals, like cooper, zinc, titanium, lead, among others, and also for non weldable metals, such as aluminium, lithium or magnesium alloys. These non weldable materials are really useful for the construction of space rockets due to their lower weight and good mechanical properties but there are few welding techniques that can weld this kind of material, like plasma arc welding (an expensive

method). Moreover, other methods affects the mechanical properties because the high temperatures involved generates thermo-mechanical stress zones. This is why FSW offers several advantages for the manufacture of non weldable metals, increasing the range of components that could be made under aluminum, lithium and magnesium alloys.

The welding techniques that involves high temperatures influence in the mechanical properties of the metals, because when the metal rich its fusion temperature, the grain will be reconstructed again in the internal structure of the material, and depending on the cooling time new secondaries phases could appear, such as martensite, this means that the welded zone will have a different kind of composition than the base metal, and this could lead to the appearance of fissures. In this sense FSW presents a huge advantage, because it doesn't need to reach the melting temperature for mixing both metals. However, despite FSW method being more and more used in the industry and the clear advantages there are still missing studies for its application along the industry.

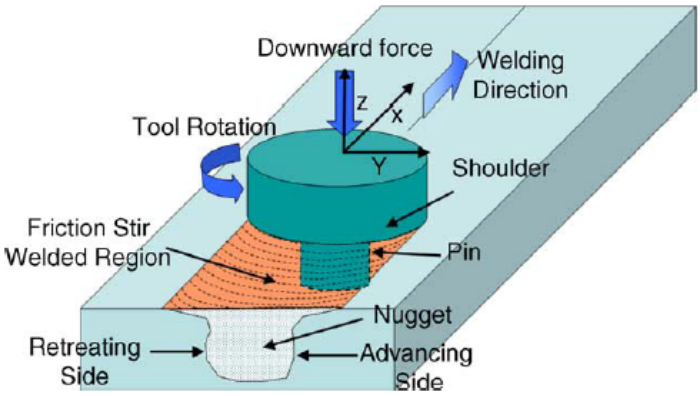

Figure 1.1: Coupling of heat transfer and plastic flow with both of them having the same characteristic length, which is the thickness of the shear layerδ.

1.1. Objectives

The main purpose of this thesis is to verify, reformulate and combine the equations proposed by Dr.Mendez and results of Dr.Tello[1] by including a new variable related to the heat loss through the plate. To achieve, this 4 aims must be accomplished:

- Rebuild Dr.Tello[1] data base with the materials she used on her work.
- Rebuild Dr.Tello[1] graphs that compare the maximum temperature, torque and shear layer thickness with the four simplifications that build the first model of FSW.
- Incorporate the new variable of heat loss through the plate and do the same graphs considering this variable.
- Analyse the results and its improvement by comparing both graphs and results.

1.2. Motivation

Speed is the main focus of attention of every transportation industry, such as cars, trains, space and maritime ships. Every year technological evolution increase the highest car speed reached by 3.5 [km/hr]. For this technological evolution, the development of materials is key, by using lighter and resistance material the weight of the transportation structures is reduced and can hold the forces involved with its movement. However this involves new challenges like welding this new materials. A clear example of this was the delay that the Tesla 3 model had to get out to the market, where 63.000 users canceled their reservation of this car because the company had trouble with the car's chassis welding.

FSW, is one of the few methods that allows the welding of exactly this kind of materials (the future materials), and it has the enormous advantage that doesn't affect the mechanical properties, so there is no need for heating treatment after its application, which in other words decrease fabrication costs. So the FSW studies and development by a mathematical model are imperative for the next technology generation. Furthermore the study of this process, could lead to the discovery of the equation that describe the temperature to deform plastically the metals, which could lead to the development of new engineering process to only use this temperature without reaching the melting temperature. All of this inspire and motivates the work of this thesis to improved the mathematical model that describes this welding process, by having better equations that describes the phenomenons behind this complex process.

1.3. Scope of work

This work consider the FSW in a general way based on the four simplifications that describe the process in a plastic deformation and heat transfer, so any other phenomenons like the formation of intermetallic structure or minimum percentage of re-crystallization are out of this scope of work.

This work is based on the information of the database available on the experiments founded in papers, where faults like the presence of pores or external conditions are not considered. Also, this thesis will use mostly aluminum alloys, so it doesn't embrace the behaviour with all the metals, and it doesn't consider in the mathematical model different kind of pin but a threadless cylindrical pin and the heat loss through the working tool.

Chapter 2

Background

2.1. FSW

The FSW technique belongs to a solid state welding method, which represents an advantage by not having flaws associated to the solidification process, unlike other techniques such as gas metal arc welding or shielded arc welding, that during the cooling down of the metal, different flaws could appear such as, the metal contraction during the cooling, which could lead to the formation of gaps or pores due to interdendritic contractions. Besides this, the FSW presents an ideal grain size, which award the material with resistance and plasticity, this is why there is no need for heat treatments for the metal recovery. This process is also considered as an autogenous one, because it doesn't require the addition of a filler material. Additionally, it works best in low melting temperature materials, because the pin tool needs to resist the friction and heat associated in the process, which is one of the limitation of this technique. On the other hand, this technique can't be executed manually because of the forces and velocities involved, and even being an automotized process the beginning and the end are complex stages and usually present some kind of flaw. One of the main conditions to avoid flaws is that there must be no gap between the two plates, nonetheless one of the advantages is that the plates can be placed in any position, because there is no melted metal that could slip off.

Mishra et al [11] studied the FSW process and the effects in the micro structure of the alloys through the process related parameters, such as velocity, temperature involved and others. The process consists of two concentric cylindrical bodies, aligned in the same axis, the first one is the pin, and has the lower radius, this tool works in the interface of the two plates and generates the plastic deformation by the friction enforced by the rotation between itself and the plates, at the same time this rotational movement combine the two metals. The second one is the shoulder, and it is the tool that confers the rotational strength, and provides heat to the plates before the pin, having a preheating role because of its wider diameter. Furthermore, it's diameter also confer a consolidation purpose, as the pin remove material the shoulder level out the removed metal. In a chronological way, the shoulder is the first one to have contact with the joint of the two plates, which removes the dirtiness that could be in the plates, and at the same time because of the friction due to the rotation it also preheat the two plates, facilitating the entrance of the pin. Then the pin makes contact with the plates and start to deform and mix them under the pressure exercised by the shoulder, which in addition, consolidate the removed metal and grant a flatten surface.

2.2. Background literature

The process of friction stir welding has been modeled both numerically and analytically. Since the process has a great potential in practical applications, it is necessary to develop simple models. Within the most relevant features of FSW modeling are the effect of heat transfer and plastic deformation on the temperature field, which can be seen in the tool contribution to the heat generation and the contact condition in the tool/plate interface.

There exists some analytical models in which the heat source is modeled as a line heat source. These models are based in Rosenthal's equation[44]. On the other side, proposing heat transfer by conduction, Schmidt et al. [2] proves that the shoulder of the tool is the major contribution to the heat generation and that a sticking condition is the prevalent contact condition in FSW. Otherwise, Chao et al. [6] combined numerical and experimental studies to determine the heat flux. They came to the result that only 5% of the heat generated flows into the tool and the rest into the workpiece of aluminum alloys. Khandkar et al. [12] proposed an inverse model in which measurements of torque are used to find important information of FSW.

Two extreme cases about the contact condition have been proposed in the literature: sliding and sticking condition. The first one appears when the contact shear stress is smaller than the material yield shear stress, thus, the material experiences only elastic deformation. Otherwise, in sticking condition the material will stick to the moving tool, and the contact shear stress will exceed the yield shear stress of the material [2]. In the case of the heat generation, it is being discussed if the heat is mainly generated by coulombic mechanisms at the tool/base plate interface (sliding boundary condition), by plastic deformation in the shear layer (sticking boundary condition); or by a combination of these two.

Schmidt et al. [3] studied the material flow using the tracer technique; they concluded that a sticking condition in the tool/workpiece interface is prevalent. Models proposed by Ulysse [24], Seidel and Reynolds et al. [47] among others ([26], [27]) considered only sticking. Schneider et al. [5], Schmidt and Hattel [[41]], and also Buck and Langerman [49] developed stickslip models. On the other hand, Xu et al. [48] developed a model of the interface pin/base plate and they proposed that the interface pin/surrounding material is mostly a slipping interface. Chao et al. [6] and McClure et al. [51] also carry out models that consider sliding friction.

Frigaard et al. [50] and Nandan et al. [43] developed mathematical models that involve the plastic deformation. There are models of the temperature field that contemplate different hypotheses, one case is whether the heat is generated by the shoulder and the pin([2],[12],[41],[39]) or only by the shoulder ([52], [6]). All the models consider that the maximum temperature is achieved at the tool/base plate interface. There are fully coupled models of this(citeKhandkar, [27], [43]). In these last, to predict temperature and shear rates, the viscoplastic flow and the heat transfer are modeled.

2.3. Coupled model for friction stir welding

2.3.1. List of symbols

Symbols	Description
Pe	Peclet number
τ_c	Shear stress within the shear layer [Pa]
k_δ	Thermal conductivity of the plate asociated to the temperature Tδ
k_0	Modified Bessel function of the second kind and order 0
T_δ	Temperature of the shear layer/base plate interface [K]
T_p	Preheat temperature due to the shoulder friction[°K]
ΔT_{max}	Temperature difference T_{max} $T_\delta(K)$.
T_{max}	Maximum temperature at the pin/shear layer interface [K]
T_m	Solidus temperature of the material [J/molK]
T_∞	Initial temperature of the base plate [K]
α_δ	Thermal diffusivity of the plates at To [m2/s]
η	Total efficiency of the process, which accounts for heat losses in the form of energy stored as dislocations in the shear layer.
η_s	Efficiency that accounts for the fraction of the mechanical energy converted into heat, excluding the small amount of mechanical energy that is accumulated as potential energy in the form of dislocations.
V	Travelling speed
ω	Rotational speed of the pin $[s^{-1}]$
a	Pin radius [m]
b	Shoulder radius [m]
t	Thickness of the plate [m]
δ	Thickness of the shear layer[m]
ΔT_1	Temperature difference within the shear layer [°K].
ΔT_δ	Temperature difference T_δ T [K].
R	Gas constant [J/mol K]
A	Constant of the Zener-Hollomom law [s1]
Q	constant of the Zener-Hollomom law. Activation energy [J/mol]
n	constant of the Zener-Hollomom law
B'	Constante
τ_R	Shear stress reference[Pa]
ω_R	Normal stress reference [Pa]
τ	shear stress experienced by an element of volume at coordinate x [Pa]
q_c'''	Volumetric heat generation within the shear layer [W/m3]
q_{out}	Volumetric heat flow from the shear layer through the pin [W/m^2]
$\dot{\gamma}$	Plastic deformation rate [1/s]
ζ	Constante
ϵ	Adimensional deformation rate associated with T_δ
$\widehat{\tau_c}$	Estimation of the shear stress within the shear layer [Pa]
$\widehat{\delta}$	Estimation of the shear layeyr thickness [m]
$\widehat{\mathcal{M}}$	Estimation of torque of the pin [Nm]

The math behind the coupled model considered the plastic deformation and the heat transfer, and is limited to the deformed area surrounding the pin, which is considered as a threadless cylindrical pin. The deformed area around the pin is called shear layer or deformation zone. In Figure 1.1 it can be observed the different variables that represent the model: the pin and shoulder diameter, named "a" and "b" respectively; the shear layer thickness named "δ" that belongs to the friction stir welded region; the travelling "V" and rotational "ω" velocity; and the torque involved named "M".

The first simplification was made by using Rosenthal's solution[44], that basically says that as the travelling speed of the heat source can be considerate as a steady state, slow moving heat point, then the isotherms can be considerate to have a circular shape, which leads to the estimation of the heat transfer to the base plate as a function of the Peclet number:

$$Pe = \frac{Va}{2\alpha} << 1 \tag{2.1}$$

The second one is made under the comparison of the shear layer deformations with the viscous layer of a body moving through a fluid, because the viscous boundary layer can be represented as the zone where the inertial and viscous forces stabilize between each other. Analogously, the shear layer of FSW can be characterized as the region in which the heat generation and heat conduction are balanced, and also, because the heat generation is lower than the melting temperature, it can be establish that the shear layer is significantly thinner than the pin diameter:

$$\delta << a \tag{2.2}$$

The third condition postulates that there is a small difference between the shear layer in front and backwards of the pin, as a consequence of the amount of incoming material, which is much less than the one removed in the whole shear layer. This can be represented as:

$$\rho\ V\ a << \rho\ \omega\ a\ \delta \Leftrightarrow V << \omega\ \delta \tag{2.3}$$

Finally the fourth simplification means that the thickness of the shear layer is larger than the difference in radius between the shoulder and the pin. This condition can be state as:

$$b - a << \delta \tag{2.4}$$

Later Dr. Mendez and Dr.Tello [20] made another simplification that helps to build the model in a more complete mode. This fifth hypothesis states that the maximum temperature near the pin is rather more affected by the concentrated heat from the deformation around the pin than by the distributed heat from the shoulder.

$$T_p - T_\infty << T_{max} - T_\infty \tag{2.5}$$

2.4. Scaling of the coupled thermal and mechanical problem

To analyze FSW process, Dr.Mendez used scaling analysis, a method for estimating the magnitudes of the terms in the governing equations that provides a systematic way to simplify the equations for a given phenomenon. Under this method, the ordinary differential equations that describe the phenomenon of FSW can be substitute by a system of four algebraic equations with four unknown variables, called characteristic values of a function or differential equation.

The procedure to formulate this four algebraic equations are:

- Heat conduction in the shear layer
- Heat generation in the shear layer
- Constitutive equation in the shear layer
- Heat conduction outside the shear layer

2.4.1. Heat conduction in the shear layer

The profile temperature illustrated in *a* of Figure 2.2 exhibits that the temperature decreases monotonically from the maximum T° in the pin(Tmax), to the T° in the outer boundary of the shear layer(T_δ), this variable is the characteristic value of the transition between the shear layer and the rest of the base plate.

On the other hand, the tangential velocity profile in the shear layer is exemplified in *b* of Figure 2.2. The tangential velocity decreased gradually from the tool/shear layer maximum value(ωa) to its minimum value, zero at the end of the shear layer.

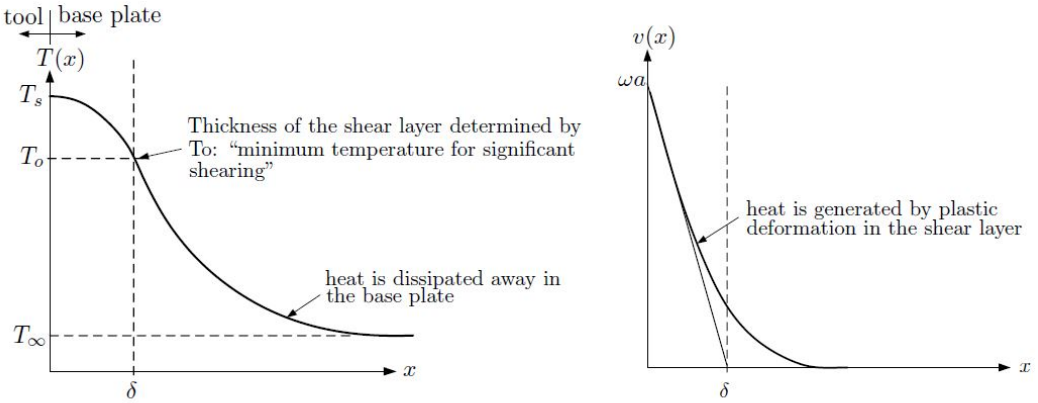

(a) Temperature profile (b) Tangential velocity profile

Figure 2.1: Coupling of heat transfer and plastic flow with both of them having the same characteristic length, which is the thickness of the shear layerδ.

Finally under the three first simplifications made in section 2.3, the heat transfer and the plastic deformation around the pin can be considered as one dimensional problem. Figure 2.2 illustrate the problem in one dimension, with the coordinate perpendicular to the pin/base plate interface and originating at that interface.

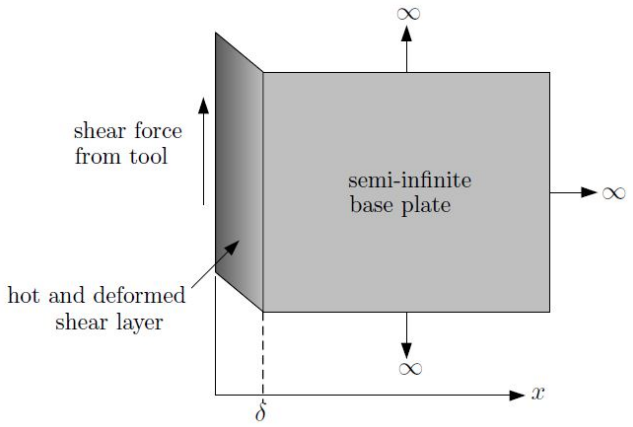

Figure 2.2: Illustration of FSW in one dimension.

Due to the above points of the temperature and tangential velocity profile and one dimension representation, the equation of conservation of energy for the steady-state, low Peclet and one dimensional problem is given by equation 2.6, where the equations assumes a balance between the heat conduction (the first term) and the volumetric heat generation (the second term). The boundary conditions are represented in Equation 2.7 and 2.8, which states that the heat lost to the tool does not significantly affect the temperature profile, and that the temperature at $x = \delta$ is T_δ:

$$\frac{\mathrm{d}^2T}{\mathrm{d}x^2} + \frac{q(x)}{k} = 0 \tag{2.6}$$

$$\left.\frac{\mathrm{dT}}{\mathrm{d}x}\right|_{x=0} \approx 0 \tag{2.7}$$

$$T|_{x=\delta} = T_\delta \tag{2.8}$$

From this equations T(x) is the temperature profile in the shear layer, q(x) is the volumetric heat generation due to the plastic deformation, and K(T) is the thermal conductivity of the base plate. The two terms of Equation 2.5 can be normalized by an estimation of their maximum values given by:

$$x = \widehat{\delta} x* \tag{2.9}$$

$$\frac{\mathrm{d}^2\mathrm{T}}{\mathrm{d}x^2} = 2\frac{\Delta\widehat{T_s}}{\widehat{\delta}^2}\left(\frac{\mathrm{d}^2\mathrm{T}}{\mathrm{d}x^2}\right)^* \tag{2.10}$$

$$q(x) = \widehat{q_c} q^*(x^*) \tag{2.11}$$

$$K(T) = k_0 k^*(T^*) \tag{2.12}$$

Where the "*" represents a normalized function. By replacing Equation 2.10, 2.11 and 2.12

in Equation 2.6, the normalized equation of conservation of energy is obtained(2.13)

$$2\frac{\Delta\widehat{T_s}}{\widehat{\delta}^2}\left(\frac{\mathrm{d}^2\mathrm{T}}{\mathrm{d}x^2}\right)^* + \frac{\widehat{q_c}}{k_o}\left(\frac{q}{k}\right)^* = 0 \tag{2.13}$$

Finally by replacing the normalized functions by +1, or-1, depending on the sign of the normalized function, equation 2.14 is obtain, which is based on the estimated values of their characteristic values, that are symbolized by the hat symbol as: $\Delta\widehat{T_s}$, $\widehat{\delta}$ and $\widehat{q_c}$.

$$-2\frac{\Delta\widehat{T_s}}{\widehat{\delta}^2} + \frac{\widehat{q_c}}{k_o} = 0 \tag{2.14}$$

2.4.2. Heat generation in the shear layer

Considering that the heat generation in the pin is only because of a sticking condition between the pin and the shear layer, the volumetric heat generated by the plastic deformation can be calculated with the shear stress rate experienced by the fraction of the mechanical energy converted into heat(η_s) of a volumetric element in the shear stress zone($\tau(x)$) and its rate($\dot{\gamma}$) with the following equation:

$$q(x) = \eta_s \tau(x)\dot{\gamma}(x) \tag{2.15}$$

However considering that the shear stress varies very little within the shear layer, as it was postulated in Equation 2.2, the shear layer is thin, and the shear stress vary in inverse proportion to the difference between the pin and shear layer radius, so the variation is small and constant. Furthermore, considering that the shear rate and tangential velocity gradient are essentially the same magnitude ($\dot{\gamma} = -dv/dx$), Equation 2.15 can be restate as Equation 2.16 with Equation 2.17 as boundary condition.

$$q(x) = -\eta_s \tau \frac{dv}{dx} \tag{2.16}$$

$$v|_{x=0} = \omega a \tag{2.17}$$

By using the tangential velocity profile of Figure 2.3 it is possible to normalize the two terms of Equation 2.16 by an estimation of their maximum values given by:

$$\frac{dv}{dx} = \frac{3}{2}\frac{\omega a}{\widehat{\delta}}\left(\frac{dv}{dx}\right)^* \tag{2.18}$$

$$\tau = \widehat{\tau_c}\tau^* \tag{2.19}$$

Replacing Equation 2.18 and 2.19 in Equation 2.16, the normalized form of the volumetric heat generation is expressed by:

$$\widehat{q_c}q^* = -\frac{3}{2}\eta_s\widehat{\tau_c}\frac{\omega a}{\widehat{\delta}}\left(\frac{dv}{dx}\right)^* \tag{2.20}$$

Where the value 3/2 present in the normalization of the derivative is related to the speed evolution inside the shear stress illustrated in Figure 2.3. Finally substituting the normalized functions by ±1 the following algebraic equation based on the characteristic values is obtained:

$$\widehat{q_c} = \frac{3}{2}\eta_s \widehat{\tau}_c \frac{\omega a}{\widehat{\delta}} \tag{2.21}$$

2.4.3. Constitutive equation in the shear layer

The constitutive equation in the shear layer is made under the assumption that there is no phase transformation, such as any amount of remelting in the base plate. The constitutive model has an intuitive interpretation based on the activation energy and strain rate measure, this is made under the assumption that the material follows a Zener-Hollomon behaviour, which has the expression:

$$\dot{\gamma} = A\left(\frac{\tau}{\tau_R}\right)^n exp\left(-\frac{Q}{RT}\right) \tag{2.22}$$

Where "A", "Q" and "n" are parameters of the model, R is the gas constant, and τ_R is an arbitrary reference stress. Considering that T=T(x) and that $\dot{\gamma} = -dv/dx$, the Equation 2.22 can be normalized as Equation 2.23 with the Equation 2.24 as boundary condition.

$$-\frac{3}{2}\frac{wa}{\widehat{\delta}}\left(\frac{dv}{dx}\right)^* = A\left(\frac{\widehat{\tau}_c \tau^*}{\tau_R}\right)^n exp\left(-\frac{Q}{RT_s}\right) f^*(x^*) \tag{2.23}$$

$$v|_{x=0} = wa \tag{2.24}$$

Also $f^*(x^*)$ is define as:

$$f^*(x^*) = exp\left(-\frac{Q}{R}\left(\frac{1}{T(\widehat{\delta}x^*)} - \frac{1}{T_s}\right)\right) \tag{2.25}$$

Now, replacing again the normalized functions by +1 or -1 in Equation 2.23 turns into:

$$\frac{3}{2}\frac{\omega a}{\widehat{\delta}} = A\left(\frac{\widehat{\tau}_c}{\tau_R}\right)^n exp\left(-\frac{Q}{R\widehat{T_s}}\right) \tag{2.26}$$

Furthermore a new simplification can be made to obtain a power law expression. Figure 2.3 illustrates how the exponential component of the constitutive equation can be divided in two asymptotic regimes. The first one is the regime at high temperature, within the shear layer, near the pin and where the shear layer rate is high. The second one is outside the shear layer with low temperatures, the characteristic temperature T_δ is the representation of the limit between this two regimes. Near the incipient melting temperature, the Arrhenius expression can be linearized as:

$$exp\left(-\frac{Q}{R\widehat{T_s}}\right) \approx \begin{cases} 0 & if \quad T \leq T_0 \\ \frac{\widehat{T_s}-T_0}{T_m-T_0} exp(-\frac{Q}{RT_m}) & if \quad T > T_0 \end{cases} \tag{2.27}$$

Where T_m is the melting temperature and T_0 can be obtained by intersecting the x-axis of Figure 2.3 with the tangent to the curve at the point of T_m, obtaining:

$$T_0 = T_m \left(1 - \frac{RT_m}{Q}\right) \tag{2.28}$$

Finally Equation 2.26 can be expressed using power laws as:

$$\frac{3}{2}\frac{\omega a}{\widehat{\delta}} \approx AB \left(\frac{\widehat{\tau_c}}{\tau_R}\right)^n \frac{\Delta\widehat{T_s}}{\Delta T_m} \tag{2.29}$$

Where $\Delta\widehat{T_s} = \widehat{T_s} - T_0$, $\Delta T_m = T_m - T_0$, and $B = exp(-Q/RT_m)$. ΔT_m, as well as B are known quantities from the material properties.

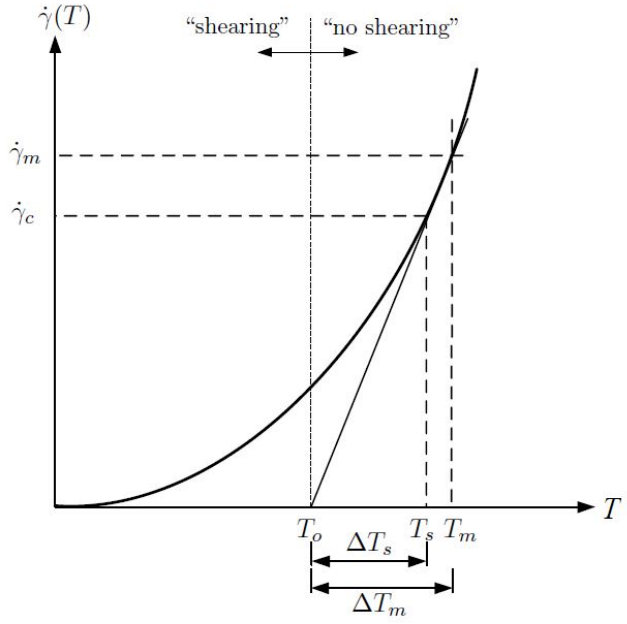

Figure 2.3: Asymptotic regimes for the constitutive behavior of the base plate.

2.4.4. Heat conduction outside the shear layer

As it was explained in section 2.3 for the Equation 2.1 Rosenthal's solution[44], explain that for a steady state heat point the isotherms corresponding to the shear layer are approximately circular and concentric. In this mathematical model Rosenthal's[44] thin plate solution will be based on a line heat source, which consider heat transfer only on the plane of the plate (one dimensional problem). Thereby as it was mention on section 1.3 is not consider the heat losses through the pin or to the atmosphere, it's also relevant to mention that Rosenthal's solution[44] assume constant materials properties and a uniform temperature T_∞ and is expressed in Equation 2.30.

$$T(x') - T_p = \frac{ql}{2\pi k_0} exp\left(-\frac{Vx'}{2\alpha}\right) K_0\left(\frac{Vr}{2\alpha}\right) \tag{2.30}$$

Where ql is the intensity of the line heat source, k_0 is the heat conductivity of the plate at $T = T_0$, and K_0 corresponds to the modified Bessel function of a second kind and order 0. The coordinates x' and r correspond to a distance in the direction of travel and a radial distance from the line heat source respectively. Then the intensity of the heat source is given by:

$$ql = \eta \text{ (torque/thickness) x (angular velocity)} = \eta(\tau 2\pi a^2)\omega \tag{2.31}$$

Where η is the total heat efficiency of the process. As it was mention before, even though the radius of the isotherm corresponding to the shear layer is $r = r_0 = a + \delta$, it can be approximated to r=a for a thin shear layer. Additionally the Pe number is small, which means that the expression $exp(-Vx'/2\alpha)$, from Equation 2.30 is 1, and $K_0(Pe)$ increases when Pe decreses (see Figure 2.4). Considering this points the Equation 2.30 can be simplified as:

$$\Delta T_\delta = T_\delta - T_\infty = \eta \frac{\omega a^2 \widehat{\tau_c}}{k_0} K_o(Pe) \tag{2.32}$$

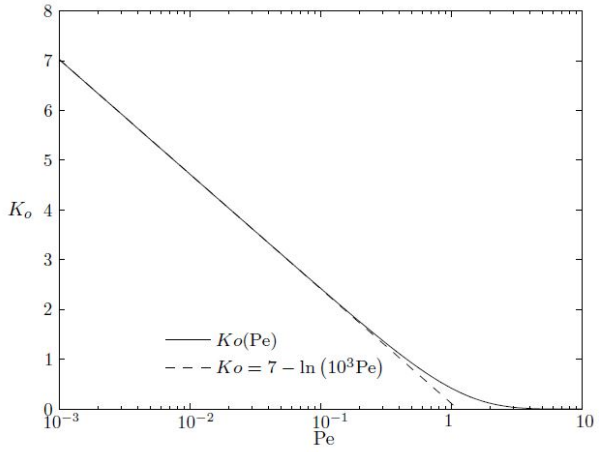

Figure 2.4: Behavior of the Bessel function Ko(Pe) and the asymptotic linearization valid for small Pe numbers (dashed line).

2.4.5. Solutions of the system of scaled equations

A system of equations to found the expression for the characteristic values can be formed by the equations 2.14, 2.18, 2.29 and 2.47. From this system of equation, $\widehat{\tau_c}$ can be solve without the other equations, and to solve $\widehat{\delta}$, $\Delta\widehat{T_s}$ and $\widehat{q_c}$ linear algebra can be used. Therefore the characteristic values are:

$$\widehat{\tau_c} = \frac{k_o \Delta T_\delta}{\eta^2 K_0} \tag{2.33}$$

$$\widehat{\delta} = a \left[\frac{8}{3} \frac{\Delta T_m}{\eta_s AB} \left(\frac{\tau_R a^2}{k_\delta} \right)^n \left(\frac{\eta K_0 \omega}{\Delta T_\delta} \right)^{n+1} \right]^{1/2} \tag{2.34}$$

$$\Delta T_s = \Delta T_m \left[\frac{3}{2} \frac{\eta_s}{AB\Delta T_m} \left(\frac{\eta K_0}{\Delta T_\delta} \right)^{n-1} \left(\frac{a^2 \tau_R}{k_\delta} \right)^n \omega^{n+1} \right]^{\frac{1}{2}} \tag{2.35}$$

$$\widehat{q_c} = \frac{3}{4}\left[\frac{3}{2}\frac{AB\eta_s^3}{\Delta T_m}\left(\frac{1}{\tau_R}\right)^n\left(\frac{1}{\omega}\right)^{n+1}\left(\frac{k_\delta}{a^2}\right)^{n+2}\left(\frac{\Delta T_\delta}{\eta K_0}\right)^{n+3}\right]^{\frac{1}{2}} \tag{2.36}$$

Additionally from Equation 4.5 is possible to obtain the equation for the torque of the pin, and is given by:

$$\widehat{M} = 2\pi\widehat{\tau_c}a^2t \tag{2.37}$$

2.5. Material Properties

2.5.1. Thermal and Mechanical Properties

All the thermal and mechanical properties are summarized in Table 2.1[22]. Also, since it is believed that FSW involves only pure shear stress, the flow shear stress of reference τ_R was calculated from Von Mises criteria in uniaxial tension and pure shear, with the following equation:

$$\tau_R = \frac{\sigma_R}{\sqrt{3}} \tag{2.38}$$

Where the normal stress of reference was assumed to be the yield stress of the alloy and the values from each material were obtained from the Metals Handbook [25].

The thermal efficiency (η) varies among the materials analyzed. According to Lienert et al. [29] the thermal efficiency of aluminum alloys is 90% and of AISI 1018 is 75%. According to Zhu et al. [30] the thermal efficiency of AISI 304 is 50%, and according to Lienert et al. [31] the thermal efficiency of Ti-6Al-4V is 47%. Furthermore, the efficiency η_s was assumed to be 100% for all materials.

Table 2.1: Thermal and mechanical properties of the materials selected.

Material	$T_{solidus}$[K]	k[W/ms]	C_p[J/kg]	ρ[kg/m^3]	σ_R[MPa]	η_s[%]	η[%]	k_{inf}
Al2024	775	185	1,100	2,670	103	100	90	162
Al2195	813	196	1,338	2,770	330	100	90	170
Al5083	847	139	1,190	2,523	214	100	90	121
Al6061	855	200	1,10	2,590	55.2	100	90	152
Al7050	761	180	861	2,827	103	100	90	180
Al7075	805	192	1,109	2,693	103	100	90	166.7
AISI 1018	1,733	33.1	699	7,314	205	100	75	25
AISI 304	1,673	33.5	720	7,350	290	100	50	20
Ti-6Al-4V	1,877	27	750	4,198	875	100	47	-

2.5.2. Zenner-Hollomon law constants

Sellars and Tegart[32] postulated that the deformation mechanisms operating in hot working processes at low level of stress can be described by:

$$\dot{\varepsilon} = A\left(\frac{\sigma}{\sigma_R}\right)^n exp\left(-\frac{Q}{RT}\right) \tag{2.39}$$

Where "A","Q", and "n" are constants. The problem with the Equation 2.39 is that it doesn't take into account the behaviour of the materials at high stresses. As a result, the authors proposed an empirical constitutive equation (see Equation 2.40) suitable at low and high level of stresses and which is capable of correlate data over a wide range of strain rate

$$\dot{\varepsilon'} = A\left[sinh\left(\frac{\sigma'}{\sigma_R}\right)\right]^{n'} exp\left(-\frac{Q'}{RT}\right) \tag{2.40}$$

Where A', Q', n' and σ'_R are constants obtained from the hot deformation model done by Dr.Tello[33]. To include the effects of Equation 2.40 to the Equation 2.39 is fundamental to found a relationship between both of them by their constants, for this the following procedure was made.

1. Take the linearized form of Equation 2.39 and 2.40.

$$ln(\dot{\varepsilon} = lnA + nln\left(\frac{\sigma}{\sigma_R}\right) - \frac{Q}{RT} \tag{2.41}$$

$$ln(\dot{\varepsilon'}) = lnA' + n'ln\left[sinh\left(\frac{\sigma'}{\sigma'_R}\right)\right] - \frac{Q'}{RT} \tag{2.42}$$

2. Calculate the partial derivatives of $\ln(\dot{\varepsilon})$ with respect to 1/T and $\ln(\sigma)$ for each equation presented in 1):

$$\frac{\partial ln(\dot{\varepsilon})}{\partial 1/T} = -\frac{Q}{RT} \tag{2.43}$$

$$\frac{\partial ln(\dot{\varepsilon})}{\partial ln(\sigma)} = n \tag{2.44}$$

$$\frac{\partial ln(\dot{\varepsilon'})}{\partial 1/T} = -\frac{Q'}{RT} \tag{2.45}$$

$$\frac{\partial ln(\dot{\varepsilon'})}{\partial ln(\sigma')} = \frac{n'\sigma'}{\sigma'_R}\frac{1}{tanh(\frac{\sigma'}{\sigma'_R})} \tag{2.46}$$

3. Evaluate each equation presented in 2) at the solidus temperature of the alloy and at average value of strain rate achieved during FSW, which is $\dot{\varepsilon}$=300(s^{-1}) . Then equating the respective partial derivatives:

$$\frac{Q}{RT} = \frac{Q'}{RT} \Rightarrow Q = Q' \tag{2.47}$$

$$n = \frac{n'\sigma'}{\sigma'_R} \frac{1}{tanh(\frac{\sigma'_R}{\sigma'})} \tag{2.48}$$

Where σ' corresponds to the shear stress calculated with Equation 2.41 at $300[s^{-1}]$ and $T_{solidus}$, in consequence "Q" and "n" can be calculated using 2.47 and 2.48 respectively.

4. Calculate the constant A from Equation 2.40.

$$ln(A) = ln(\dot{\varepsilon})|_{300s^{-1}} - nln\left(\frac{\sigma'}{\sigma_R}\right)\Bigg|_{\left(\begin{smallmatrix}300s^{-1}\\ T_{solidus}\end{smallmatrix}\right)} + \frac{Q}{RT_{solidus}} \tag{2.49}$$

Table 2.2 summarizes the values of the constants obtained by using the procedure previously described.

Table 2.2: Values of constants for the Zenner-Hollomon constitutive Equations 2.39 and 2.40.

Material	A'$[s^{-1}]$	n'	Q'=Q[kJ/mol]	σ'_R[MPa]	A(s^{-1})	n
Al2024	2.29 x 10^{11}	5.46	178	47.7	6.52 x 10^{14}	11.5
Al2195	2.29 x 10^{12}	2.38	162	293	1.73 x 10^{12}	3.54
Al5083	2.29 x 10^{11}	2.44	173	34.8	1.78 x 10^{15}	8.44
Al6061	2.29 x 10^{11}	5.33	191	60.7	1.72 x 10^{13}	7.68
Al7075	2.29 x 10^{11}	3.47	160	33.9	1.74 x 10^{12}	11.95
Al7050	2.29 x 10^{11}	3.39	165	32.5	6.48 x 10^{13}	10.7
AISI 1018	2.29 x 10^{11}	4.32	371	56.6	6.95 x 10^{16}	5.67
AISI 304	2.29 x 10^{11}	4.69	441	119	4.36 x 10^{18}	5.51
Ti-6Al-4V	3.37 x 10^{8}	3.39	231	47.9	3.96 x 10^{14}	4.63

Chapter 3

Materials and methods

3.1. Methodology

This thesis is based on the previous work of Dr.Mendez et al[20] and Dr.Tello thesis [1]. Relying on their work this thesis consists in remake Dr.Tello results and compare them with the new results that embrace the mathematical variable of heat loss in the FSW model. In order to achieve this purpose the following steps where conducted:

1. Study and inspect the mathematical model in Dr.Tello's thesis [1].
2. Study and compare the FSW mathematical model of Dr.Mendez et al.[20] with Dr.Tello's work.
3. Order and rebuild Dr.Tello's[1] data base constructed from different publications.
4. Calculate the characteristic values $\widehat{\delta}$, $\widehat{\tau_c}$, ΔT_s and $\widehat{M}$ for the data base of Dr.Tello[1].
5. Calculate the five assumptions; Pe«1, $\widehat{\delta}/a$«1, $(b-a)/\widehat{\delta}$«1, $V/\omega\delta$«1 and T_P/T_{max}«1.
6. Build the main graphs that Dr.Tello[1] determined to observe the accuracy of the mathematical model, which are; $(T_{max}-T_\infty)/(\widehat{T_{max}}-T_\infty)$, $\delta/\widehat{\delta}$, and $M/\widehat{M}$ v/s the four assumptions and the graph of Figure 10 of Dr.Mendez[20] work $(T_{max}-T_\infty)/(\widehat{T_{max}}-T_\infty)$ vs $(T_P-T_\infty)/(\widehat{T_{max}}-T_\infty)$.
7. Analyze the incorporation of the new mathematical value associated to the heat loss by the study of the importance of the convective values related to the heat loss through the bottom and top of the plate.
8. Recalculate the characteristic values and assumptions considering the incorporation of the new mathematical variable ξ.
9. Rebuild the graphs mentioned in point 6.
10. Calculate the logarithmic error and the correction factors.
11. Analyze the results and compare them with Dr.Tello's[1] results.

3.2. Experiment selection

3.2.1. Data Base

The data base was formed by choosing papers that had the information or allowed to calculate numerically the experimental measured or computer simulation of the shear layer thickness, maximum temperature and torque. This allowed the comparison with the estimations made by the mathematical model. In addition, thermal and mechanical properties of the material were also compiled.

As previously mentioned, the main focus of FSW is to weld unweldable material such as aluminium alloys, but due to its benefits is also important to compare the results with other materials like steel metals or titanium. Therefore the specific materials that conform the data base are:

- Al2024
- Al2195
- Al5083
- Al6061
- Al7050
- Al7075
- AISI 1018
- AISI 304
- Ti-6Al-4V

3.2.2. Measurement Forms

In this section the measurement forms during the experiments are detailed, due to the importance of knowing the source of the information in the data base, and the procedure that was made to measured the temperature, force, and shear layer size. This understanding allows the comprehension of possible error origins.

- **Temperature measure** In general most of the temperature measures where made by the use of a thermocouple k-type coupled to the plate in different heights of its width and length, allowing to have a temperature profile and its evolution through time. There have also been experiments where the thermocouple is inside the rotational tool(the smallest possible off-the-shelf type K thermocouple was chosen to reduce the temperature response time (sheath diameter 0.25 mm, part no. TJ36-CAXL-010U; Omega Corp.)), which also shows the variation of the temperature but with a proportional variation compared to the temperature measured in the plate. There are also measures with infrared cameras(Mikron M7815 Infrared Thermal Imaging Camera) or thermoelectric methods.

- **Force and Torque measure** The most common methods for this are dynamometer, load cells(SEWHA, 2000kg capacity, R.O:2.0008mV/V or LowStir™ device) and strain gauge. Less common measures are related to the energy measures and from this the torque and forces are calculated.

- **Shear layer measure** The shear layer length measure requires a cross-section sample from the path made by the pin, which is subjected to a chemical attack that allows to distinguish the deformed zone by the welding process from the one that wasn't. Once this is completed, it is possible to measure the width of the deformed area to a quarter of the height of the base plate and considering that this measure is twice the pin radius and two times the thickness of the deformation layer (see Figure 3.1) is possible to calculate it.

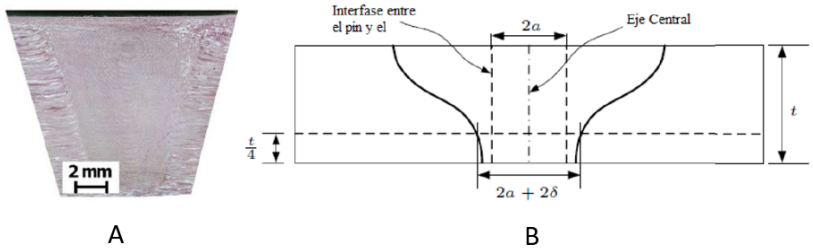

Figure 3.1: A: Cross-section sample of FSW. B: Diagram for the shear layer measurement.

3.3. Resources

The resources for the realization of this thesis where:

- MATLAB ®: this software was used to construct the graphs.

- Excel: this software was used to rebuild the data base; calculate the characteristic values and generate the trial graphs.

- Bibliography material:

  - Research papers: the bibliography was used to extract the data that contains the experiments and to search or verify previous information.
  - Dr. Tello thesis[1] and Dr.Mendez paper[20]: The study of previous thesis related to FSW to understand the evolution of the equations and different results related to their respective changes.
  - Book: Metals Handbook [22] was used to verify mechanical properties of the alloys.

Chapter 4

Adjustment of coupled model for FSW

Chapter 2.4.4 mentioned that heat loss through the plate in Rosenthal's solution[44] is not considered, therefore in this section the importance of its consideration will be proved to incorporate it in the model and improve the results.

4.1. Influence of the heat loss through the plate

Previously the Bessel function was calculated using only Peclet number (see Equation 2.30) because it was believed that the heat loss through convection and conduction from the bottom and top of the plate was insignificant due to the fact that FSW is considered a low heat welding process, compared to other kinds of welding.

The heat loss through the plate can be represented as:

$$\frac{h + h'}{k_\delta d} \tag{4.1}$$

Where h and h' are the coefficients of heat loss by convection and conduction of the top and bottom part from the plate and their values are 10[W/M2°K] and 10000[W/M2°K][53] respectively for all the materials, "d" is the thickness of the plate and k_δ is the thermal conductivity associated with the temperature at $x = \delta$.

On the other hand the heat loss through thermal diffusivity is expressed by:

$$\frac{V^2}{4\alpha^2} \tag{4.2}$$

To proved that the heat loss by convection of the top and bottom part from the plate matters, the Equation 4.3 will be graph with the Equation 4.4.

$$\lambda = \frac{h + h'}{k_\delta d} \Big/ \frac{v^2}{4\alpha^2} = \frac{4\alpha^2(h + h')}{k_\delta d v^2} \tag{4.3}$$

$$M/\widehat{M} \tag{4.4}$$

Where M is the torque measured in the experiments and $\widehat{M}$ is the estimation made by

the mathematical model. Thus if the heat loss of the top and bottom is equally or more significant than the heat loss through thermal diffusivity, Equation 4.3 should tend to 1 or more. Something similar happens with Equation 4.4, because if the estimated torque is close to the measure of it, then their division should be 1, or similar. Figure 4.1 effectively prove the influence of λ, this can be easily notice by looking that experiments are set from 1 until 100 in the λ axis. Furthermore in the $M/\widehat{M}$ axis the experiments also are located near 1, proving that the mathematical model works.

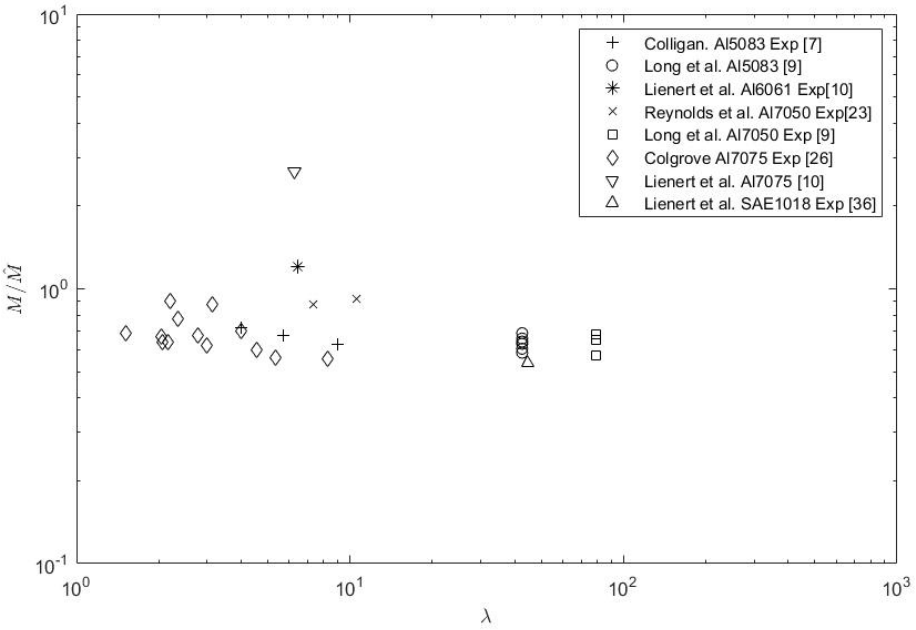

Figure 4.1: Ratio of torque as a function of simplification λ (Equation 4.3).

4.2. Modification of the coupled model for FSW

The section 2.4.4 explained the heat conduction outside the shear layer should now incorporate the heat loss by convection and conduction of the top and bottom of the plate, for this, the following equation is presented:

$$\xi = r\sqrt{\left(\frac{V}{2\alpha_\delta}\right)^2 + \frac{h+h'}{k_\delta t}} \tag{4.5}$$

The variable ξ will replace the Pe number in the Bessel equation, beside this, the system of scaled equations shown in section 2.4.5 remains intact.

Chapter 5

Results

5.1. Ratio of measurement and numerical results to estimations

To have a better conception of how the estimations match up with the measurement (X) and numerical results ($\widehat{X}$), the ratio between them is calculated. For this purpose, three ratios are defined: maximum temperature ratio, shear layer thickness and torque given by the Equations 2.34, 2.35, and 2.37. There is no ratio made for the volumetric heat $\widehat{q_c}$ because there are no suitable techniques to measure it. So the ratios that will be use are:

$$\theta = \frac{T_s - T_\infty}{\widehat{T_s} - T_\infty} \tag{5.1}$$

$$\frac{\delta}{\widehat{\delta}} \tag{5.2}$$

$$\frac{M}{\widehat{M}} \tag{5.3}$$

Where the terms without the hat symbol corresponds to the measurement and numerical results reported in the literature. Each ratio will be plotted with the four simplifications stated in Equations 2.1, 2.2, 2.3, and 2.4. If the ratios are constant near one, it means that the estimations made by the mathematical model could capture the proper order of magnitude of the target variable, and the graph behaviour should always present their values near one (in the "Y" axis).

Two graphs will be presented and analyze, first the graphs that Dr.Tello built in her thesis[1], where the Bessel function was evaluated with the Peclet number, and second the graphs that consider the Bessel function evaluated with ξ. The aforementioned will relate the ratio $(X/\widehat{X})$ with a simplification, where a subset of available data is used. This subset data consists of tests that fulfill all the simplifications except the one that is being used as the horizontal axis, and those experiments that use a Trivex-type pin. Following, the comparison between the estimations of the model and the measurement and numerical results will be presented for the maximum temperature, thickness of the shear layer and torque. The data compiled, and the results of the estimations are summarized in Appendix B (tables B.1, B.2),B.3, B.6, B.4, B.5), and C (C.2, C.3, C.3, C.4, C.5, C.6).

Finally a last graph will be rebuild from Figure 10 from Dr.Mendez paper[20] to incorporate the fifth assumption (Equation 2.5). Is also important to explain that usually one paper have several experiments with different materials, and that with one specific material, different kind of tests, where the variables changed as, for example, the velocity, pin or shoulder radius. So in this way the *experiments* refer to the different materials in one same study, and *tests* refer to the change of variable in one experiment.

5.1.1. Estimation of maximum temperature

Figure 5.1 presents the ratio of maximum temperature as a function of simplification given by Equation 2.4. Only in this case, the simplification is satisfied by being bigger than one($(b-a)/\widehat{\delta}>1$) for all the experiments, because the shear layer thickness is expected to be always lower than the shoulder's length. For Figure 5.1.A the ratio is between the range 0.5 and 1, and in Figure 5.1.B the ratio θ is between 0.4 and 1. In addition the Figure 5.1.A has 17 experiments and 36 tests plotted, and Figure 5.1.B has 13 experiments and 49 tests.

The Figure 5.2 presents the ratio of maximum temperature as a function of simplification given by Equation 2.1, where the result shows that the simplification is satisfied(Pe<1). The same happens for Figure 5.2.B, with the exception of one point doesn't fulfill the assumption and corresponds to the experiment of Nandal et al. AISI 1018[43], which is 1.01. In addition, the range of the ratio θ is between 0.65-1, with 17 experiments and 38 tests and between 0.55-1, with 13 experiments and 44 tests for Figure 5.2.A and B, respectively.

The Figure 5.3 presents the ratio of maximum temperature as a function of simplification given by Equation 2.3. In this case the simplification was not always satisfied for both graphs, because the $V/\omega\widehat{\delta}$ reaches values of 100 and 1000 for Figure 5.3.A and B, respectively. In this case is also evident that the data in both graphs differs, due to the fact that the incorporation of the ξ factor changes the values of the simplifications, which, at the same time also modifies the data that fulfilled the assumptions. In addition, this result presents a range of the ratio θ between 0.49-1.1, with 21 experiments and 51 tests and between 0.5-1.8, with 26 experiments and 107 tests for Figure 5.3.A and B, respectively.

Finally, the Figure 5.4 presents the ratio of maximum temperature as a function of simplification given by the Equation 2.2. Figure 5.4.A in which the Bessel equation is evaluated with the Peclet number, the curve decreases as $\widehat{\delta}/a$ increase, meanwhile in graph "B" all the data remains constant except for the experiment of Colgrove and Shercliff. Al7075 [26] and Colligan Al5083[7], which present a lower tendency to decrease as the $\widehat{\delta}/a$ increases. This can also be verify because this figure present a range of the ratio θ between 0.1-1.1, with 19 experiments and 61 tests and between 0.45-1, with 17 experiments and 61 tests for Figure 5.4.A and B, respectively. In addition, is also important to emphasize that the simplification is mostly satisfied in graph 5.4.B, for the exception of two test belonging to the experiment of Colegrove and Shercliff. Al7075 Exp[26], meanwhile graph 5.4.A doesn't satisfy the assumptions.

A

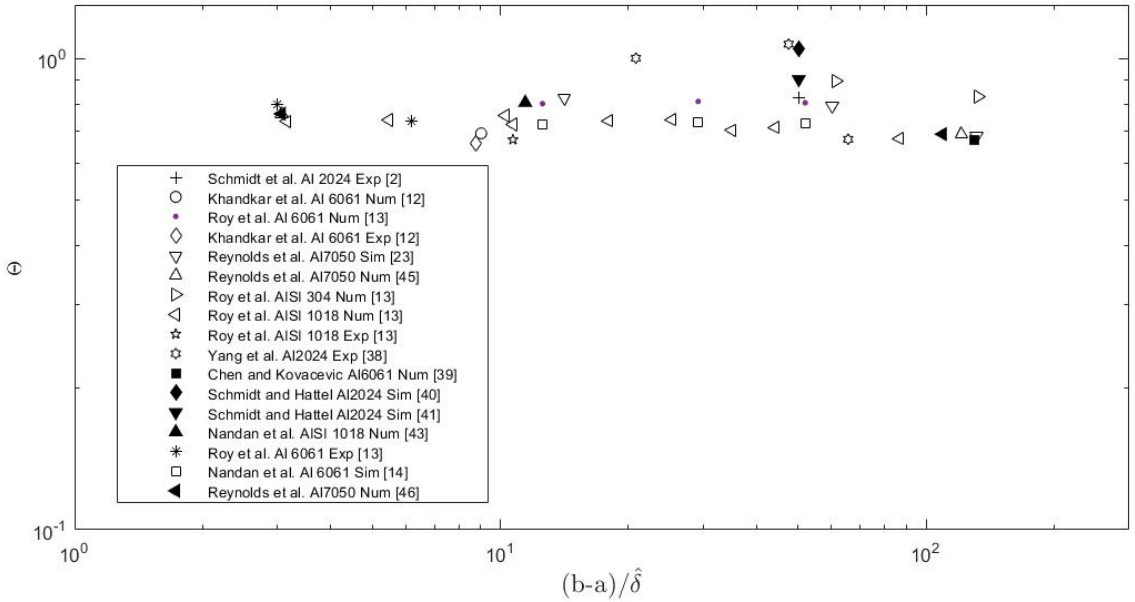

B

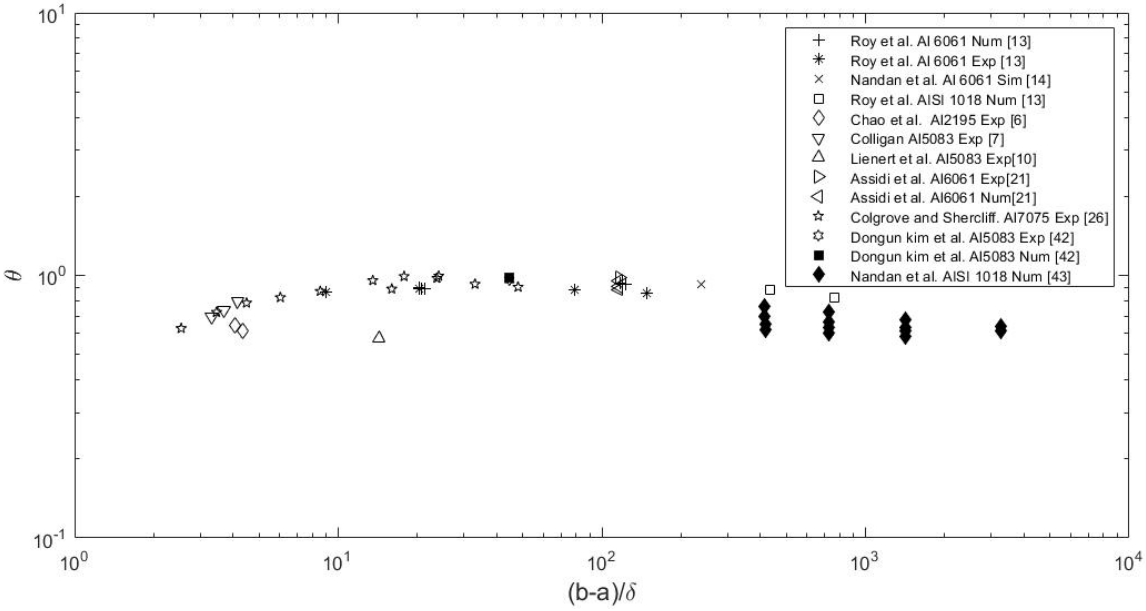

Figure 5.1: Comparison between the ratio of maximum temperature (θ) as a function of (b-a)/δ (Equation 2.4) without accounting for surface heat losses (Figure A) and accounting for surface heat losses (Figure B).

A

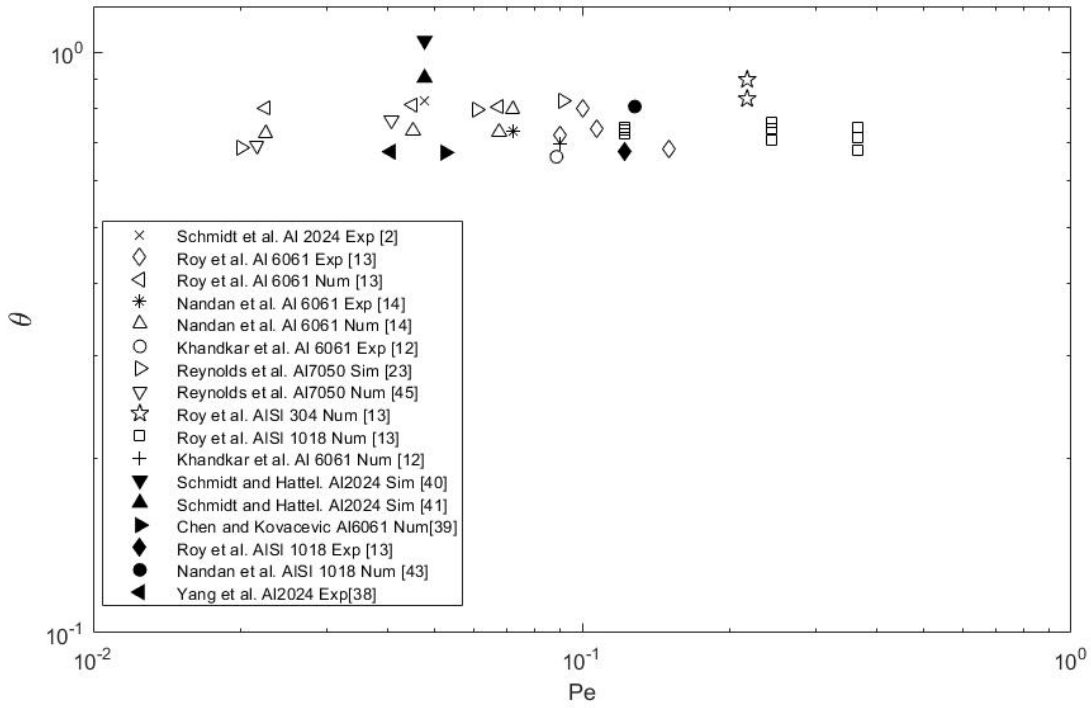

B

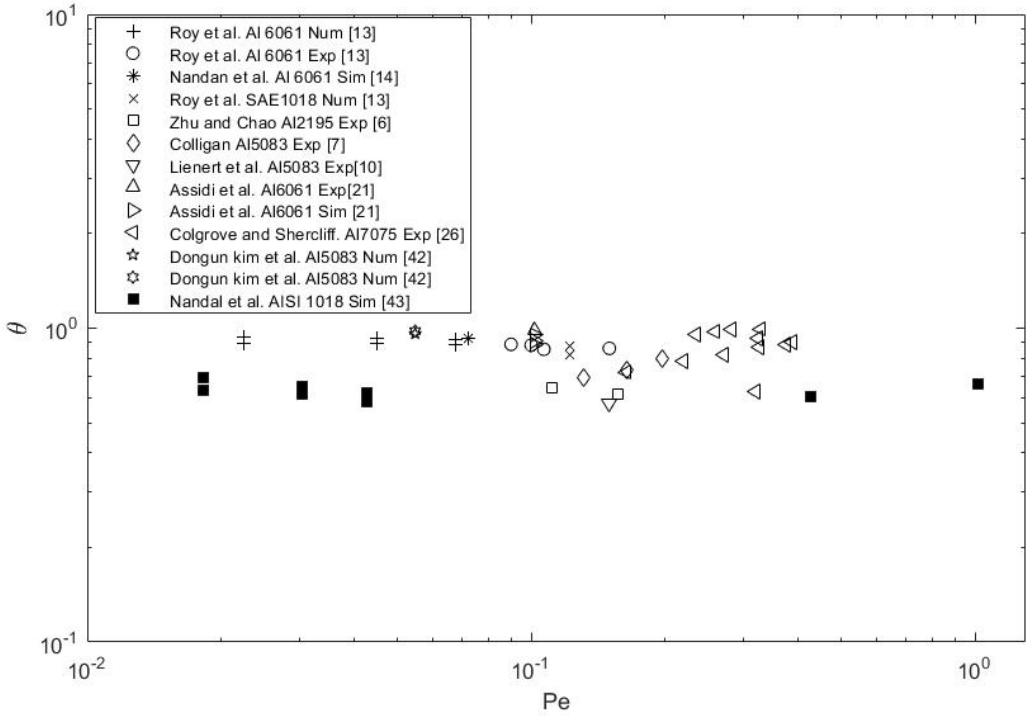

Figure 5.2: Comparison between the ratio of maximum temperature (θ) as a function of Pe (Equation 2.1) without accounting for surface heat losses (Figure A) and accounting for surface heat losses (Figure B).

A

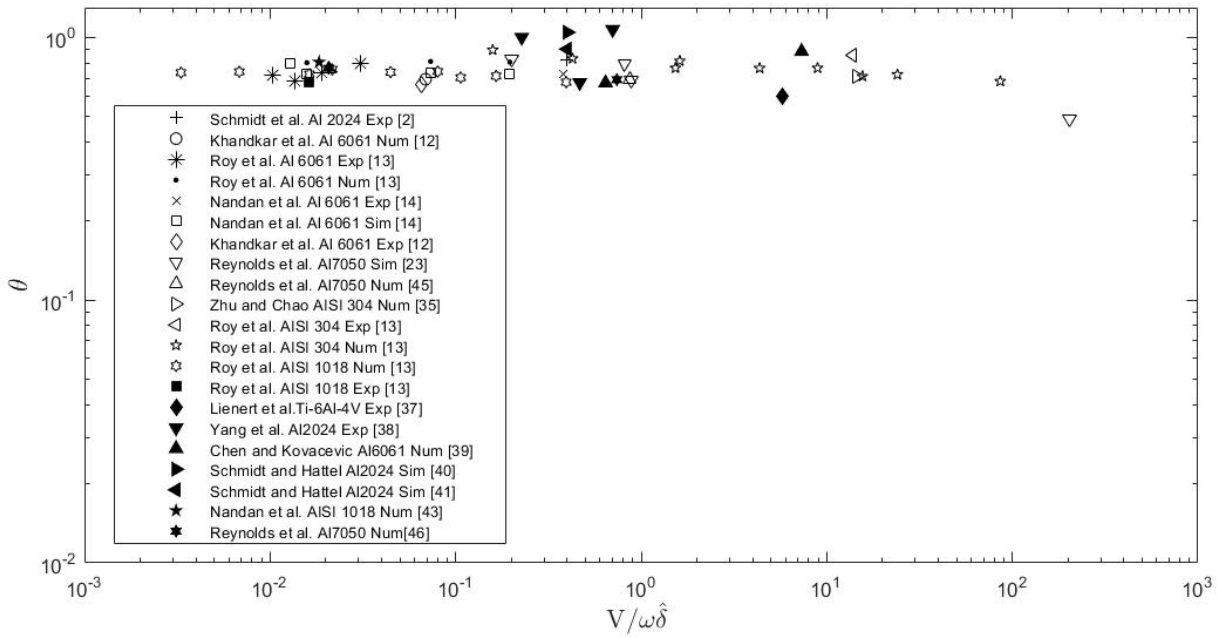

B

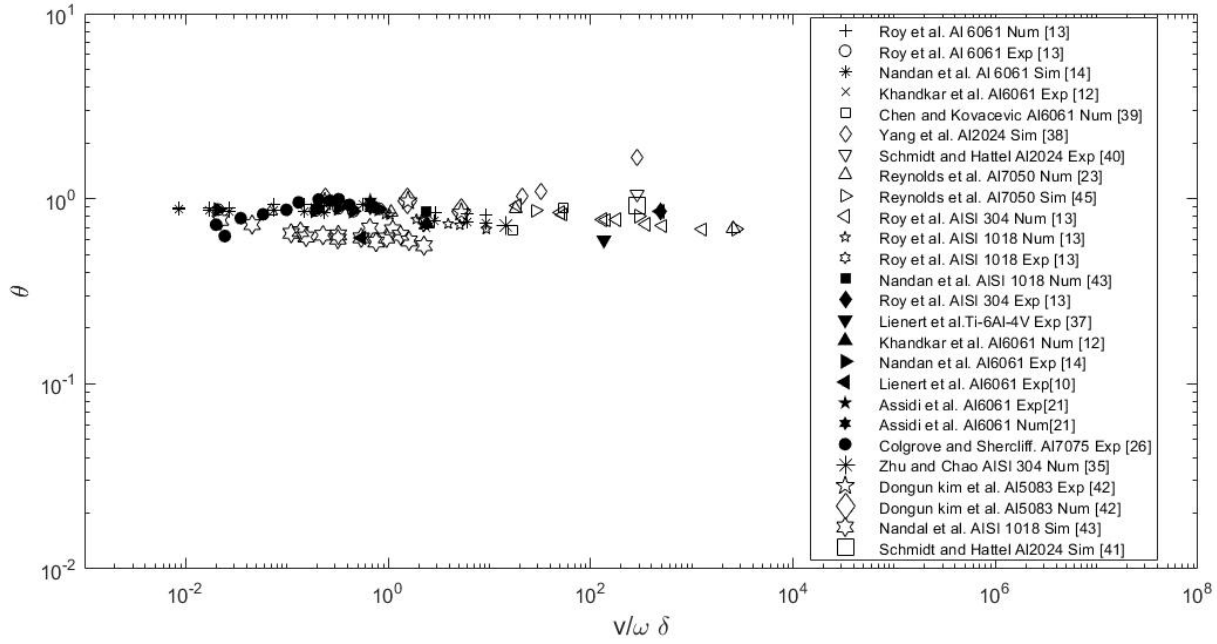

Figure 5.3: Comparison between the ratio of maximum temperature (θ) as a function of $V/\omega\delta$ (Equation 2.3) without accounting for surface heat losses (Figure A) and accounting for surface heat losses (Figure B).

A

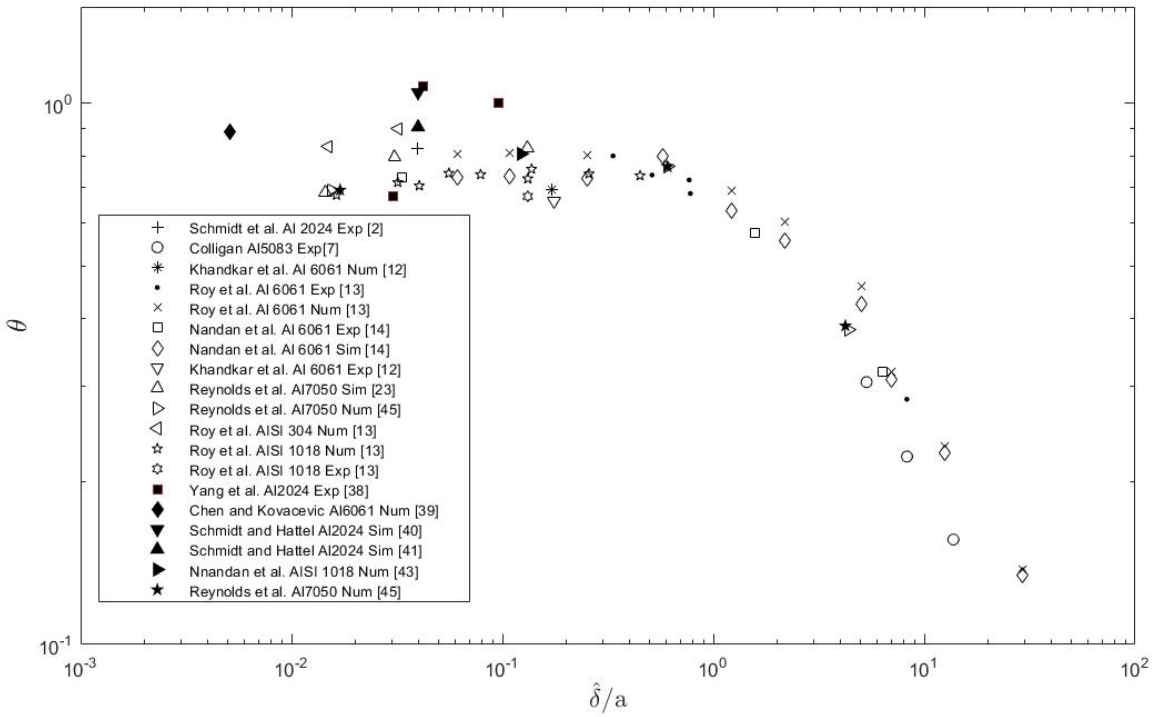

B

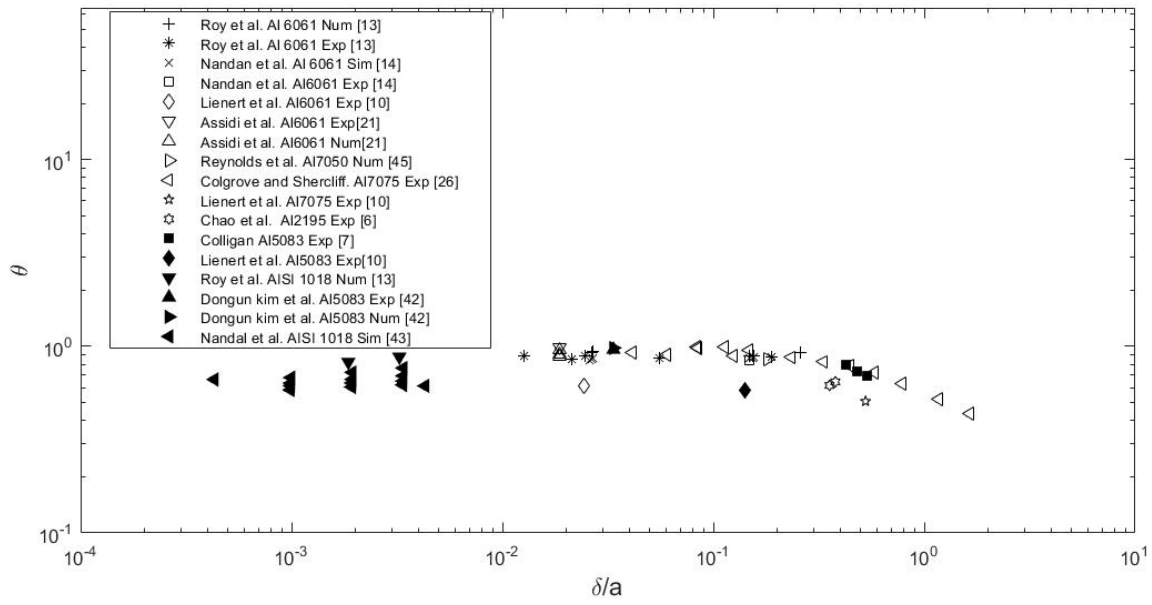

Figure 5.4: Comparison between the ratio of maximum temperature (θ) as a function of δ/a (Equation 2.2) without accounting for surface heat losses (Figure A) and accounting for surface heat losses (Figure B).

5.1.2. Estimation of torque

The results for the graphs of $M/\widehat{M}$ usually presents less data, due that the torque was not as frequently measured as the temperature, considering the higher difficulty that this presents. Figure 5.5 shows the ratio of torque as a function of simplification given by Equation 2.4. The simplifications did satisfied either of the graphs, because $(b-a)/\widehat{\delta}$ reach 100 and 10000(bigger than one) in Figures 5.5.A and B respectively. The ratio $M/\widehat{M}$ present a range between 1-2, with 9 experiments and 15 tests and between 0.5-1, with 7 experiments and 40 tests for Figure 5.5.A and B, respectively. Nonetheless Figure 5.5.B presents two exceptions for this affirmation; the experiment of Lienert et al. Al5083[10] and the experiment of Lienert et al[10]. AL7075, where the ratio $M/\widehat{M}$ are 2 and 5 respectively. In addition Figure 5.5.A has its ratio $M/\widehat{M}$ above one, meanwhile in Figure 5.5.B the ratio is under one.

The Figure 5.6 presents the ratio of torque as a function of simplification given by Equation 2.1. In this case, both graphs satisfied completely the simplification, and the ratio $M/\widehat{M}$ remains in a range between 1-4, with 9 experiments and 16 tests and between 0.5-1, with 7 experiments and 25 tests for Figure 5.6.A and B, respectively. Again, in Figure 5.6.B there are two exceptions for this statement; the experiment of Lienert et al. Al5083[10] and the experiment of Lienert et al. AL7075[10], where their ratio $M/\widehat{M}$ are 2 and 5 respectively. In this case the position of the ratio $M/\widehat{M}$ for Figure 5.6.B is, once more lower than one, meanwhile the Figure 5.6.A is higher than one.

The Figure 5.7 presents the ratio of torque as a function of simplification given by Equation 2.3. In this result the simplification was not fulfilled for neither graph A or B, due to the fact that $V/\omega\widehat{\delta}$ reached values of 10^2 and 10^6 in Figures 5.7. A and B, respectively. Additionally the position of the ratio $M/\widehat{M}$ is, once more, under one only for the Figure 5.7.B. The ratio $M/\widehat{M}$ present a range between 0.7-2, with 11 experiments and 28 tests, and between 0.4-1.6, with 13 experiments and 77 tests for Figure 5.7.A and B, respectively. As previously observed, in Figure 5.7.B there are two exceptions for this statement; the experiment of Schmidt et al. Al2024[2] and Lienert et al. Al5083[10], where their ratio $M/\widehat{M}$ are 2 and 6 respectively.

Finally, Figure 5.8 presents the ratio of torque as a function of simplification given by Equation 2.2. Again the ratio $M/\widehat{M}$ is under one for the Figure 5.8.B and over one for Figure 5.8.A, where it's ratio $M/\widehat{M}$ remains in a range between 1-2, with 10 experiments and 38 tests and between 0.5-1, with 8 experiments and 43 tests for Figure 5.6.A and B, respectively, with the exception of Lienert et al. Al5083[10], which has a ratio of 5 in 5.8.B. In addition is also important to emphasize that once more, the simplification is fully satisfied in Figure 5.8.B, except for two test from Colegrove and Shercliff. Al7075[26] and Long et al. Al5083[9]. On the other hand 5.8.A has values of $\widehat{\delta}/a$ that reach values of 10^3.

A

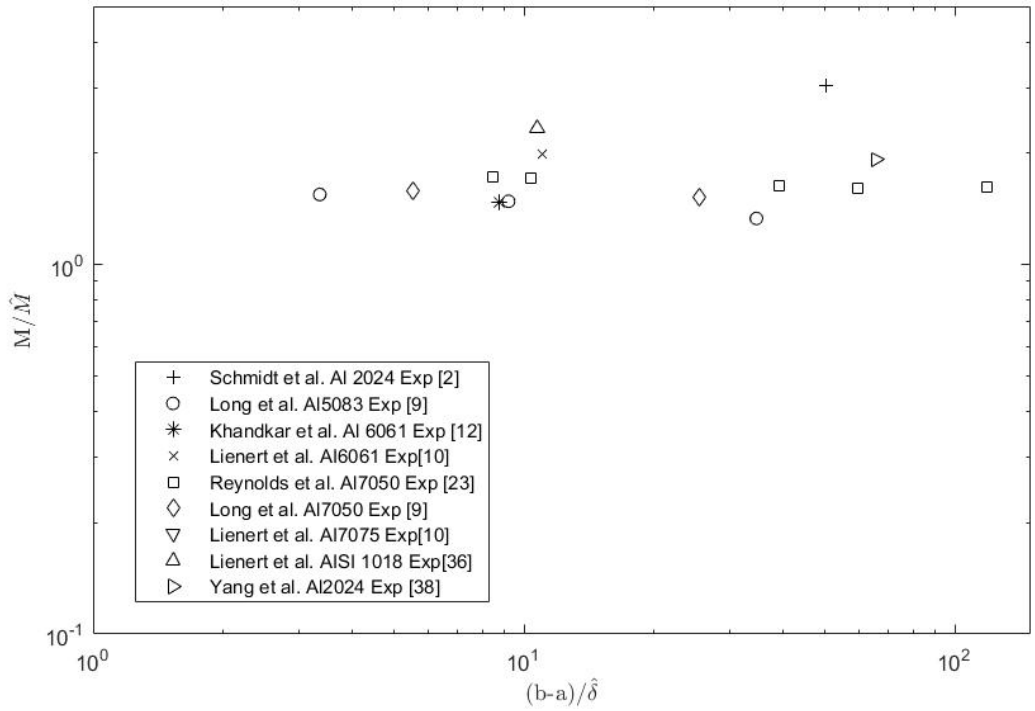

B

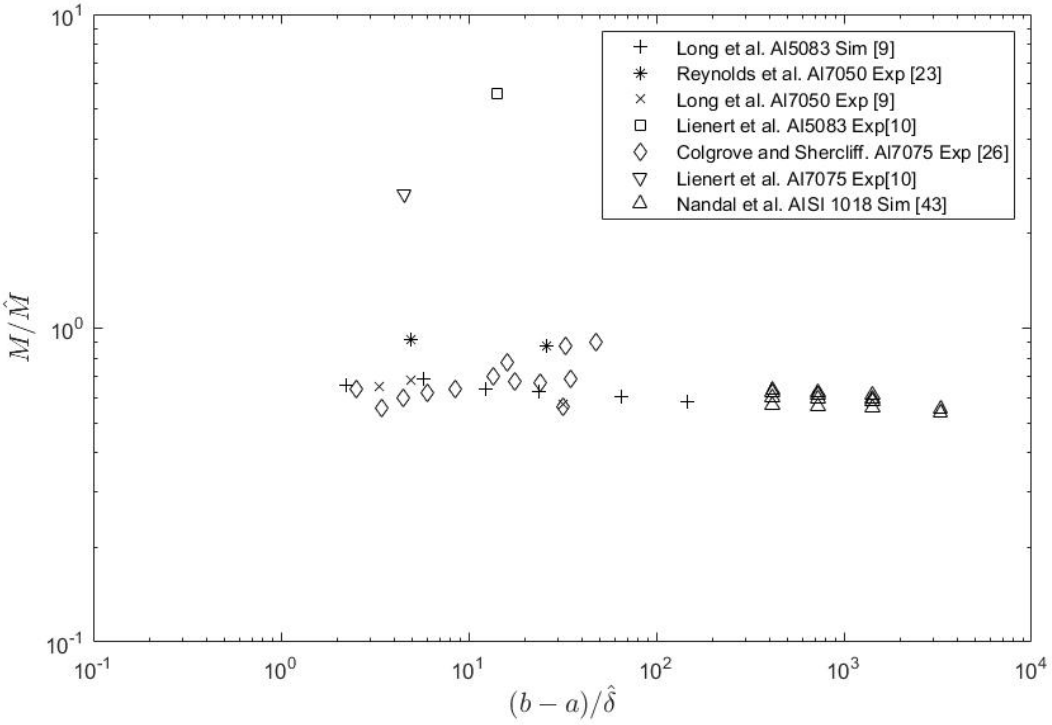

Figure 5.5: Comparison between the ratio of torque as a function of (b-a)/δ (Equation 2.4) without accounting for surface heat losses (Figure A) and accounting for surface heat losses (Figure B).

A

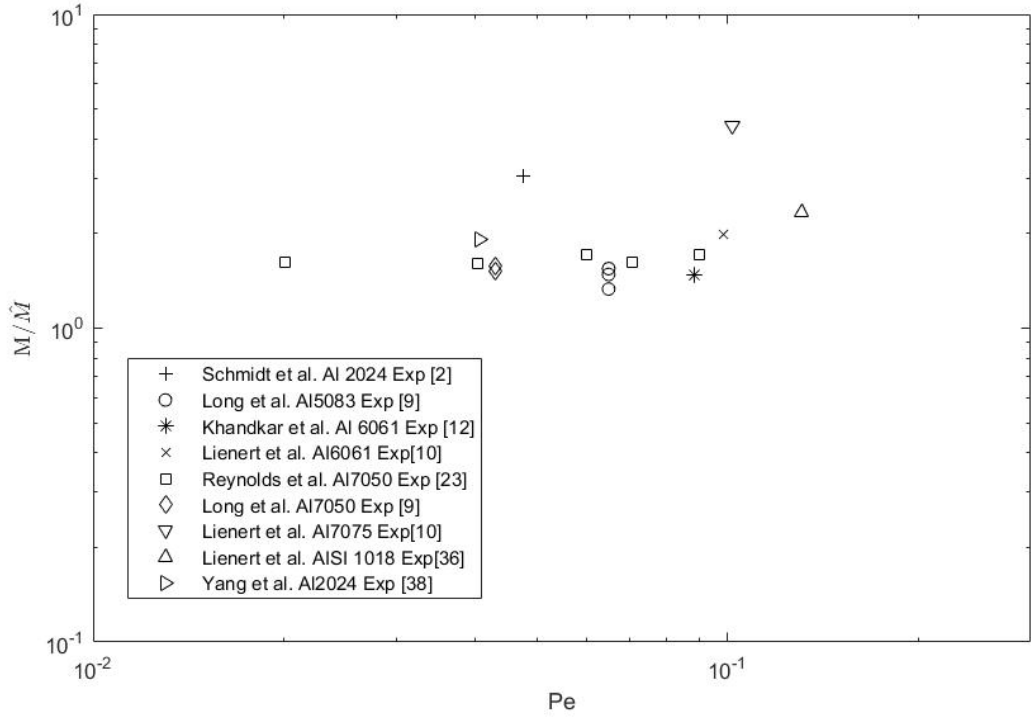

B

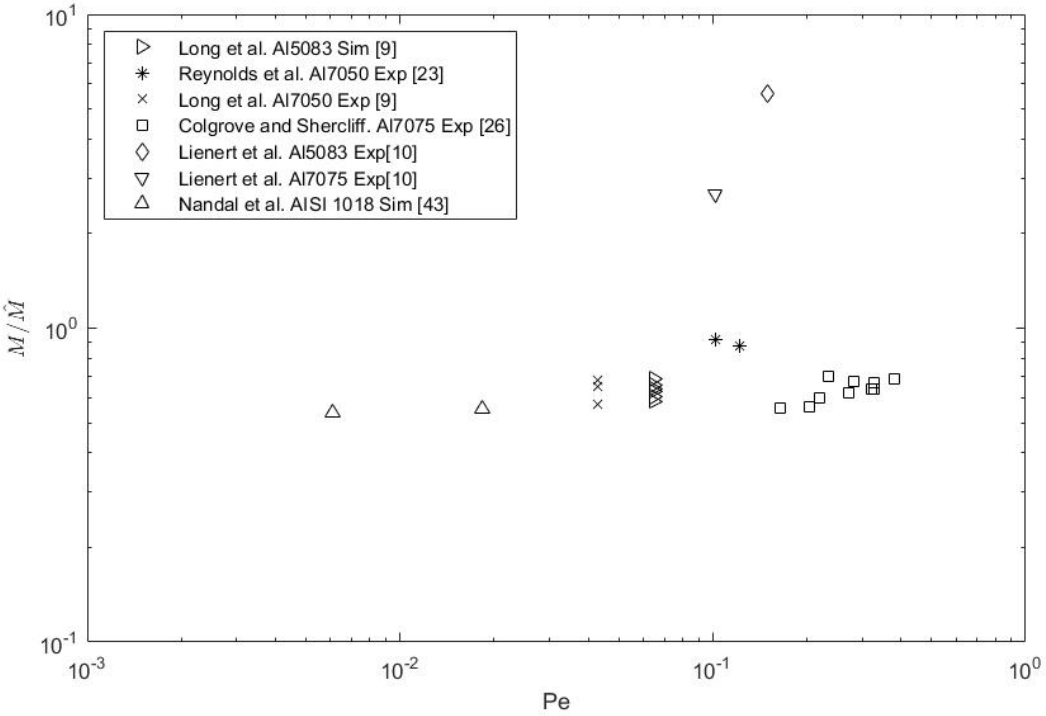

Figure 5.6: Comparison between the ratio of torque as a function of Pe (Equation 2.1) without accounting for surface heat losses (Figure A) and accounting for surface heat losses (Figure B).

A

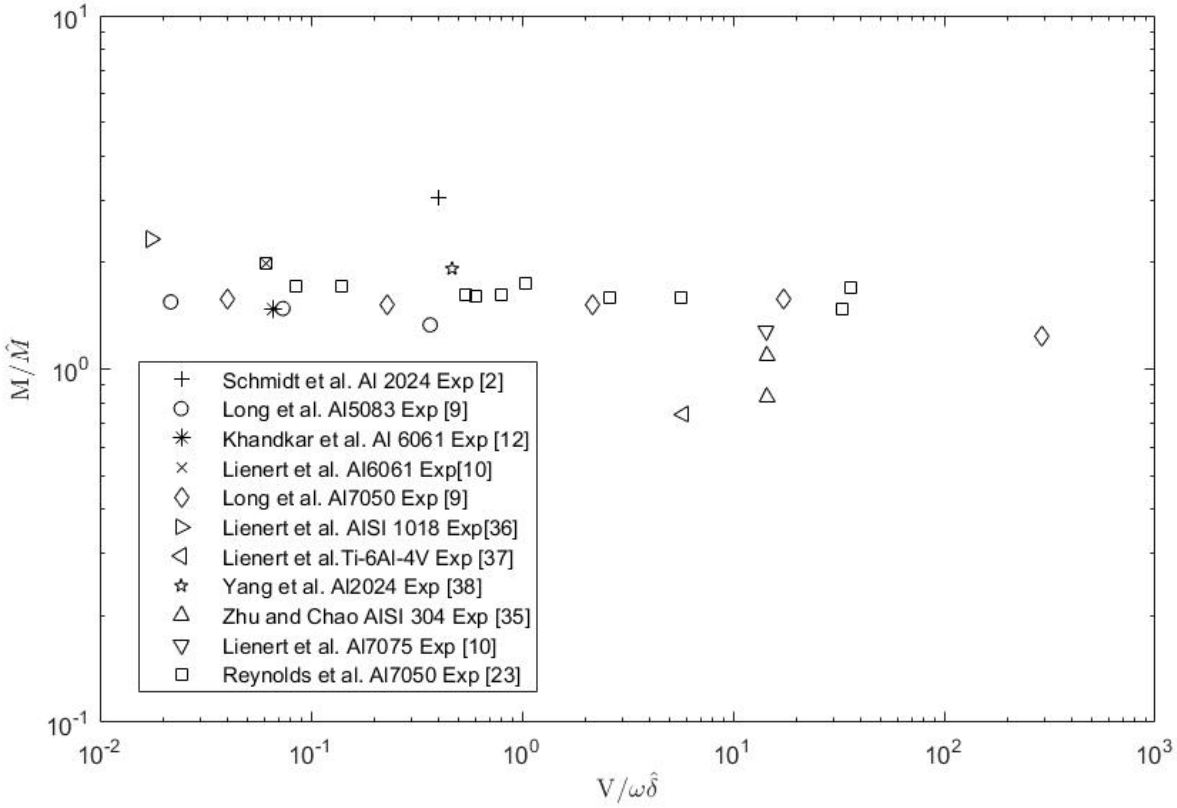

B

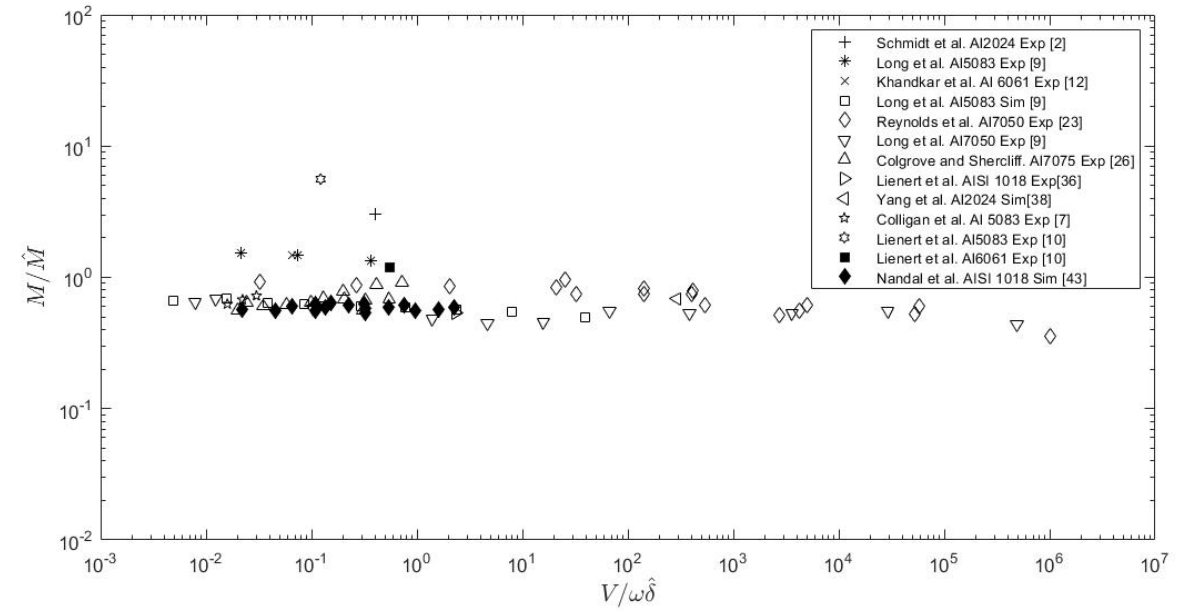

Figure 5.7: Comparison between the ratio of torque as a function of $V/\omega\delta$ (Equation 2.3) without accounting for surface heat losses (Figure A) and accounting for surface heat losses (Figure B).

A

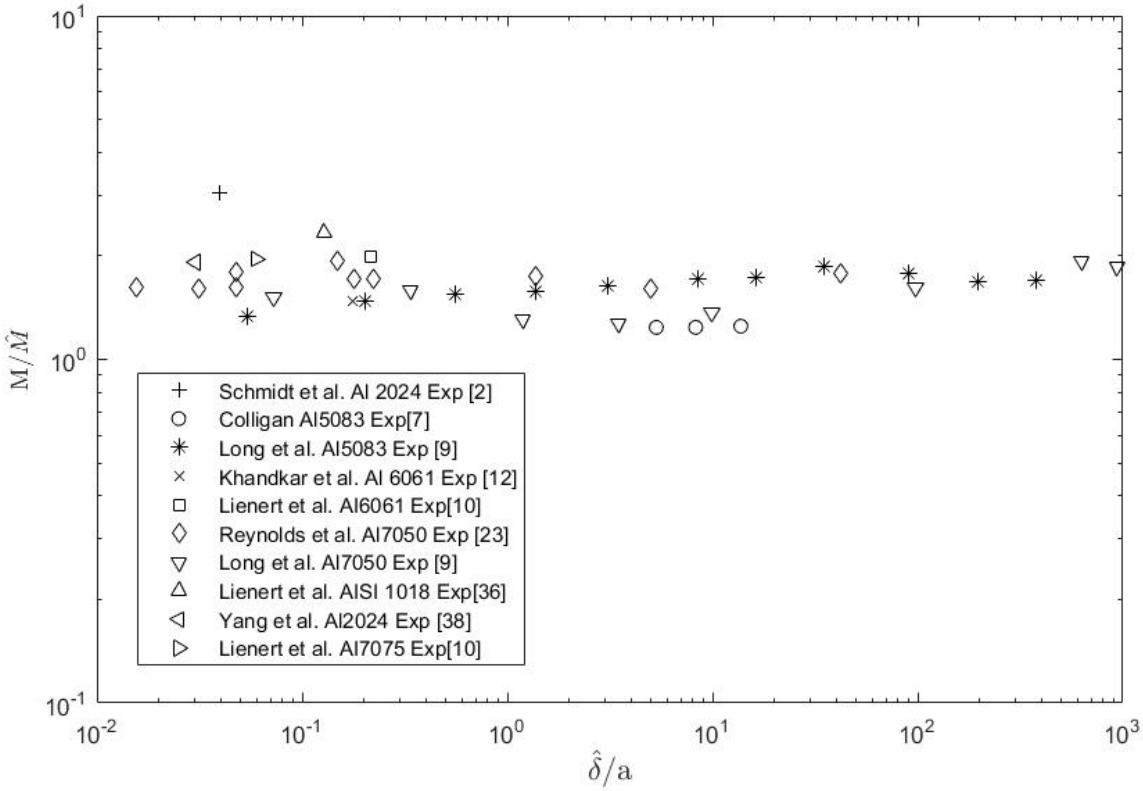

B

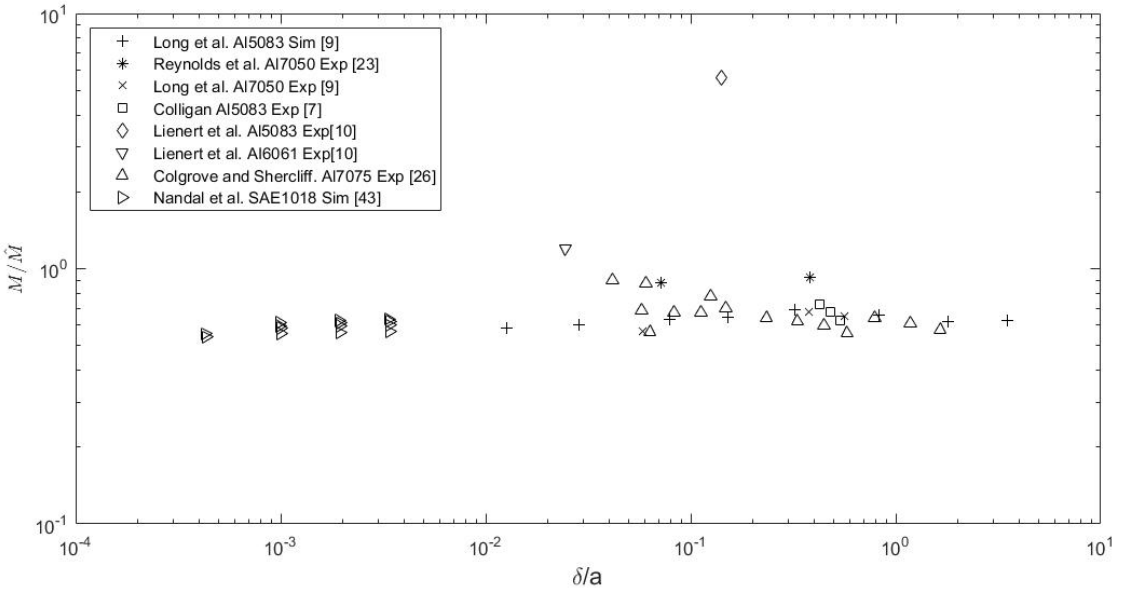

Figure 5.8: Comparison between the ratio of torque as a function of δ/a (Equation 2.2) without accounting for surface heat losses (Figure A) and accounting for surface heat losses (Figure B).

5.1.3. Estimation of shear layer thickness

The results for the graphs of $\delta/\widehat{\delta}$ usually presents few data (never more than 9 research publications), considering the higher difficulty that this measure implies (as explained in section 3.2.2). Figure 5.9 presents the ratio of the shear layer thickness as a function of simplification given by Equation 2.4. Figure 5.9.A satisfied the assumption because $(b-a)/\widehat{\delta}$ reached values of 100. Data presented in 5.9.B does fulfilled the assumption. Regarding the ratio $\delta/\widehat{\delta}$, it has a crescent slope between 0.1-4, with 4 experiments and 11 tests and between 0.3-1, with 7 experiments and 8 tests for Figure 5.9.A and B, respectively.

The Figure 5.10 presents the ratio of the shear layer thickness as a function of simplification given by Equation 2.1. In this case, both graphs satisfied completely the simplification, and the ratio $\delta/\widehat{\delta}$ remains between 0.6-4, with 4 experiments and 9 tests and between 0.2-1, with 6 experiments and 7 tests for Figure 5.10.A and B, respectively. Moreover Pe values in Figure 5.10 have values of $10^{-2} - 10^{-1}$ and $0.06 - 0.2$ for A and B respectively.

The Figure 5.11 presents the ratio of the shear layer thickness as a function of simplification given by Equation 2.3. Figure 5.11.A and B present a crescent slap as $v/\omega\widehat{\delta}$ increase, and their respective range $\delta/\widehat{\delta}$ is between 0.4-5, with 4 experiments and 12 tests and 0.2-110, with 9 experiments and 22 test. In addition Figure 5.11.A fulfilled the assumption, with the exception of 2 test of Atharifar et al. Al6061[18], and Figure 5.11.B doesn't follow through the assumption because the value of $v/\omega\widehat{\delta}$ for 14 tests are greater than one, reaching values of 100.

Finally the Figure 5.12 presents the ratio of the shear layer thickness as a function of simplification given by Equation 2.2. Both cases of A and B present a decreasing slope as $\widehat{\delta}/a$ increase. Once again as in Figure 5.4 and 5.12 the simplification is satisfied only by Figure 5.12.B with the exception of 2 test belonging to the experiment of Colegrove and Shercliff. Al 7075[26]. that are between 1 and 2. The ratio $\delta/\widehat{\delta}$ remains between 10^{-2}-10, with 7 experiments and 15 tests and between $0.2 - 10$, with 7 experiments and 8 tests for Figure 5.12.A and B, respectively.

A

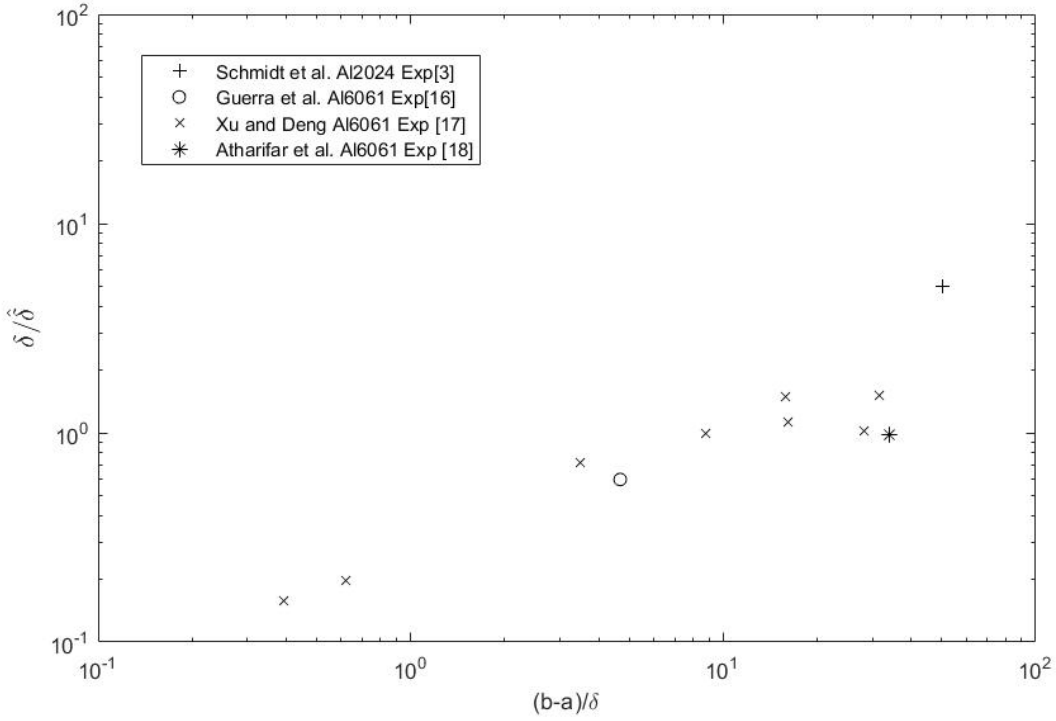

B

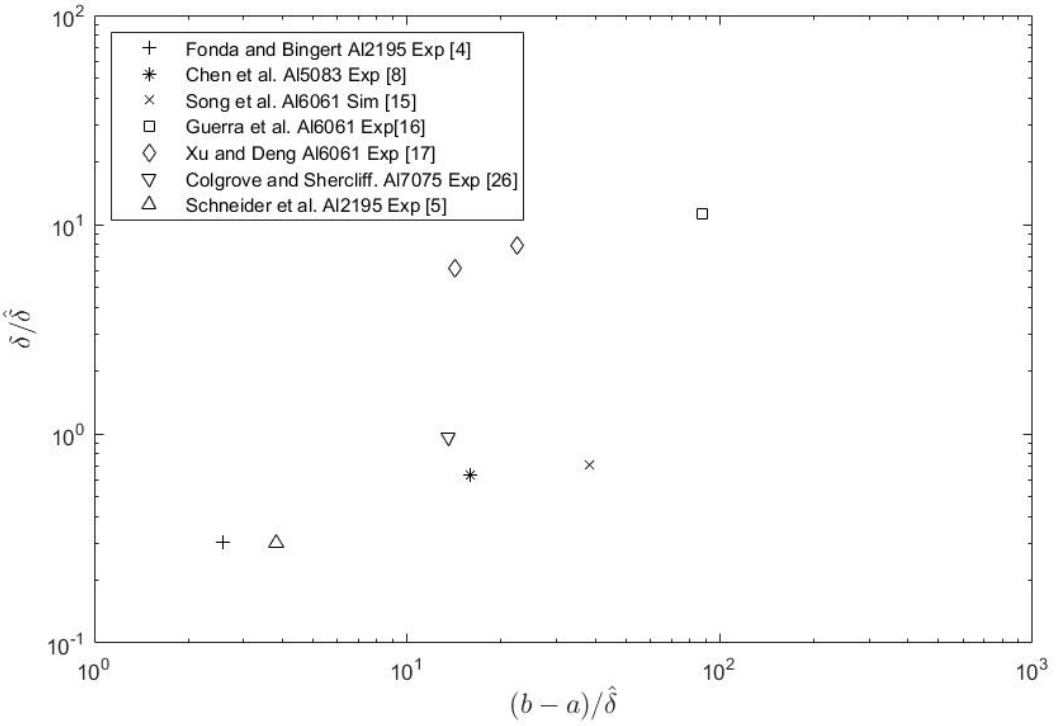

Figure 5.9: Comparison between the ratio of the shear layer thickness as a function of (b-a)/δ (Equation 2.4) without accounting for surface heat losses (Figure A) and accounting for surface heat losses (Figure B).

A

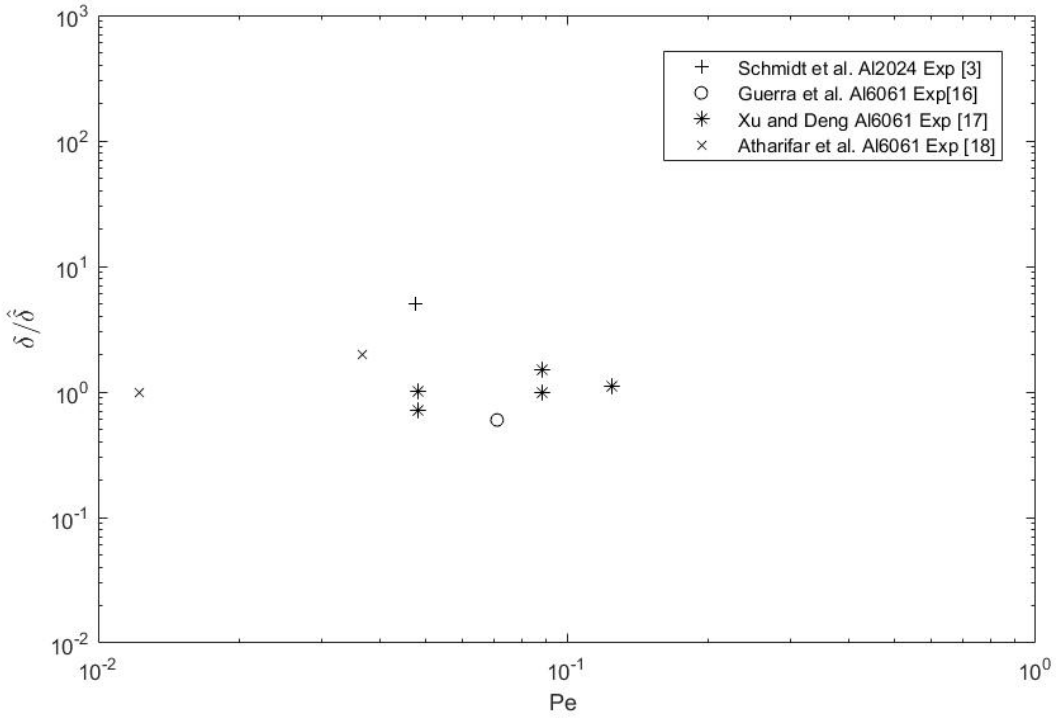

B

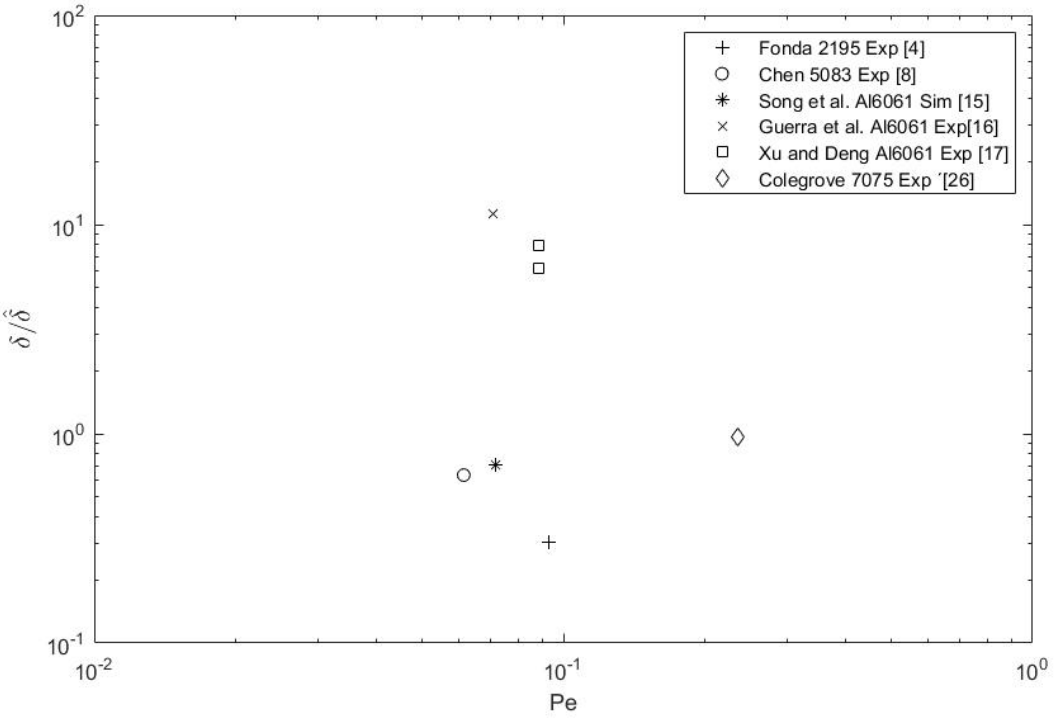

Figure 5.10: Comparison between the ratio of the shear layer thickness as a function of Pe (Equation2.1) without accounting for surface heat losses (Figure A) and accounting for surface heat losses (Figure B).

A

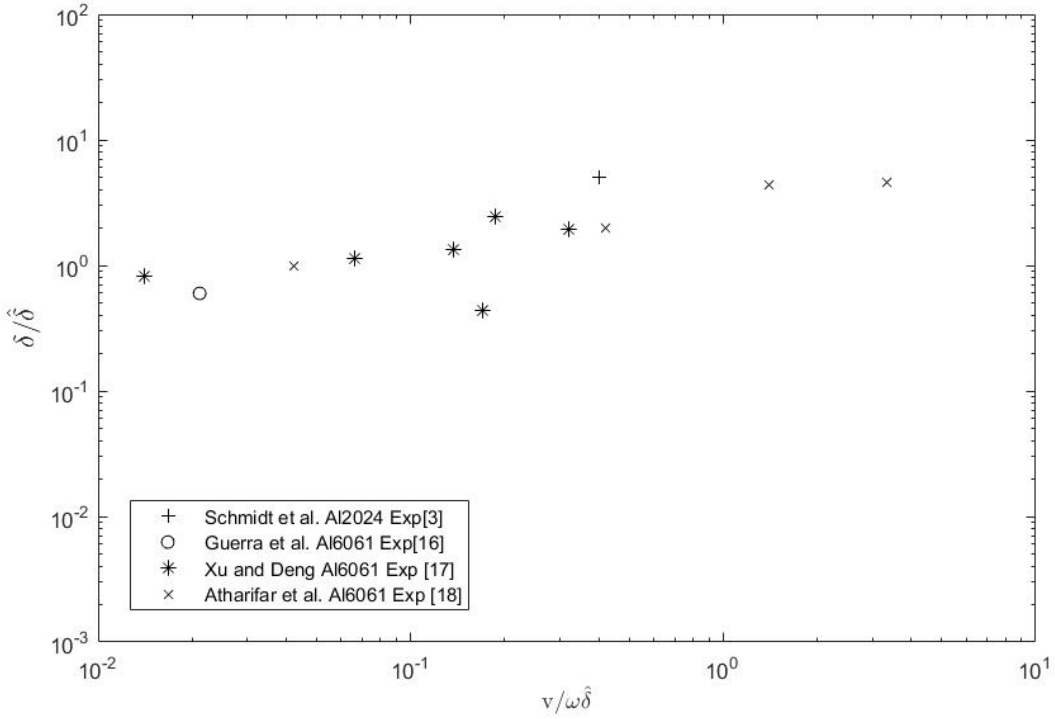

B

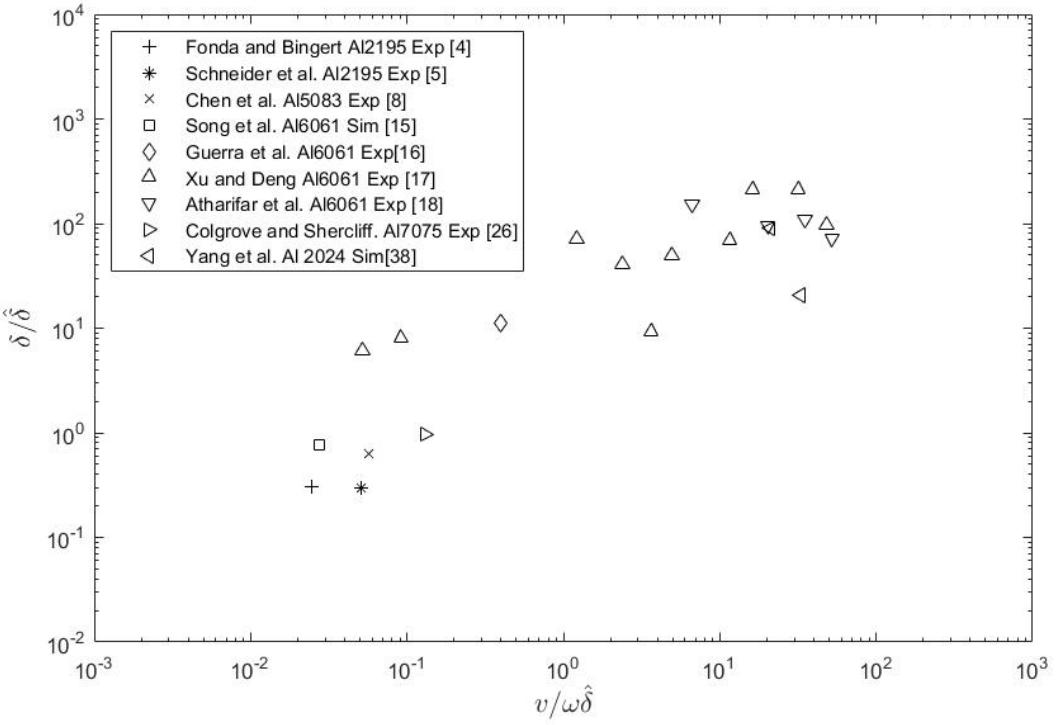

Figure 5.11: Comparison between the ratio of the shear layer thickness as a function of $V/\omega\delta$ (Equation 2.3) without accounting for surface heat losses (Figure A) and accounting for surface heat losses (Figure B).

A

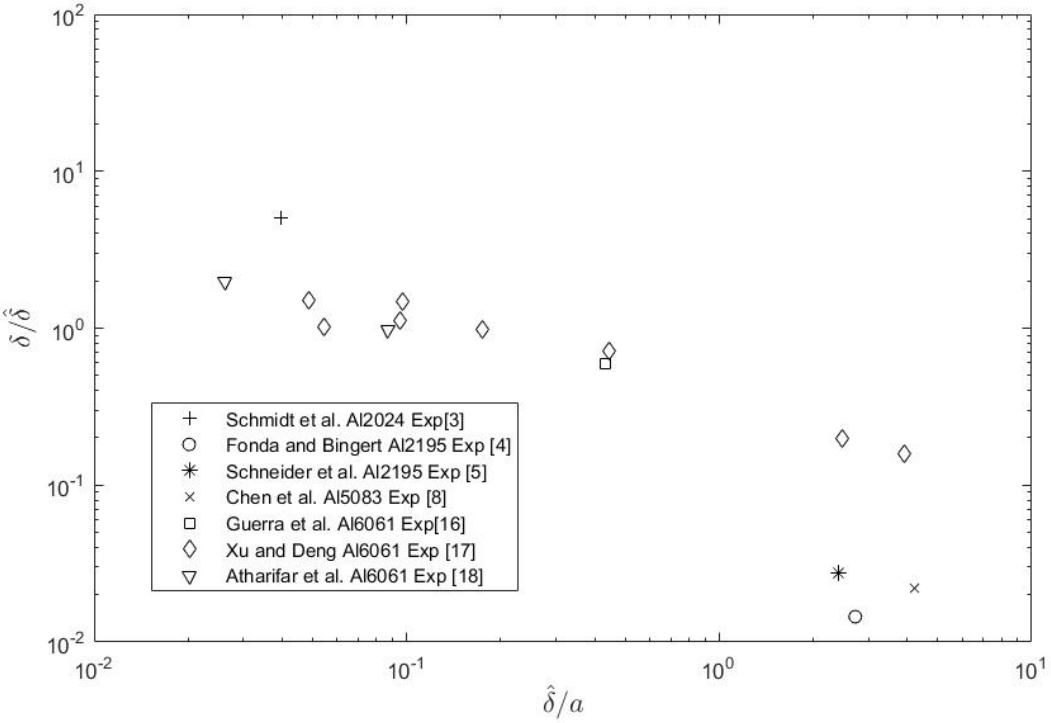

B

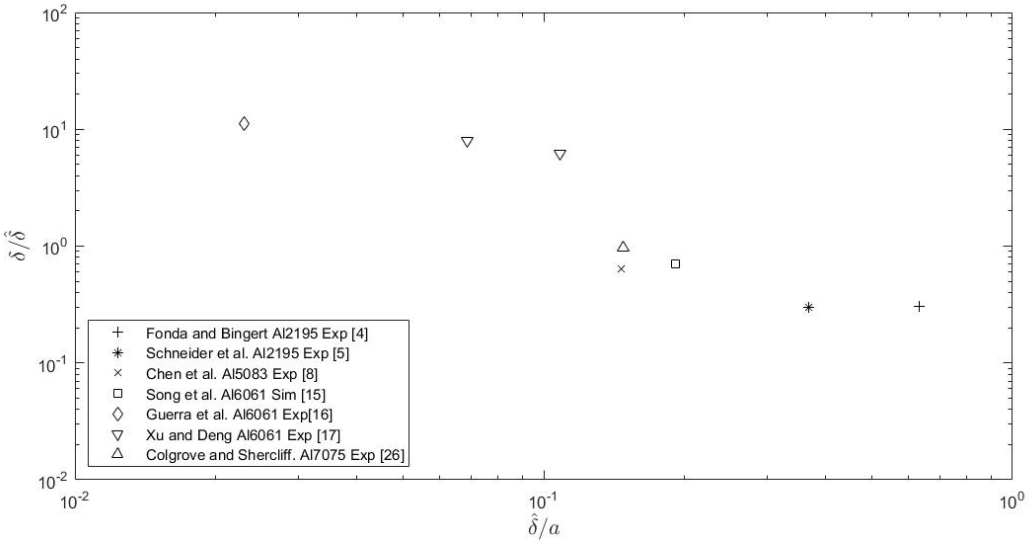

Figure 5.12: Comparison between the ratio of the shear layer thickness as a function of δ/a (Equation 2.2) without accounting for surface heat losses (Figure A) and accounting for surface heat losses (Figure B).

5.1.4. Correlation between the estimated and measured maximum temperature, torque and shear layer thickness

This section presents three graphs 5.13, 5.14, and 5.15, where the estimated and measured maximum temperature are compared, as well as the measured and estimated torque and shear layer thickness. This graphs should present a behaviour of X:Y = 1:1, which means that their values are similar, and therefore the proportion of their division is 1:1. In a contrary example if the curve of a graph is X:Y = 1:2 this means that the value of "Y" is two times the value of "X", which means that the estimated and measured values are not the same.

Figure 5.13 presents the correlation between $T_s - T$ and $\widehat{T_s} - T_\infty$ for the case where the model evaluate the Bessel function with the Peclet number (case A), and with ξ factor (case B). In both cases it can be see that there is a tendency to 1:1. Is also possible to observe that the material AISI 1018 have a different behaviour for figure A and B for being located between 900 and 1200, meanwhile the rest of the materials are located between 200 and 600 in the $T_s - T_\infty$ axis. The incorporation of the factor ξ allows more experiments to fulfill the assumptions because Figure 5.13.B count with 16 experiments, and 59 tests, and 5.13.A has 14 experiments and 31 tests.

Figure 5.14 present 12 and 16 experiments with 50 and 92 tests in Figures 5.14.A and B respectively. The two cases fall very close to the line 1:1, but Figure 5.14.A have one test of Lienert et al. Ti-6Al-4V[37], Reynolds et al.Al7050[23], Lienert et al. Al7075[10] and Scchmidt et al. Al2024[2] that escapes from the line 1:1. Figure 5.14.B also present data that doesn't follow the line 1:1 such as Lienert et al. Al5083, and Al7075[10]. Additionally both figures (A and B) are between 20 - 140 in the M axis, so none of them fulfilled the assumption.

In Figure 5.15 only the materials Al6061, Al2024, Al2195 and Al5083 could be included because there are no many experiments that actually measured the shear layer thickness. Therefore Figure 5.15.A has 7 experiments and 19 tests, where all of them follow the proportion 1:1 with the exception of 1 test from; Xu and Deng. Al6061[17], and the experiments of Chen et al.Al 5083[8], Schneider et al. Al2195[5] and Fonda and Bingert. Al2195[4]. From the data presented in Figure 5.15.B none of the experiments follow the proportion of 1:1 and presented 7 experiments and 8 test plotted. Additionally both of them fulfilled the assumption reaching values of 10^{-2}.

A

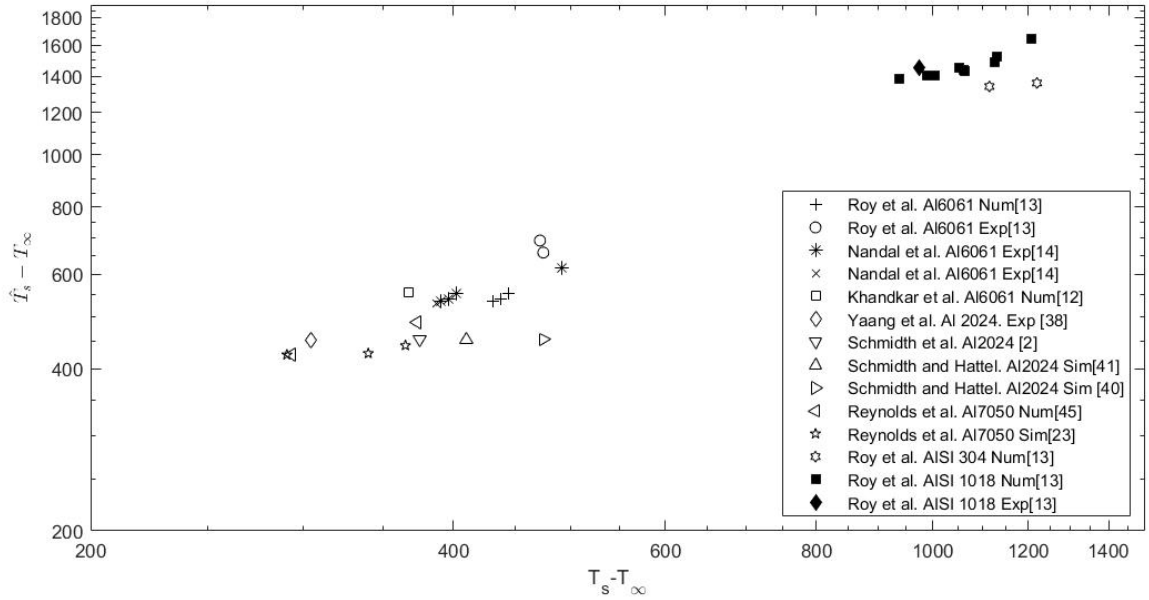

B

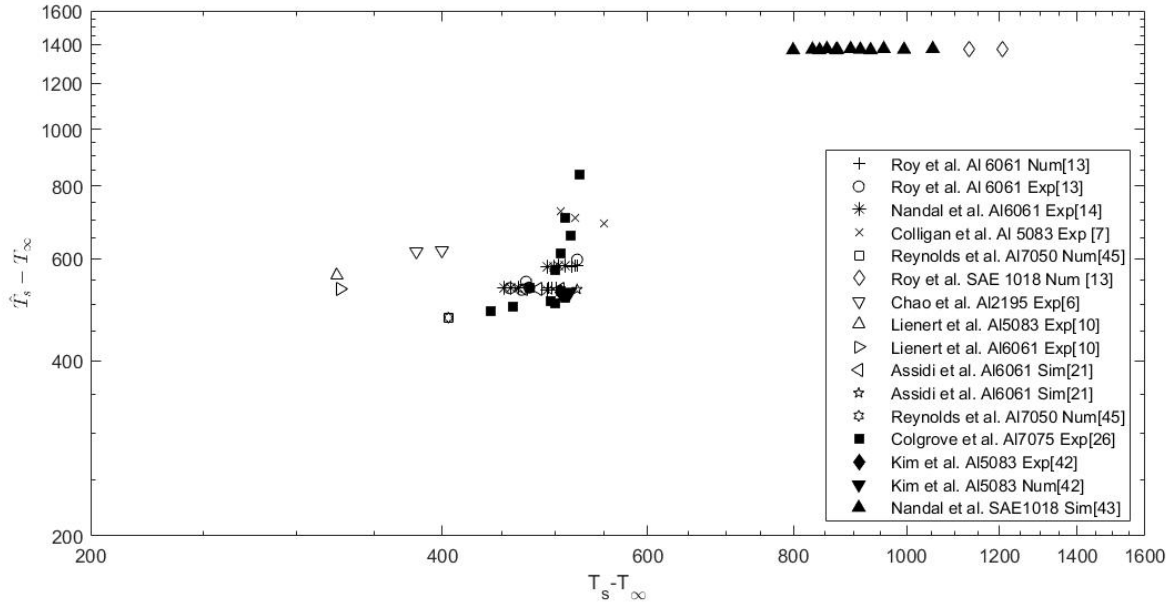

Figure 5.13: Comparison between the correlation between the maximum temperature reported in the literature ($T_s - T_\infty$) and the estimated maximum temperature ($\widehat{T_s} - T_\infty$) without accounting for surface heat losses (Figure A) and accounting for surface heat losses (Figure B).

A

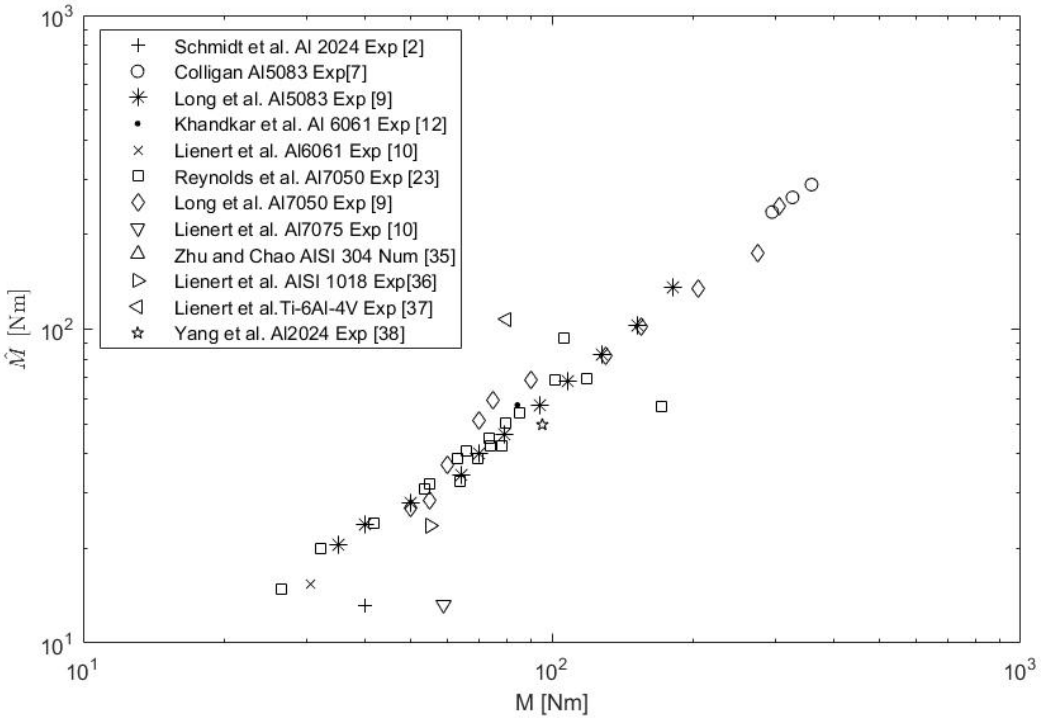

B

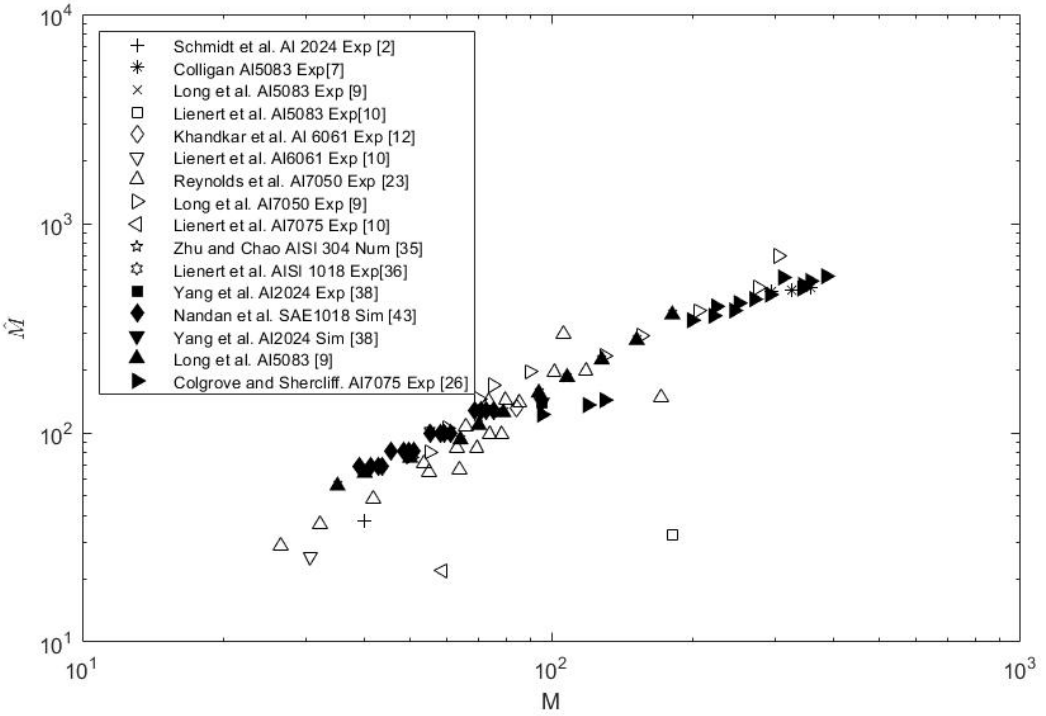

Figure 5.14: Comparison between the correlation between the torque reported in the literature (M) and the estimated torque($\widehat{M}$) without accounting for surface heat losses (Figure A) and accounting for surface heat losses (Figure B).

A

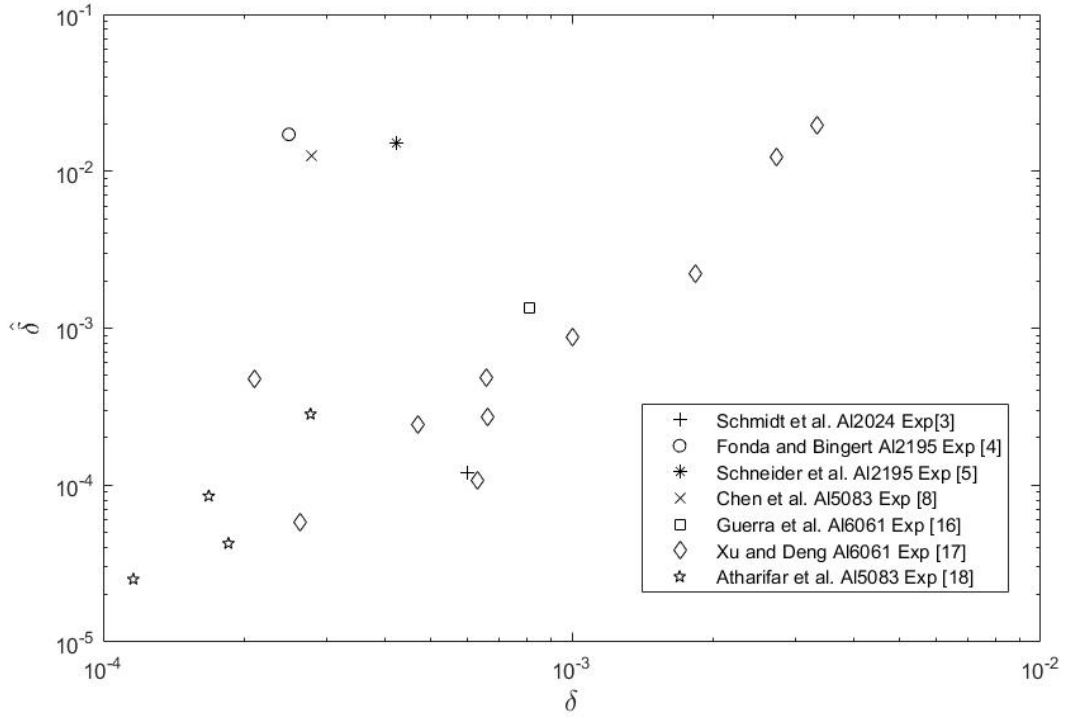

B

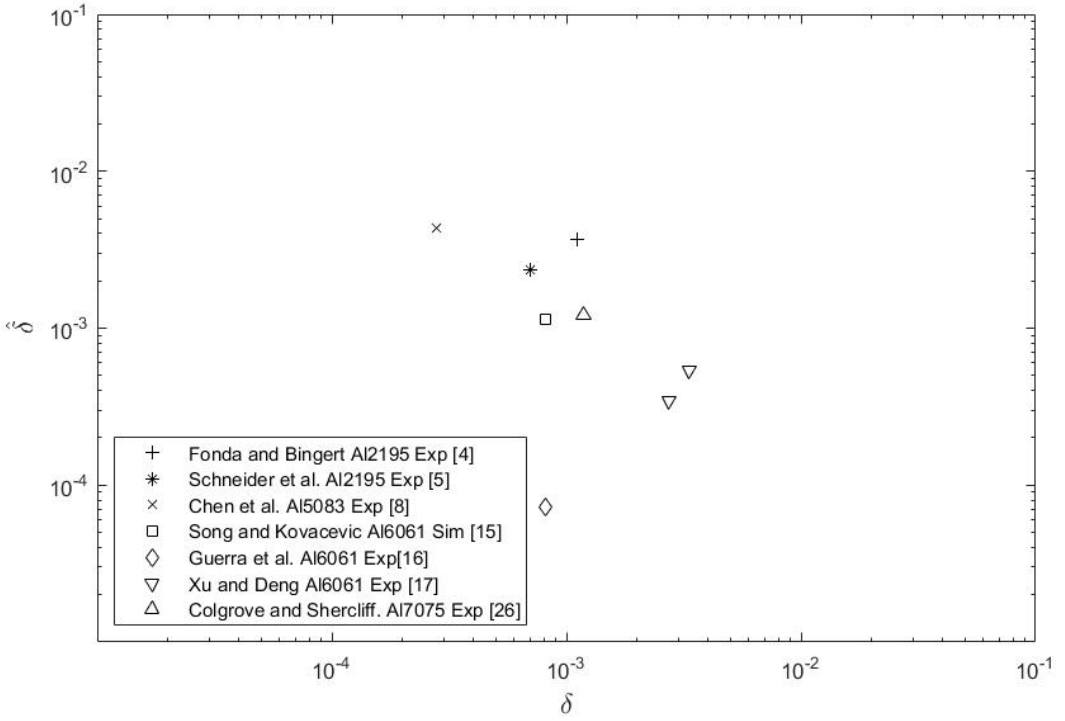

Figure 5.15: Comparison between the correlation between the shear layer thickness reported in the literature (δ) and the estimated shear layer thickness ($\widehat{\delta}$) without accounting for surface heat losses (Figure A) and accounting for surface heat losses (Figure B).

As a summary of which graphs satisfied or not the assumptions, the following Table (5.1) is presented:

Table 5.1: Fulfillment of the assumption in the Figures of the ratios of temperature, torque and shear layer and the four conditions.

Graph	Without accounting for surface heat losses	Accounting for surface heat losses
θ vs $(b-a)/\widehat{\delta}$	YES	YES
θ vs Pe	YES	YES
θ vs $v/\omega\widehat{\delta}$	NO	NO
θ vs $\widehat{\delta}/a$	NO	YES
$M/\widehat{M}$ vs $(b-a)/\widehat{\delta}$	YES	YES
$M/\widehat{M}$ vs Pe	YES	YES
$M/\widehat{M}$ vs $v/\omega\widehat{\delta}$	NO	NO
$M/\widehat{M}$ vs $\widehat{\delta}/a$	NO	YES
$\delta/\widehat{\delta}$ vs $(b-a)/\widehat{\delta}$	YES	YES
$\delta/\widehat{\delta}$ vs Pe	YES	YES
$\delta/\widehat{\delta}$ vs $v/\omega\widehat{\delta}$	YES	NO
$\delta/\widehat{\delta}$ vs $\widehat{\delta}/a$	NO	YES

5.1.5. Incorporation of the fifth assumption

For further analysis, one more assumption will be added corresponding to Equation 2.5. Figure 5.16 shows the correlation between θ and ϕ, where ϕ incorporate the preheat temperature of the shoulder with the following equation:

$$\phi = \frac{T_p - T_\infty}{\widehat{T_s} - T_\infty} \tag{5.4}$$

Equation 5.4 is calculated with the data base with the Bessel equation evaluated with the Peclet number (see table D.1) number and with the ξ factor (see table D.2) for their comparison. Their graphs are plotted it with θ, in this way Figure 5.16 is obtained.

In Figure 5.16.A, the experiments fulfilled the assumption with the exception of the experiment from Roy et al. AISI 304[13] that has a value 1.2 in the ϕ axis, and in Figure 5.16.B the data presented also satisfied the assumption with the exception of the experiment of Roy et al. Al 6061 Num[13], 4 test of the experiment Colgrove et al. Al7075[27] and 1 test of Roy et al. Al 6061 Exp[13], where all of them have a value of 1.2. In addition these results present a range of the ratio θ between 0.6-1.1, with 17 experiments and 39 tests and between 0.4-1, with 13 experiments and 51 tests for Figure 5.16.A and B, respectively. Another observation is that only Figure 5.16.B presents all of their values under one in the θ axis.

A

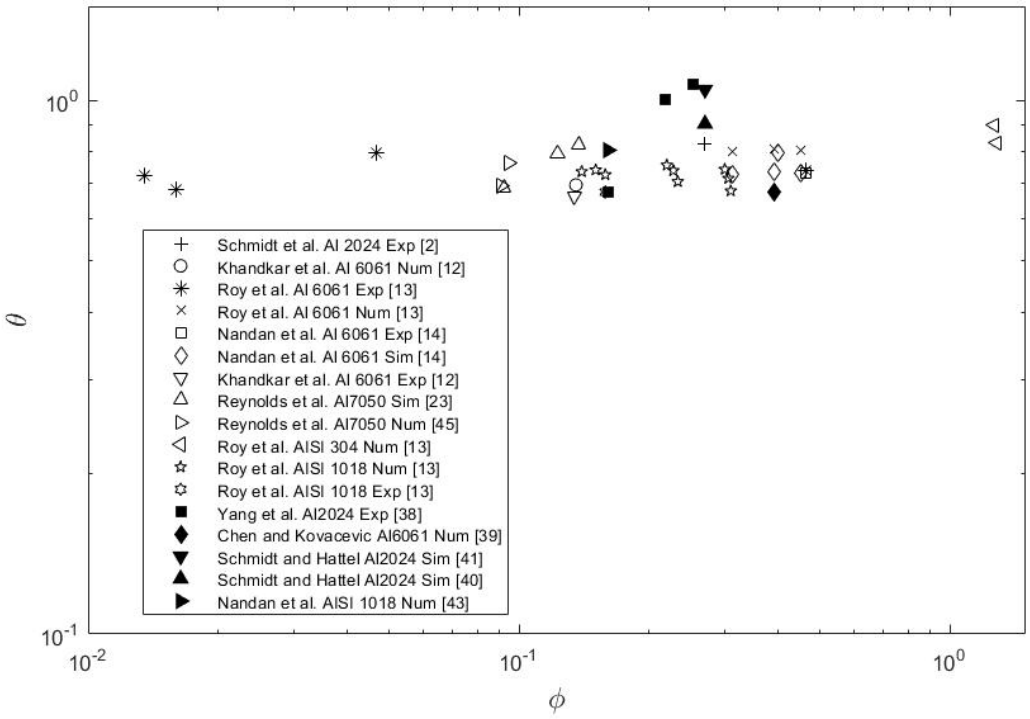

B

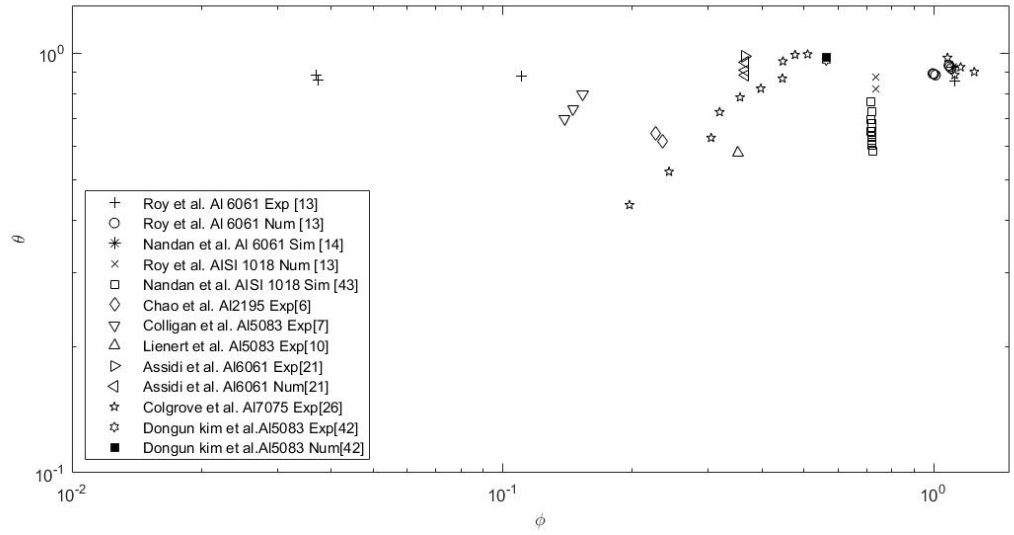

Figure 5.16: Comparison between the ratio of maximum temperature in the base plate θ against the hypothesis given by Equation. (2.5) without accounting for surface heat losses (Figure A) and accounting for surface heat losses (Figure B).

5.2. Error and Correction factors

All the previously plotted data is found in tables B.1, B.2, B.3, B.4, B.5, B.6, C.1, C.2, C.3, C.4, C.5, and C.6, where in addition, to calculate the percentage of error, the Equation 5.5 was used, and summarized in table 5.2.

$$\text{Error } \% = 100 \ln\left(\frac{\widehat{u}}{u}\right) \tag{5.5}$$

Table 5.2: Error calculated with Equation 5.5.

	θ %	M %	δ %
Accounting for surface heat losses	32.21	40.56	-308.67
Without accounting for surface heat losses	87.73	-62.97	74.86

The table 5.3 present the mean of the correction factor, which are calculated with the mean of the values that satisfied the assumptions of each graph, and for each case(Temperature, Torque and shear layer thickness) and it is represented by Equation 5.6.

$$u = \text{Correction factor } \widehat{u} \tag{5.6}$$

which, could also be written as:

$$\text{Correction factor} = \left|\frac{u}{\widehat{u}}\right| \tag{5.7}$$

Table 5.3: Correction factors of graphs presented in Chapter 5.

Correction Factor	Accounting for surface heat losses	Without accounting for surface heat losses
θ	.3215	.9706
$M/\widehat{M}$	.4771	.6356
$\delta/\widehat{\delta}$	2.64611	.6982

Chapter 6

Discussion

The main equations to calculate the shear stress, the shear layer thickness, the maximum temperature and the volumetric heat generation are given by Equations 2.33, 2.34, 2.35 and 2.36 respectively (see the system of scale equation in section 2.4.5). This equations that conform the mathematical model for the FSW process are independent of the material chosen, as it was proven with the material AISI 1018 and AISI 304, where the model was equally use for steels as it was for the aluminium materials. The solution proposed aim to capture the right order of magnitude and accurate trend of 1 in the "Y" axis, despite this, the comparison between the measured and estimated results that where established in Dr.Tello[1] thesis of maximum temperature, torque and shear layer thickness are incredibly close. Furthermore this new study aspire to get even closer results with the incorporation of the heat losses by the ξ factor (see Equation 4.5).

The estimation of maximum temperature is studied with θ (see Equation 5.1) which correspond to the ratio between the difference of the measured and estimated maximum temperature and the room temperature. Figures 5.1, 5.2, 5.3, 5.4, 5.13 and 5.16 compare the behaviour of maximum temperature considering, without accounting the heat losses, which in other words means that the Bessel function is evaluated in Pe (corresponding always to Figure A) and accounting the heat losses, by considering ξ (Figure B). In Figure 5.1.B is possible to see a greater proximity to one and also more aligned data than in 5.1.A, which, in other words means that the estimated values of the maximum temperature are closer to the measured ones. Beside this, to analyze the decrease or increase of the ratios, the Equation 6.1 helps to explain its conduct. Therefore the ratio of the temperature in Figure 5.1.B tends to decrease when $(b-a)/\delta$ is lower, which is expected because this is a result of a reduction in the shoulder's radius. This can be verified with the experiment of Colgrove with Al7075[26] (see Table A.1), which shows a variation on the preheated temperature, due to the shoulder's radius and this results in a lower measured maximum temperature than the calculated maximum temperature. Beside this observation, is also important to highlight the fact that the tests of the material AISI 1018 presented in Figure 5.1.B, unlike Figure 5.1.A, are located only at the right part of the graph, where the values of $(b-a)/\delta$ are higher, which is also expected because this materials are steel, meaning that their density is higher and therefore the shear layer thickness is lower due to the same reason of the viscous layer explained in section 2, to build the assumption represented in Equation 2.2, where due to the high viscosity of this material the resistance to deform is higher, resulting in a thinner shear layer and the temperature of the process is lower, giving as a result a lower measured

maximum temperature than the estimated maximum temperature.

$$\frac{X-W}{Y-W}\downarrow \Rightarrow X-W<Y-W \Rightarrow X\downarrow or Y\uparrow \tag{6.1}$$

In terms of proximity to one and data alignment, all the other graphs related to the maximum temperature shows more promising results considering the heat losses. In Figure 5.3, it can be observed that a higher number of experiments where added to Figure 5.3.B, due to the fact that the simplification of Equation 2.3 restricted more experiments than the other simplifications, because is more often bigger than one on account of a lower shear layer thickness estimation. Similar to graphs 5.1 and 5.2 it is possible to observe in Figure 5.3.B, that the experiments of steel are below one in the θ axes, which suggests the addition of a correction factor to the model for its improvement.

The impact of considering the heat losses to the model is clearly observed in the Figure 5.4, because the curve in Figure 5.4.A has a negative trend as δ/a increase, and with the incorporation of the ξ factor there is a much more constant tendency to one of the θ ratio in the vertical axis. Once again the experiment of Colgrove with Aluminium 7075[27] has a small decreasing behaviour, but now it happens when δ/a increase, which implies that when the difference between the shear layer thickness and the pin radius increase, the variation among the estimated and measured maximum temperature increases as well. Also, it is expected to observe the steel experiments in the left part of the graphs due to the thinner shear layer that this materials have.

In previous years, the mathematical model didn't contemplate the importance of the preheat temperature given by the shoulder, but now, with the addition of the ξ factor, it is clearly recognizable and proven by the Figure 5.16, where the ratio of the maximum temperature in Figure 5.16.A have almost a constant behaviour under one, which in other words means that the measure maximum temperature is lower than the estimated one, even if the preheat temperature increases. In contrast, Figure 5.16.B shows that if the preheat temperature increase this difference between the measured and estimated temperature decrease, and the increasing of the preheat temperature is given by a bigger shoulder radius, which is why in Figure 5.1.B the difference between the radius of the pin and shoulder increase the ratio of θ tending to one (without considering the steel materials). Meanwhile in Figure 5.1.A there is no variation.

Finally as discussion for the maximum temperature, Figure 5.13 compare the difference between the estimated (Y axes) and measured (X axis) maximum temperature and the room temperature. As it was expected, a 1:1 trend is present in both graphs, but the consideration of heat losses allows that more experiments fulfills the assumptions, and this add more distortion to the graph presented in Figure 5.13.B. Beside this, both of them have a similar behaviour in terms of the separation between the aluminium alloys and the steel ones, but in Figure 5.13.B there is a constant tendency for the steels, where when the measured maximum temperature increase the estimated one doesn't.

Regarding to the torque, Figures 5.5, 5.6, 5.7, 5.8, and 5.14, compare the ratio given in Equation 5.3 with the four simplifications and the behaviour of the torque ratio considering the Bessel function evaluated in Pe (corresponding always to Figure A) and with ξ (Figure B). In the first figure of torque (see fig 5.5), for both graphs there is no dependency of the torque and $(b-a)/\delta$, and both of them had a constant ratio in the vertical axis, but as it was mention before only in Figure 5.5.B the tendecy of the ratio is in all the graphs under one, and above one in the A cases of the Figures. This means that when the heat losses are incorporated the estimated torque is bigger than the measured one, and contrary when the Bessel equation is calculated with the Peclet number the measured torque is bigger than the estimated one. This is expected, due to the fact that the incorporation of the heat loss means a decrease of the temperature in the plate and therefor a highest force must be apply to deform the metal, increasing the torque applied by the tool. However it seems that heat loss is oversize, because is similarly far from one as it was before (when the Bessel function was calculated with the Peclet number). Is also important to outline that for Figure "b" of 5.5 the steel AISI 1018 is, once more, located at the right part of the graph, where $(b-a)/\delta$ is bigger due to the thinner shear layer thickness.

Figure 5.6 shows in both graphs a slight increasing tendency of the data as the Peclet number increase, which in another words means that when the velocity of translation increase the difference between the measured and estimated torque decrease. Is also important that in this case only in Figure "B" the assumption is satisfied, so it is a dependency between the Torque and the Peclet number. On the other hand there is no dependency of the torque and $V/\omega\delta$ in Figure 5.7, but the inclusion of the ξ factor allow the incorporation of more experiments, and there is a much more clear tendency, and alignment of the data near one. Moreover, is not excessive to outline that the steels from Figure "B" in this graph is next to the aluminium metals, the same happens with case "B" of Figure 5.3, where the steels are next to the aluminum, due to the fact that the velocity of translation is related to the rotational velocity, and therefor the relation is proportional to both metals.

Finally for the graph 5.14 the measured and estimated torque are compared, for the case where the ξ factor is added, there are more experiments that fulfill the assumption and therefore there is a little more of distortion than the case A, but the data follows more the line 1:1 than the case A, proving that the mathematical model is closer to the measured data.

Ultimately for the shear layer thickness the graphs 5.9, 5.10,5.11,5.12, and 5.15 compare measured and estimated shear layer is analyzed with the four restrictions. Due to the restrictions the amount of experiments involve for this study are lower than the previous graphs. All Figures in both cases have experiments that are above one, meaning that the measured shear layer is bigger than the estimated one. Figure 5.9 have a crescent behaviour for the case "a" so when the difference between the the radius of the pin shoulder increase the difference between the measured and estimated shear layer thickness decrease as well, and tends to one. A similar behaviour but less evident can be observed in Figure 5.9.B. This conduct is easily understandable by looking the Equation 6.1, because as the estimated shear layer decrease the ratio of $\delta/\widehat{\delta}$ increase and $(b-a)/\widehat{\delta}$ increase as well.

Figure 5.10 doesn't present a similar behaviour for its cases, Figure 5.10.A has a constant ratio of $\delta/\widehat{\delta}$ in the Y axis, indicating that there is no dependence between the shear layer and Pe. Meanwhile, for Figure 5.10.B the experiments of Chen 5083[8], Song et al. Al 6061 Sim[15], Fonda 2195 Exp[4] and Colgrove 7075 Exp[27] are near one (in the Y axis), but the experiments of Xu and Deng Al6061 Exp[17], Guerra et al. Al6061 Exp[16] are above one, indicating that the mathematical model didn't predict expected results in all the cases.

A better analyze can be made for graph 5.11, for both cases there is a crescent tendency, but more strong for Figure 5.11.B, so there is a dependency between $v/\omega\widehat{\delta}$ and the ratio of $\delta/\widehat{\delta}$. If the difference between the translation and rotational velocity increases the difference between the estimated and measured shear layer increase as well, having a lower estimated shear layer. A theory that could explain this might be that if the translation velocity decrease (making bigger the difference than it has with the rotational velocity) then the heat produced by the friction due to the pin, is bigger than the estimated. This is directly connected to the ξ factor because by including the heat loss through the plate then the heat involved in the process is lower and therefore the shear layer is also thinner.

Finally. regarding the analysis of the figures, for graph 5.12 both of the cases presents a decreasing behaviour in the ratio of $\delta/\widehat{\delta}$ as $\widehat{\delta}/a$ increase, once again this is expected by Equation 6.1, because if $\widehat{\delta}$ increase, the $\delta/\widehat{\delta}$ will decrease and $\widehat{\delta}/a$ will decrease as well. Figure 5.15 present the measured and estimated δ, effectively in Figure 5.12.A the data follow the line 1:1, meanwhile in Figure 5.12.B there is no similar behaviour, due to the few data.

Lastly, respecting the error, there are mainly three kind of errors:

1. Experimental: errors that occurs during the experimental trials, or during test measurements that lead to the disruption of the data.

2. Material properties: the properties of the material where measured as well, and during this study they are taken from the literature, and a lot of expression or constants used in this model comes from the properties, such as ΔT_m or B (from the Zenner Hollomon constants). Beside this, the Rosenthal's solution[44] assumes constant materials properties, which is not true because some of them changes with the variation of the T°.

3. Mathematical simplification: errors are also related to the mathematical simplifications. An example of this is the heat loss through the plate or the process efficiency that where assumed as constant to all of the experiments and they should vary. This also lead to a percentage of error.

4. Physical assumptions: to build this model, several physical assumption were made, such as assuming that the translation velocity of the tool is infinitely slow compared to the rotational one, or to assure that the shear layer thickness is extremely lower than the pin radius, because this varies depending on the kind of material. Is also important to highlight that in the measurement of the shear layer is well done, due to the fact that is still not clear if the shear layer belongs to the heat affected zone or the thermomechanically affected zone, so this could lead to the error in the shear layer study.

The error comparing the results of the estimated and measured data for the maximum temperature, torque and shear layer thickness of all the data are presented in tables B.1, B.2, B.3, B.4, B.5, B.6, C.1, C.2, C.3, C.4, C.5, and C.6. They are summarized in Table 5.2. However a better idea of the difference between this model and the previous one is obtain by looking Table 5.3 where is possible to observed the variation between the correction factors of both graphs, in other words with and without considering the heat losses. In Table 5.2 the minus sign means that the average of data is under one, or conversely, if it is positive the average is above one. Observing the Torque case is possible to verify that when the heat losses are considered, the trend of the data are above one, as it was already explained before. Analyzing Table 5.3, is possible to see that each rate have the mean of every graph, where in the θ graphs the correction factor considering ξ is 0.32, meanwhile without considering the heat loss the correction factor is 0.97, in other words the correction factor is 0.65 less considering the heat losses. The second case, accounting the heat losses the average of the correction factor is 0.47, and 0.63 for the previous case, so is possible to ensure is lower considering ξ. Finally the last case of δ the correction factor is lower for the case without accounting the heat losses by 0.99.

Finally analyzing table 5.2 the error is effectively lower in the cases of θ and Torque by 55.52% and 22.41% respectively for the cases that considered ξ, meanwhile the δ case is lower by 233.81% for the case that doesn't consider the heat losses, but as it was mention is important to consider that this case has lower data than the others. Is also crucial to emphasize that the average of the correction factors multiplied by 100 is similar to the error results, which is expected because the correction factor is the average of the difference between the trend of the data and one, which could be also understood as the error.

Chapter 7

Conclusions

The couple behaviour of heat and plastic deformation involved in the friction stir welding has been modeled for two cases; the previous model, where the Bessel function was calculated from the Peclet number(without considering the heat losses), and the actual model that incorporates the heat loss through convection and conduction from the bottom and top of the plate by the ξ factor, and calculate the Bessel function with this new factor. Both models generate closed-form expressions for the maximum temperature(Equation 2.35), torque(Equation 2.37), shear layer thickness(Equation 2.34) and volumetric heat generation(Equation 2.36). All the equations that conformed the model are based in known process parameters without the need of any measured data for its application.

The incorporation of the ξ factor was valid and necessary as it was shown in Figure 4.1 due to the fact that λ was always bigger than one, proving that the heat loss given by ξ matters as much, or more than the heat loss by thermal diffusivity, and therefor the study was made comparing the previous result without accounting the heat losses and the actual model, which does include it.

Literature data was used to study the truthfulness of the models, and compare them to view the influence of the addition of ξ. The error presented by both cases where presented in Appendix "B" and "C", and the difference between the error of the ratios of temperature, torque, and shear layer thickness was presented in Table 5.2 having a 55.52% and 22.41% less error accounting the heat losses for temperature and Torque, respectively. There is also more proximity with one in the torque for the actual model and a worst difference in the shear layer thickness for the this model, as well, as 233.81% of more error. Nevertheless the analysis made for the graphs, shows important behaviour changes, especially for Figure 5.4, so it's important to see the conducts of the graphics too, because as it was mention, the data selected due to their compliance with the assumptions changes with the addition of ξ.

In respect of the graphs as it was summarized in Table 5.1, all of the figures that are plotted versus $(b-a)/\widehat{\delta}$ satisfied the assumptions, and, those that were plotted versus Peclet, always satisfied the assumptions too, those who were plotted versus $v/\omega\widehat{\delta}$ didn't accomplish the assumptions for θ and $M/\widehat{M}$, but did achieve the assumption for the Pe case in $\delta/\widehat{\delta}$, but only in the ξ cases the assumptions were accomplish for the graphs that were plotted against $\widehat{\delta}/a$, which as it was discuss is directly related to the improvement of the Figure 5.4.

Ultimately the FSW process is very important to the development of welding techniques for the joining of advance materials, such as aluminium alloys because allows to work and build different technologies with unwelldable materials being of great interest for areas such as aerospace and transportation. So its mathematical development matters to improve this process and applied to more manufacturing areas.

7.1. Future work

From this research, it is consider that a lot of progress was achieved, nevertheless more analysis needs to be done to continue improving this mathematical model, between them there are:

- Realization of more experiments where the temperature, torque and shear layer are measured.
- Research of more papers and literature experiments to enlarge the data.
- Add more materials to the investigation, to verify that the model works for several metals.

Bibliography

[1] Karem E.Tello,"*Coupled Model Of Heat Transfer and Plastic Deformation for Friction Stir Welding Using Scaling Analysis*", Master thesis, University of Alberta, 2009.

[2] H. Schmidt, J. Hattel and J. Wert,"An analytical model for the heat generation in friction stir welding" *Modelling and Simulation in materials Science and Engineering*, 12:143-157, 2003

[3] H.N.B. Schmidt , T.L. Dickerson, J.H. Hattel, "Material Flow in butt friction stir welds in AA2024-T3". Acta Materialia, 54(4):1199-1209, 2006.

[4] R.W. Fondaa and J.F. Bingert,"Texture variations in an aluminum friction stir weld"Scripta Materialia,57(11):1052-1055,2007.

[5] Judy Schneider, Ronald Beshears, Arthur C. Nunes Jr., "Interfacial sticking and slipping in the friction stir welding process" Materials Science and Engineering A, 435-436:297-304, 2006.

[6] Yuh J. Chao, X. Qi and W. Tang,"Heat Transfer in Friction Stir Welding — Experimental and Numerical Studies" Journal of Manufacturing Science and Engineering, 125(1):8, 2003.

[7] Kevin J. Colligan, "Relationships between process variables related to heat generation in friction stir welding of aluminum" Friction Stir Welding Processing IV, 4:39-54, 2007.

[8] Z.W. Chen, T. Pasang, Y. Qi, "Shear flow and formation of Nugget zone during friction stir welding of aluminium alloy 5083-O". Materials Science and Engineering A,474(1-2):312-316, 2008.

[9] T. Long, W. Tang and A. P. Reynolds, "Process response parameter relationships in aluminium alloy friction stir welds" Sciece and Technology of Welding and Joining, 12(4):311-317, 2007.

[10] T.J. Lienert, W.L. Stellwag and H. Shao , "Determination of Load, Torque, and Tool Temperatures During FSW of Aluminum Alloys", 2000.

[11] R.S. Mishra, Z.Y. Ma. *Friction stir welding and processing*Materials Science and Engineering, 50:1–2 (2005).

[12] Khandkar, M. Z. H., Khan, J. A., and Reynolds, A. P., "Prediction of temperature distribution and thermal history during friction stir welding: Input torque based model" Science and Technology of Welding and Joining, 8(3):165-174, 2003. 1362-1718.

[13] G.G. Roy, R. Nandan, T. DebRoy, "Dimensionless Correlation to estimate Peak Temperature During FSW" Science and Technology of Welding and Joining, 11:606-608, 2006.

[14] R. Nandan, G.G. Roy, T. DebRoy , "Numerical simulation of 3D Heat Transfer and

Plastic Flow During friction stir Welding" Metallurgical and Materials Transactions A, 37A(4):1247-1259, 2006.

[15] M. Song and R. Kovacevic, "Thermal Modeling of FSW in a moving coordinate system and its validation" International Journal of Machine Tool and Manufacture, 43:605-615, 2003.

[16] M. Guerra, C. Schmidt, J.C. McClure, L.E. Murr, A.C. Nunes, "Flow patterns during friction stir welding". Materials Characterization, 49:95-101, 2003.

[17] Shaowen Xu and Xiaomin Deng, "A study of texture patterns in friction stir welds" Acta Materialia, 2008.

[18] H. Atharifar, D. C. Lin, and R. Kovacevic , "Studying Tunnel-like Defect in Friction Stir Welding Process Using Computational Fluid Dynamics". Numerical, Mathematical, and Physical Modelling Tools for Materials Processes II, pages 375-391, 2007.

[19] Wanchuck Woo, Levente Balogh, Tamás Ungár, Hahn Choo, Zhili Feng, "Grain structure and dislocation density measurements in a friction-stir welded aluminum alloy using X-ray peak profile analysis" Materials Science and Engineering A, 498(1-2):308-313, 2008.

[20] Patricio F. Mendez, Karem E. Tello, and Thomas J. Lienert,"Scaling of coupled heat transfer and plastic deformation around the pin in friction stir welding",Acta Materialia, vol. 58, no. 18, pp. 6012–6026, 2010.

[21] Assidi, Mohamed, Fourment, Lionel, Guerdoux, Simon, Nelson, Tracy, "Friction models for friction stir welding process simulation: calibrations from welding experiments" International Journal of Machine Tools and anufacture, 50(2):143-155, 2010.

[22] ASM Handbook Volume 01: Properties and Selection: Irons, Steels, and High-Performance Alloys. ASM International, 10th edition, 1990.

[23] A.P. Reynolds, Z. Khandkar, T. Long, W. Tang and J. Khan, "Utility of relatively simple models for understanding process parameter effects of FSW". Thermec'2003, 426-4(1):2959-2964, 2003.

[24] P. Ulysse, "Three-dimensional modeling of the friction stir-welding process. International Journal of Machine Tools and Manufacture"International Journal of Machine Tools and Manufacture, 42(14):1549-1557, 2002.

[25] ASM Handbook Volume 02: Properties and Selection: Nonferrous Alloys and Special-Purpose Materials. ASM International, 10th edition, 1990.

[26] P.A. Colgrove and H.R. Shercliff, "Experimetal and Numerical analysis of Al 7075-T7351 FSW". Science and Technology of Welding and Joining, 8(5):360-368, 2003.

[27] P.A. Colgrove and H.R. Shercliff, "Development of a Trivex FSW tool Part 2 - 3D flow modeling".Science and Technology of Welding and Joining, 9(4):352-361, 2004.

[28] G. Buffa, L. Fratini, R. Shivpuri, "CDRX modelling in friction stir welding of AA7075-T6 aluminum alloy: Analytical approaches" Journal of Mteroals Processing Technology, 191(1-3):356-359, 2007.

[29] T. J. Lienert, W. E. Stellwag, and H. Shao. "Determination of load, torque, and tool temperatures during friction stir welding of aluminum alloys". Summary report sr0019, EWI, 2000.

[30] X. K. Zhu and Y. J. Chao. "Numerical simulation of transient temperature and residual stresses in friction stir welding of 304L stainless steel. Journal Of Materials Processing Technology", 146(2):263–272, 2004. 0924-0136.

[31] T. J. Lienert, Jr. W. L. Stell, B. B. Grimmett, and R. W. Warke. "Friction stir welding studies on mild steel". Welding Journal, pages 1–9, January 2003.

[32] C. Sellars and W. M. Tegart, "Hot workability," International Metallurgical Reviews, p. 17:1–23, 1972.

[33] K. E. Tello1, A. P. Gerlich and P. F. Mendez,"Constants for hot deformation constitutive models for recent experimental data", Science and Technology of Welding Joining 15(3), 2010.

[34] R. Nandan, G. G. Roy, T. J. Lienert T. DebRoy , "Numerical modelling of 3D plastic flow and heat transfer during friction stir welding of stainless steel" Science and Technology of Welding and Joining, 11(5):526-537, 2006.

[35] X.K. Zhu, Y.J. Chao , "Numerical Simulation of Transient Temperature and Residual Stresses in Friction Stir Welding of 304L Stainless Steel" Journal of Materials Processing Technology, 146(2):263-272, 2004.

[36] T.J. Lienert, W.L. Stellwag, Jr., B.B. Grimmet and R. W. Warke, "Friction Stir Welding Studies on Mild Steel". Welding Journal Supplement, 82(1):1-s -9-s, 2003.

[37] T.J. Lienert, W.L. Stellwag, Jr. and L.R. Lehman , "Process Results for FSW of Ti-6Al-4V". Welding Journal, pages 1-9, January 2003.

[38] Bangcheng Yang, Junhui Yan, Michael A. Sutton, Anthony P. Reynolds , "Banded microstructure in AA2024-T351 and AA2524-T351 aluminum friction stir welds". Materials Science and Engineering A364, 364:55-65, 2004.

[39] C.M. Chen, R. Kovacevic, "Finite element modeling of friction stir welding—thermal and thermomechanical analysis" International Journal of Machine Tools and Manufacture, 43:1319-1326, 2003.

[40] H. Schmidt and J. Hattel , "A local model for the thermomechanical conditions in friction stir welding". Modelling and Simulation In Materials Science and Engineering. 13(1):77-93, 2005.

[41] H. Schmidt J. Hattel , "Modelling heat flow around tool probe in friction stir welding". Science and Technology of Welding and Joining, 10(2):176-186, 2005.

[42] Dongun Kim, Harsha Badarinarayan, Ji Hoon Kim, Chongmin Kim, Kazutaka Okamoto, R.H. Wagoner, Kwansoo Chung , "Numerical simulation of friction stir butt welding process for AA5083-H18 sheets". European Journal of Machine, A/solids, 29(2):204-2015. 2010.

[43] R. Nandan, G.G. Roy, T.J. Lienert, T. Debroy , "Three-dimensional heat and material flow during friction stir welding of mild steel". Acta Materialia, 55(3):883-895, 2007.

[44] D. Rosenthal. "The theory of moving sources of heat and its application to metal treatments. Transactions of the A.S.M.E.", pages 849–866, 1946.

[45] A.P Reynolds, W. Tang, Z. Khandkar, J.A Khan and K.Linder, "Relationship between weld parammeters, hardness distribution and temperature history in alloy 7050 friction stir welding". Science and Technology of Welding and Joining, 10(2):190-199, 2005.

[46] A.P. Reynolds, W. Tang, Z. Khandkar, J.A. Khan and K. Lindner, "Relationship between weld parameters, hadrness distribution and temperature history in alloy 7050 FSW".

[47] T. U. Seidel and A. P. Reynolds. "Two-dimensional friction stir welding process model based on fluid mechanics." Science And Technology Of Welding And Joining, 8(3):175–183, 2003. 1362-1718.

[48] S. Xu, X. Deng, A. P. Reynolds, and T. U. Seidel. "Finite element simulation of material flow in friction stir welding." Science And Technology Of Welding And Joining, 6(3):191–193, 2001. 1362-1718.

[49] G. A. Buck and M. Langerman. "Non-Dimensional Characterization of the friction stir/spot welding process using a simple couette flow model Part I: Constant property Bingham Plastic solution." In S. Ghosh, J. C. Castro, and J. K. Lee, editors, American Institute of Physics Conference Series, volume 712 of American Institute of Physics Conference Series, pages 1283–1288, June 2004.

[50] O. Frigaard, O. Grong, and O. T. Midling. "A process model for friction stir welding of age hardening aluminum alloys." Metallurgical And Materials Transactions A-Physical Metallurgy And Materials Science, 32(5):1189–1200, 2001. 1073-5623.

[51] J. C. McClure, W. Tang, L. E. Murr, X. Guo, Z. Feng, and J. E. Gould. "A thermal model of friction stir welding." In Trends in Welding Research, pages 590–595, Pine Mountain, GA, 1998.

[52] J. C. McClure, W. Tang, L. E. Murr, X. Guo, Z. Feng, and J. E. Gould. A thermal model of friction stir welding. In Trends in Welding Research, pages 590–595, Pine Mountain, GA, 1998.

[53] A. Simar, J. Lecomte-Beckers, T. Pardoen B. de Meester. Effect of boundary conditions and heat source distribution on temperature distribution in friction stir welding. Science and Technology of Welding and Joining, 2006

Annexes

Annexed A

Measured of pin and shoulder for Colgrove Al7075

Table A.1: Measured of pin and shoulder for Colgrove and Shercliff experiment with Al7075

Author	Material	Specification	Pin radious[m]	Shoulder radious[m]
P.A. Colgrove and H.R. Shercliff	Aluminum	AA7075	0.00825	0.02475
P.A. Colgrove and H.R. Shercliff	Aluminum	AA7075	0.00825	0.02475
P.A. Colgrove and H.R. Shercliff	Aluminum	AA7075	0.00825	0.02475
P.A. Colgrove and H.R. Shercliff	Aluminum	AA7075	0.00825	0.02475
P.A. Colgrove and H.R. Shercliff	Aluminum	AA7075	0.00825	0.02475
P.A. Colgrove and H.R. Shercliff	Aluminum	AA7075	0.00825	0.02475
P.A. Colgrove and H.R. Shercliff	Aluminum	AA7075	0.00825	0.02475
P.A. Colgrove and H.R. Shercliff	Aluminum	AA7075	0.00825	0.02475
P.A. Colgrove and H.R. Shercliff	Aluminum	AA7075	0.00825	0.02475
P.A. Colgrove and H.R. Shercliff	Aluminum	AA7075	0.00825	0.02475
P.A. Colgrove and H.R. Shercliff	Aluminum	AA7075	0.00825	0.02475
P.A. Colgrove and H.R. Shercliff	Aluminum	AA7075	0.00825	0.02475
P.A. Colgrove and H.R. Shercliff	Aluminum	AA7075	0.00635	0.01905
P.A. Colgrove and H.R. Shercliff	Aluminum	AA7075	0.00635	0.01905
P.A. Colgrove and H.R. Shercliff	Aluminum	AA7075	0.00635	0.01905
P.A. Colgrove and H.R. Shercliff	Aluminum	AA7075	0.00635	0.01905
P.A. Colgrove and H.R. Shercliff	Aluminum	AA7075	0.00635	0.01905

Annexed B

Summary of data compiled from literature without accounting for surface heat losses

Table B.1: Error for the maximum temperature without accounting for surface heat losses

Error for the maximum temperature without accounting for surface heat losses part 1						
Author	Material	Especification	T_s	$\widehat{T_s}$	θ	Error %
H. Schmidt	Aluminum	AA2024	673	751.682826	0.826569	19.04
Yuh J. Chao	Aluminum	AA2195	698	1143.640385	0.473014	74.86
Yuh J. Chao	Aluminum	AA2195	678	1078.530501	0.486848	71.98
Kevin J. Colligan	Aluminum	AA5083	803	3529.102925	0.156293	185.60
Kevin J. Colligan	Aluminum	AA5083	818	2635.204837	0.222488	150.28
Kevin J. Colligan	Aluminum	AA5083	848	2099.142582	0.305362	118.62
T.J. Lienert	Aluminum	AA5083	623	1151.793309	0.380654	96.58
Khandkar	Aluminum	AA6061	683	852.7807656	0.693968	36.53
G.G. Roy	Aluminum	AA6061	820	2136.80958	0.283879	125.92
G.G. Roy	Aluminum	AA6061	770	991.0178371	0.681079	38.40
G.G. Roy	Aluminum	AA6061	773	956.1628661	0.721706	32.61
G.G. Roy	Aluminum	AA6061	766	883.5484475	0.799251	22.40
G.G. Roy	Aluminum	AA6061	755	918.1388765	0.736932	30.52
G.G. Roy	Aluminum	AA6061	742	851.4415587	0.802253	22.033
G.G. Roy	Aluminum	AA6061	736	837.9996242	0.811112	20.93
G.G. Roy	Aluminum	AA6061	729	832.6936946	0.806069	21.55
G.G. Roy	Aluminum	AA6061	791	1012.755246	0.689747	37.14
G.G. Roy	Aluminum	AA6061	795	1118.98875	0.605368	50.19
G.G. Roy	Aluminum	AA6061	799	1388.118564	0.459583	77.74
G.G. Roy	Aluminum	AA6061	820	4083.796381	0.137884	198.13
G.G. Roy	Aluminum	AA6061	818	2530.370545	0.232936	145.69
G.G. Roy	Aluminum	AA6061	814	1917.187379	0.318678	114.35

Table B.2: Error for the maximum temperature without accounting for surface heat losses

Error for the maximum temperature without accounting for surface heat losses part 2						
Author	Material	Especification	T_s	$\widehat{T_s}$	θ	Error %
R. Nandan	Aluminum	AA6061	790	1836.645738	0.319762	114.36
R. Nandan	Aluminum	AA6061	745	1072.498374	0.577148	54.97
R. Nandan	Aluminum	AA6061	685	828.5538994	0.729426	31.55
R. Nandan	Aluminum	AA6061	790	914.6946203	0.797802	22.59
R. Nandan	Aluminum	AA6061	700.2	851.4415587	0.726725	31.92
R. Nandan	Aluminum	AA6061	694.4	837.9996242	0.734075	30.91
R. Nandan	Aluminum	AA6061	688.2	832.6936946	0.729764	31.50
R. Nandan	Aluminum	AA6061	762.7	1388.118564	0.426284	85.26
R. Nandan	Aluminum	AA6061	756	1118.98875	0.557864	58.36
R. Nandan	Aluminum	AA6061	749.6	1012.755246	0.631825	45.91
R. Nandan	Aluminum	AA6061	807.4	4083.796381	0.134556	200.58
R. Nandan	Aluminum	AA6061	801.5	2530.370545	0.225545	148.92
R. Nandan	Aluminum	AA6061	797.3	1917.187379	0.308365	117.65
Khandkar	Aluminum	AA6061	665	853.4303833	0.660749	41.44
T.J. Lienert	Aluminum	AA6061	625	843.4707016	0.599482	51.17
Assidi	Aluminum	AA6061	820	864.7436851	0.921051	8.22
Assidi	Aluminum	AA6061	768	864.7436851	0.829299	18.71
Assidi	Aluminum	AA6061	781	864.7436851	0.852237	15.98
Assidi	Aluminum	AA6061	803	864.7436851	0.891055	11.53
A.P. Reynolds	Aluminum	AA7050	506	721.7697721	0.490833	71.16
A.P. Reynolds	Aluminum	AA7050	589	723.0274252	0.684662	37.88
A.P. Reynolds	Aluminum	AA7050	638	725.4918577	0.795337	22.89
A.P. Reynolds	Aluminum	AA7050	663	740.2395645	0.825345	19.19
A.P. Reynolds	Aluminum	AA7050	592	723.1305859	0.691552	36.88
A.P. Reynolds	Aluminum	AA7050	671	786.3973526	0.763722	26.95
A.P. Reynolds	Aluminum	AA7050	661	1250.725153	0.381012	96.49
A.P. Reynolds	Aluminum	AA7050	703	4368.3757	0.099499	230.76
P. Ulysse	Aluminum	AA7050	533	17618.62716	0.013568	430
P. Ulysse	Aluminum	AA7050	493	1506.598324	0.161344	182.42
P. Ulysse	Aluminum	AA7050	483	6286.136975	0.030894	347.71
P. Ulysse	Aluminum	AA7050	498	3718.173448	0.058477	283.91
P. Ulysse	Aluminum	AA7050	478	839.5057975	0.332406	110.13
P. Ulysse	Aluminum	AA7050	578	381114.7128	0.000735	721.52
P.A. Colgrove	Aluminum	AA7075	803	39087.26396	0.013019	434.13
P.A. Colgrove	Aluminum	AA7075	813	15169.61511	0.03463	336.3
P.A. Colgrove	Aluminum	AA7075	823	6838.414922	0.08027	252.23
P.A. Colgrove	Aluminum	AA7075	808	20281.52918	0.025521	366.82
P.A. Colgrove	Aluminum	AA7075	813	8423.461105	0.063381	275.85
P.A. Colgrove	Aluminum	AA7075	803	4328.656613	0.12529	207.71
P.A. Colgrove	Aluminum	AA7075	798	2497.147314	0.227361	148.12
P.A. Colgrove	Aluminum	AA7075	803	2952.532469	0.190241	165.94
P.A. Colgrove	Aluminum	AA7075	808	1886.317317	0.321095	113.6
P.A. Colgrove	Aluminum	AA7075	798	1370.754552	0.46609	76.33
P.A. Colgrove	Aluminum	AA7075	773	2633.29226	0.203401	159.25
P.A. Colgrove	Aluminum	AA7075	793	3791.733153	0.141682	195.41
P.A. Colgrove	Aluminum	AA7075	758	2027.537395	0.265967	132.43
P.A. Colgrove	Aluminum	AA7075	738	1339.394753	0.42251	86.15
P.A. Colgrove	Aluminum	AA7075	773	792.0688534	0.961404	3.93
R. Nandan, G	Steel	304SS	604	767.5736225	0.651655	158.27
X.K. Zhu, Y.J. Chao	Steel	304SS	570	1622.240263	0.205401	33.75
G.G. Roy	Steel	304SS	1243	1622.38162	0.713541	15.7
G.G. Roy	Steel	304SS	1430	1622.470219	0.854681	18.46
G.G. Roy	Steel	304SS	1412	1637.851642	0.831435	10.88
G.G. Roy	Steel	304SS	1518	1658.18472	0.896937	26.64
G.G. Roy	Steel	304SS	1316	1626.784249	0.766114	26.86
G.G. Roy	Steel	304SS	1313	1625.78618	0.76443	20.49

Table B.3: Error for the maximum temperature without accounting for surface heat losses

Error for the maximum temperature without accounting for surface heat losses part 3						
Author	Material	Especification	T_s	$\widehat{T_s}$	θ	Error %
G.G. Roy	Steel	304SS	1385	1632.195005	0.814723	33.96
G.G. Roy	Steel	304SS	1241	1622.297826	0.712075	38.31
G.G. Roy	Steel	304SS	1200	1621.051686	0.681757	32.39
G.G. Roy	Steel	304SS	1256	1622.4349	0.723327	26.7
G.G. Roy	Steel	SAE1018	1314	1624.976151	0.765651	30.02
G.G. Roy	Steel	SAE1018	1428	1823.641127	0.740672	30.77
G.G. Roy	Steel	SAE1018	1506	1941.285284	0.735113	32.09
G.G. Roy	Steel	SAE1018	1349	1746.638941	0.725509	35.07
G.G. Roy	Steel	SAE1018	1286	1701.05904	0.704176	39.08
G.G. Roy	Steel	SAE1018	1236	1684.510828	0.676518	30.31
G.G. Roy	Steel	SAE1018	1359	1734.665813	0.738516	33.66
G.G. Roy	Steel	SAE1018	1301	1702.362488	0.714203	27.97
G.G. Roy	Steel	SAE1018	1423	1786.010336	0.756043	39.59
G.G. Roy	Steel	SAE1018	1361	1729.636306	0.742507	27.09
T.J. Lienert	Titanium	Ti-6Al-4V	[43]	1715.19572	0.596248	51.71
Bangcheng Yang	Aluminum	AA2024	1143	754.5073135	1.073367	-7.08
Bangcheng Yang	Aluminum	AA2024	788	762.0490733	1.002049	-0.2
Bangcheng Yang	Aluminum	AA2024	763	750.4073298	0.674171	39.43
C.M. Chen	Aluminum	AA6061	603	826.524307	0.671682	39.8
C.M. Chen	Aluminum	AA6061	653	824.2560726	0.8855	12.16
H. Schmidt	Aluminum	AA2024	764	751.682826	1.046987	-4.59
H. Schmidt	Aluminum	AA2024	773	751.6828903	0.903715	10.12
Dongun Kim	Aluminum	AA5083	708	946.3714135	0.771163	25.99
Dongun Kim	Aluminum	AA5083	798	946.3714135	0.771163	25.99
Dongun Kim	Aluminum	AA5083	798	843.5144861	0.797412	22.64
Dongun Kim	Aluminum	AA5083	733	843.5144861	0.810244	21.04
Dongun Kim	Aluminum	AA5083	740	1386.667222	0.46387	76.82
Dongun Kim	Aluminum	AA5083	803	1386.667222	0.473055	74.85
R. Nandan	Steel	SAE1018	813	1742.65753	0.806419	21.52
R. Nandan	Steel	SAE1018	1463	1919.426797	0.537798	62.03
R. Nandan	Steel	SAE1018	1170	1811.861202	0.554608	58.95
R. Nandan	Steel	SAE1018	1137.6	1773.058429	0.548385	60.08
R. Nandan	Steel	SAE1018	1106.9	1751.193999	0.52505	64.43
R. Nandan	Steel	SAE1018	1061	2251.995954	0.476562	74.12
R. Nandan	Steel	SAE1018	1229.2	2003.406487	0.510142	67.31
R. Nandan	Steel	SAE1018	1168	1913.731339	0.521188	65.16
R. Nandan	Steel	SAE1018	1140.1	1863.201549	0.510605	67.22
R. Nandan	Steel	SAE1018	1097.2	2810.135117	0.395958	92.64
R. Nandan	Steel	SAE1018	1292.7	2324.870227	0.450201	79.81
R. Nandan	Steel	SAE1018	1210.5	2149.817754	0.470889	75.31
R. Nandan	Steel	SAE1018	1170	2051.179895	0.473597	74.74
R. Nandan	Steel	SAE1018	1128.3	3662.861704	0.312821	116.21
R. Nandan	Steel	SAE1018	1350.6	2816.003435	0.379626	96.86
R. Nandan	Steel	SAE1018	1253.9	2510.511246	0.404608	90.48
R. Nandan	Steel	SAE1018	1193.2	2338.373743	0.418698	87.06
A.P. Reynolds	Aluminum	AA7050	1152.3	723.2560326	0.691348	36.91
A.P. Reynolds	Aluminum	AA7050	592	786.3973526	0.763722	26.96
A.P. Reynolds	Aluminum	AA7050	671	1233.608761	0.387983	94.68
A.P. Reynolds	Aluminum	AA7050	661	4368.3757	0.099499	230.76

Table B.4: Error for the torque without accounting for surface heat losses.

Error for the torque without accounting for surface heat losses part 1					
Author	Material	Especification	M	$\widehat{M}$	Error %
H. Schmidt	Aluminum	AA2024	40	13.13074285	-111.39
Kevin J. Colligan	Aluminum	AA5083	295	236.0963535	-22.27
Kevin J. Colligan	Aluminum	AA5083	326	262.9264972	-21.50
Kevin J. Colligan	Aluminum	AA5083	358	288.8122443	-21.48
T. Long	Aluminum	AA5083	181	135.7943064	-28.74
T. Long	Aluminum	AA5083	152	102.4705502	-39.43
T. Long	Aluminum	AA5083	128	82.68663209	-43.7
T. Long	Aluminum	AA5083	108	68.17428442	-46.01
T. Long	Aluminum	AA5083	94	57.39759341	-49.33
T. Long	Aluminum	AA5083	79	46.26786615	-53.5
T. Long	Aluminum	AA5083	70	40.24746911	-55.34
T. Long	Aluminum	AA5083	64	34.2971246	-62.38
T. Long	Aluminum	AA5083	50	28.0246639	-57.89
T. Long	Aluminum	AA5083	40	23.75917451	-52.09
T. Long	Aluminum	AA5083	35	20.64610591	-52.78
T.J. Lienert	Aluminum	AA5083	181	19.25829063	-224.06
Khandkar	Aluminum	AA6061	84.4	57.33559068	-38.66
T.J. Lienert	Aluminum	AA6061	30.62	17.89613664	-53.71
A.P. Reynolds	Aluminum	AA7050	73.46273863	45.13327081	-48.72
A.P. Reynolds	Aluminum	AA7050	118.4408879	69.62584674	-53.13
A.P. Reynolds	Aluminum	AA7050	171.5561491	56.51784759	-111.04
A.P. Reynolds	Aluminum	AA7050	78.37008922	42.6318552	-60.88
A.P. Reynolds	Aluminum	AA7050	69.27153671	38.54286616	-58.63
A.P. Reynolds	Aluminum	AA7050	63.71057417	32.88969428	-66.12
A.P. Reynolds	Aluminum	AA7050	26.5153383	14.84364264	-58.02
A.P. Reynolds	Aluminum	AA7050	79.88050498	50.29811407	-46.26
A.P. Reynolds	Aluminum	AA7050	65.78226736	40.91040851	-47.5
A.P. Reynolds	Aluminum	AA7050	53.47648869	31.07148775	-54.3
A.P. Reynolds	Aluminum	AA7050	41.77850679	24.00336754	-55.42
A.P. Reynolds	Aluminum	AA7050	32.08569944	20.04585281	-47.04
A.P. Reynolds	Aluminum	AA7050	106.0661574	93.31372169	-12.81
A.P. Reynolds	Aluminum	AA7050	101.3537555	68.77385854	-38.71
A.P. Reynolds	Aluminum	AA7050	85.56303957	53.87265706	-46.26
A.P. Reynolds	Aluminum	AA7050	73.81569813	42.35446999	-55.55
A.P. Reynolds	Aluminum	AA7050	62.80619328	38.54286616	-48.83
A.P. Reynolds	Aluminum	AA7050	54.81374197	32.00468919	-53.81
T. Long	Aluminum	AA7050	305	246.5230003	-21.29
T. Long	Aluminum	AA7050	275	174.0162355	-45.76
T. Long	Aluminum	AA7050	205	134.4670911	-42.17
T. Long	Aluminum	AA7050	155	102.0095174	-41.84
T. Long	Aluminum	AA7050	130	82.17433344	-45.87
T. Long	Aluminum	AA7050	90	68.79711637	-26.86
T. Long	Aluminum	AA7050	75	59.16552008	-23.71
T. Long	Aluminum	AA7050	70	51.00475869	-31.66
T. Long	Aluminum	AA7050	60	36.97845005	-48.4
T. Long	Aluminum	AA7050	55	28.44496158	-65.94
T. Long	Aluminum	AA7050	50	26.89341822	-62.01
P.A. Colgrove	Aluminum	AA7075	199.2071804	175.5688697	-12.63
P.A. Colgrove	Aluminum	AA7075	221.3413116	207.0936243	-6.65

Table B.5: Error for the torque without accounting for surface heat losses.

Error for the torque without accounting for surface heat losses part 2					
Author	Material	Especification	M	$\widehat{M}$	Error %
P.A. Colgrove	Aluminum	AA7075	245.0564521	239.580694	-2.26
P.A. Colgrove	Aluminum	AA7075	224.4084698	191.2078986	-16.01
P.A. Colgrove	Aluminum	AA7075	250.4724322	223.9033233	-11.21
P.A. Colgrove	Aluminum	AA7075	270.5634033	254.742882	-6.03
P.A. Colgrove	Aluminum	AA7075	292.2084755	287.6783146	-1.56
P.A. Colgrove	Aluminum	AA7075	342.2142352	269.7777044	-23.78
P.A. Colgrove	Aluminum	AA7075	343.7746771	301.9093452	-12.99
P.A. Colgrove	Aluminum	AA7075	356.2755744	334.8195276	-6.21
P.A. Colgrove	Aluminum	AA7075	384.8149494	373.2152747	-3.06
P.A. Colgrove	Aluminum	AA7075	311.4754379	287.5290217	-8.00
P.A. Colgrove	Aluminum	AA7075	95.49714498	70.5091999	-30.34
P.A. Colgrove	Aluminum	AA7075	119.4267993	73.45661491	-48.6
P.A. Colgrove	Aluminum	AA7075	129.7056234	83.85053327	-43.62
T.J. Lienert	Aluminum	AA7075	56.02253997	51.3752888	-67.24
X.K. Zhu, Y.J. Chao	Aluminum	AA7075	42.7808487	51.3752888	-8.66
X.K. Zhu, Y.J. Chao	Steel	304SS	55	23.6121351	18.31
T.J. Lienert	Steel	304SS	80	107.4114654	-84.56
T.J. Lienert	Steel	SAE1018	68.8	12.59955318	29.46
R. Nandan	Titanium	Ti-6Al-4V	70.9	15.96054075	-169.75
R. Nandan	Steel	SAE1018	72.6	18.21812038	-149.12
R. Nandan	Steel	SAE1018	75.5	20.08710187	-138.25
R. Nandan	Steel	SAE1018	55.2	9.799652471	-132.41
R. Nandan	Steel	SAE1018	58	12.41375391	-172.86
R. Nandan	Steel	SAE1018	59.2	14.16964918	-154.16
R. Nandan	Steel	SAE1018	61.1	15.62330145	-142.98
R. Nandan	Steel	SAE1018	45.6	8.017897476	-136.37
R. Nandan	Steel	SAE1018	48.4	10.15670775	-173.82
R. Nandan	Steel	SAE1018	49.8	11.59334933	-156.14
R. Nandan	Steel	SAE1018	51	12.78270119	-145.76
R. Nandan	Steel	SAE1018	38.9	6.784374788	-138.37
R. Nandan	Steel	SAE1018	41.3	8.594137325	-174.64
R. Nandan	Steel	SAE1018	42.8	9.809757127	-156.98
R. Nandan	Steel	SAE1018	43.7	10.81613177	-147.32

Table B.6: Error for the shear layer thickness with the Bessel function evaluated with the Peclet number

Error for the shear layer thickness without accounting for surface heat losses.					
Author	Material	Especification	δ	$\widehat{\delta}$	Error %
H.N.B. Schmidt	Aluminum	AA2024	0.0006	0.000119421	-161.43
R.W. Fondaa	Aluminum	AA2195	0.000249	0.017170354	423.34
Judy Schneider	Aluminum	AA2195	0.000423	0.015237132	358.41
Z.W. Chen	Aluminum	AA5083	0.000278	0.012653728	381.80
M. Song	Aluminum	AA6061	0.000811	0.049977277	412.10
M. Guerra	Aluminum	AA6061	0.000811	0.001355779	51.38
Shaowen Xu	Aluminum	AA6061	0.000278	0.000271772	-2.26
Shaowen Xu	Aluminum	AA6061	0.000121	0.000107446	-11.88
Shaowen Xu	Aluminum	AA6061	0.000263	5.85528E-05	-150.22
Shaowen Xu	Aluminum	AA6061	0.000369	0.000243514	-41.56
Shaowen Xu	Aluminum	AA6061	0.000723	0.000485424	-39.83
Shaowen Xu	Aluminum	AA6061	0.001598	0.002217316	32.75
Shaowen Xu	Aluminum	AA6061	0.000865	0.000876624	1.33
Shaowen Xu	Aluminum	AA6061	0.000535	0.000477716	-11.32
Shaowen Xu	Aluminum	AA6061	0.002441	0.012417087	162.66
Shaowen Xu	Aluminum	AA6061	0.003102	0.019581762	184.25
H. Atharifar	Aluminum	AA6061	0.000277	0.000283147	2.19
H. Atharifar	Aluminum	AA6061	0.000168	8.51365E-05	-67.97
H. Atharifar	Aluminum	AA6061	0.000185	4.24821E-05	-147.12
H. Atharifar	Aluminum	AA6061	0.000116	2.51242E-05	-152.97
P.A. Colgrove	Aluminum	AA7075	0.00118	0.07485765	415.00
Bangcheng Yang	Aluminum	AA2024	0.000075	0.000168198	80.76
Bangcheng Yang	Aluminum	AA2024	0.000375	0.000384268	2.44

Annexed C

Summary of data compiled from literature accounting for surface heat losses

Table C.1: Error for the maximum temperature accounting for surface heat losses.

Error for maximum temperature accounting for surface heat losses part 1						
Author	Material	Especification	T_s	$\widehat{T_s}$	θ	Error %
H. Schmidt,	Aluminum	AA2024	673	746.992744	0.835203	18.00
Yuh J. Chao	Aluminum	AA2195	698	918.6521939	0.644483	43.93
Yuh J. Chao	Aluminum	AA2195	678	913.8002355	0.617083	48.27
Kevin J. Colligan	Aluminum	AA5083	803	1020.935241	0.698541	35.87
Kevin J. Colligan	Aluminum	AA5083	818	1004.089031	0.736451	30.59
Kevin J. Colligan	Aluminum	AA5083	848	986.4396864	0.798908	22.45
T.J. Lienert	Aluminum	AA5083	623	860.6480341	0.577626	54.88
Khandkar	Aluminum	AA6061	683	825.13499	0.730363	31.42
G.G. Roy	Aluminum	AA6061	820	895.4539354	0.873708	13.50
G.G. Roy	Aluminum	AA6061	770	845.3190343	0.862386	14.80
G.G. Roy	Aluminum	AA6061	773	832.7076115	0.888336	11.84
G.G. Roy	Aluminum	AA6061	766	828.087891	0.882872	12.45
G.G. Roy	Aluminum	AA6061	755	831.4919039	0.85662	15.47
G.G. Roy	Aluminum	AA6061	742	823.7334243	0.844534	16.89
G.G. Roy	Aluminum	AA6061	736	823.7266781	0.833133	18.25
G.G. Roy	Aluminum	AA6061	729	823.715743	0.819835	19.86
G.G. Roy	Aluminum	AA6061	791	833.0017708	0.921492	8.17
G.G. Roy	Aluminum	AA6061	795	833.2207097	0.928589	7.40
G.G. Roy	Aluminum	AA6061	799	833.3557802	0.935826	6.63
G.G. Roy	Aluminum	AA6061	820	881.6879631	0.894313	11.16
G.G. Roy	Aluminum	AA6061	818	880.9083319	0.892079	11.42
G.G. Roy	Aluminum	AA6061	814	879.6446101	0.88714	11.97
R. Nandan	Aluminum	AA6061	790	879.3378989	0.846324	16.68
R. Nandan	Aluminum	AA6061	745	824.3982614	0.849167	16.34
R. Nandan	Aluminum	AA6061	685	823.3654457	0.73663	30.56
R. Nandan	Aluminum	AA6061	790	828.2918552	0.927791	7.49
R. Nandan	Aluminum	AA6061	700.2	823.7334243	0.765026	26.78
R. Nandan	Aluminum	AA6061	694.4	823.7266781	0.754004	28.23
R. Nandan	Aluminum	AA6061	688.2	823.715743	0.742226	29.81
R. Nandan	Aluminum	AA6061	762.7	833.3557802	0.868021	14.15
R. Nandan	Aluminum	AA6061	756	833.2207097	0.855722	15.58
R. Nandan	Aluminum	AA6061	749.6	833.0017708	0.844109	16.94
R. Nandan	Aluminum	AA6061	807.4	881.6879631	0.872727	13.61
R. Nandan	Aluminum	AA6061	801.5	880.9083319	0.863772	14.64
R. Nandan	Aluminum	AA6061	797.3	879.6446101	0.858428	15.26
Khandkar	Aluminum	AA6061	665	825.1391303	0.696211	36.21
T.J. Lienert	Aluminum	AA6061	625	830.4959104	0.614089	48.76

Table C.2: Error for the maximum temperature accounting for surface heat losses.

Error for maximum temperature accounting for surface heat losses part 2						
Author	Material	Especification	T_s	$\widehat{T_s}$	θ	Error %
Assidi	Aluminum	AA6061	820	829.294681	0.982506	1.76
Assidi	Aluminum	AA6061	768	829.294681	0.884631	12.25
Assidi	Aluminum	AA6061	781	829.294681	0.9091	9.53
Assidi	Aluminum	AA6061	803	829.294681	0.950508	5.07
A.P. Reynolds	Aluminum	AA7050	506	721.7588633	0.490845	71.16
A.P. Reynolds	Aluminum	AA7050	589	721.7601103	0.686709	37.58
A.P. Reynolds	Aluminum	AA7050	638	721.78205	0.802299	22.02
A.P. Reynolds	Aluminum	AA7050	663	722.0185999	0.860811	14.98
A.P. Reynolds	Aluminum	AA7050	592	721.7602783	0.693788	36.55
A.P. Reynolds	Aluminum	AA7050	671	721.949792	0.879821	12.80
A.P. Reynolds	Aluminum	AA7050	661	724.9466038	0.850223	16.22
A.P. Reynolds	Aluminum	AA7050	703	772.7323789	0.853112	15.88
P.A. Colgrove	Aluminum	AA7075	803	879.0083725	0.404469	83.30
P.A. Colgrove	Aluminum	AA7075	813	733.7757207	0.447478	65.04
P.A. Colgrove	Aluminum	AA7075	823	869.1187673	0.323926	46.41
P.A. Colgrove	Aluminum	AA7075	808	858.468936	0.356844	32.29
P.A. Colgrove	Aluminum	AA7075	813	731.1050604	0.415604	24.19
P.A. Colgrove	Aluminum	AA7075	803	30915.59098	0.009145	19.36
P.A. Colgrove	Aluminum	AA7075	798	1459.655229	0.434725	13.86
P.A. Colgrove	Aluminum	AA7075	803	1284.941626	0.521814	4.44
P.A. Colgrove	Aluminum	AA7075	808	1133.092209	0.628673	0.87
P.A. Colgrove	Aluminum	AA7075	798	1002.423697	0.723996	0.55
P.A. Colgrove	Aluminum	AA7075	773	953.9673184	0.7851	11.90
P.A. Colgrove	Aluminum	AA7075	793	910.9335849	0.823907	2.47
P.A. Colgrove	Aluminum	AA7075	758	872.343325	0.870559	7.62
P.A. Colgrove	Aluminum	AA7075	738	825.9542117	0.956522	10.21
P.A. Colgrove	Aluminum	AA7075	773	812.4639325	0.991323	-1.19
T.J. Lienert	Aluminum	AA7075	604	800.7734586	0.994484	67.84
R. Nandan	Steel	304SS	570	833.0512908	0.887765	158.27
X.K. Zhu	Steel	304SS	1243	805.4284492	0.975507	33.75
G.G. Roy	Steel	304SS	1430	794.4673599	0.926546	15.54
G.G. Roy	Steel	304SS	1412	785.3254067	0.902887	17.18
G.G. Roy	Steel	304SS	1518	763.8014866	1.019748	8.14
G.G. Roy	Steel	304SS	1316	901.0796756	0.507396	26.16
G.G. Roy	Steel	304SS	1313	1622.229928	0.205402	26.47
G.G. Roy	Steel	304SS	1385	1622.370008	0.713547	19.66
G.G. Roy	Steel	304SS	1241	1620.411457	0.856012	33.81
G.G. Roy	Steel	304SS	1200	1620.826177	0.842136	38.25
G.G. Roy	Steel	304SS	1256	1621.510866	0.921791	32.24
G.G. Roy	Steel	304SS	1314	1620.453498	0.769781	26.39
G.G. Roy	Steel	SAE1018	1428	1620.70199	0.767369	19.46
G.G. Roy	Steel	SAE1018	1506	1621.24336	0.821466	13.05
G.G. Roy	Steel	SAE1018	1349	1620.40732	0.713093	26.53
G.G. Roy	Steel	SAE1018	1286	1620.355302	0.682116	32.69
G.G. Roy	Steel	SAE1018	1236	1620.562098	0.724352	37.86
G.G. Roy	Steel	SAE1018	1359	1620.942024	0.767985	25.73
G.G. Roy	Steel	SAE1018	1301	1670.765131	0.823156	31.30
G.G. Roy	Steel	SAE1018	1423	1674.494291	0.877592	20.12
G.G. Roy	Steel	SAE1018	1361	1668.324265	0.766972	25.71
G.G. Roy	Steel	SAE1018	1273	1668.109881	0.72111	34.03
T.J. Lienert	Titanium	Ti-6Al-4V	1143	1667.805315	0.684769	51.42
Bangcheng Yang	Aluminum	AA2024	788	1670.346637	0.773128	-8.67
Bangcheng Yang	Aluminum	AA2024	763	1669.752101	0.731182	-3.43
Bangcheng Yang	Aluminum	AA2024	603	1673.763959	0.817727	38.66
C.M. Chen	Aluminum	AA6061	653	1672.726406	0.773245	39.22
C.M. Chen	Aluminum	AA6061	764	1668.324265	0.71151	12.00
H. Schmidt and J. Hattel	Aluminum	AA2024	773	1668.401266	0.651432	5.63
H. Schmidt & J. Hattel	Aluminum	AA2024	708	1711.104106	0.597974	9.08

Table C.3: Error for the maximum temperature accounting for surface heat losses.

Error for maximum temperature accounting for surface heat losses part 3						
Author	Material	Especification	T_s	$\widehat{T_s}$	θ	Error %
Dongun Kim	Aluminum	AA5083	798	747.2731261	1.090651	2.86
Dongun Kim	Aluminum	AA5083	798	747.3116629	1.034916	2.86
Dongun Kim	Aluminum	AA5083	733	746.9893178	0.679303	16.75
Dongun Kim	Aluminum	AA5083	740	823.4947494	0.675554	15.16
Dongun Kim	Aluminum	AA5083	803	823.4492485	0.88686	4.02
Dongun Kim	Aluminum	AA5083	813	746.992744	1.057924	2.06
R. Nandan	Steel	SAE1018	1463	746.9927443	0.913155	16.23
R. Nandan	Steel	SAE1018	1170	812.5425493	0.971737	45.09
R. Nandan	Steel	SAE1018	1137.6	812.5425493	0.971737	48.88
R. Nandan	Steel	SAE1018	1106.9	812.3686615	0.845697	52.60
R. Nandan	Steel	SAE1018	1061	812.3686615	0.859306	58.45
R. Nandan	Steel	SAE1018	1229.2	823.7318039	0.960566	38.63
R. Nandan	Steel	SAE1018	1168	823.7318039	0.979587	45.43
R. Nandan	Steel	SAE1018	1140.1	1668.31649	0.850169	48.69
R. Nandan	Steel	SAE1018	1097.2	1666.903389	0.637006	53.92
R. Nandan	Steel	SAE1018	1292.7	1666.902703	0.613338	32.22
R. Nandan	Steel	SAE1018	1210.5	1666.901332	0.590912	40.85
R. Nandan	Steel	SAE1018	1170	1666.89928	0.557382	45.38
R. Nandan	Steel	SAE1018	1128.3	1668.401735	0.679509	50.28
R. Nandan	Steel	SAE1018	1350.6	1668.400149	0.634851	26.84
R. Nandan	Steel	SAE1018	1253.9	1668.396981	0.614493	36.48
R. Nandan	Steel	SAE1018	1193.2	1668.39224	0.583191	43.04
R. Nandan	Steel	SAE1018	1152.3	1670.916357	0.724516	47.71

Table C.4: Error for the torque accounting for surface heat losses.

Error for torque accounting for surface heat losses part 1					
Author	Material	Especification	M	$\widehat{M}$	Error %
H. Schmidt	Aluminum	AA2024	40	37.67975132	-5.97
Kevin J. Colligan	Aluminum	AA5083	295	471.0883432	46.80
Kevin J. Colligan	Aluminum	AA5083	326	481.8232913	39.06
Kevin J. Colligan	Aluminum	AA5083	358	494.423486	32.28
T. Long	Aluminum	AA5083	181	367.4787699	70.81
T. Long	Aluminum	AA5083	152	277.2999307	60.12
T. Long	Aluminum	AA5083	128	223.7618253	55.85
T. Long	Aluminum	AA5083	108	184.4893416	53.54
T. Long	Aluminum	AA5083	94	155.326078	50.22
T. Long	Aluminum	AA5083	79	125.2074479	46.05
T. Long	Aluminum	AA5083	70	108.9153945	44.20
T. Long	Aluminum	AA5083	64	92.81291315	37.17
T. Long	Aluminum	AA5083	50	75.83873943	41.65
T. Long	Aluminum	AA5083	40	64.2957165	47.46
T. Long	Aluminum	AA5083	35	55.87130866	46.77
T.J. Lienert	Aluminum	AA5083	181	32.32760243	-172.25
Khandkar	Aluminum	AA6061	84.4	131.5487226	44.38
T.J. Lienert	Aluminum	AA6061	30.62	25.48622852	-18.35
A.P. Reynolds	Aluminum	AA7050	73.46273863	141.7628962	65.73
A.P. Reynolds	Aluminum	AA7050	118.4408879	197.1806736	50.97
A.P. Reynolds	Aluminum	AA7050	171.5561491	147.3714757	-15.19
A.P. Reynolds	Aluminum	AA7050	78.37008922	98.3126712	22.67
A.P. Reynolds	Aluminum	AA7050	69.27153671	84.4871087	19.85
A.P. Reynolds	Aluminum	AA7050	63.71057417	66.24019214	3.89
A.P. Reynolds	Aluminum	AA7050	26.5153383	28.76610888	8.14
A.P. Reynolds	Aluminum	AA7050	79.88050498	142.4444582	57.84
A.P. Reynolds	Aluminum	AA7050	65.78226736	106.6747502	48.34
A.P. Reynolds	Aluminum	AA7050	53.47648869	71.83442206	29.51
A.P. Reynolds	Aluminum	AA7050	41.77850679	48.56194691	15.04
A.P. Reynolds	Aluminum	AA7050	32.08569944	36.45004996	12.75
A.P. Reynolds	Aluminum	AA7050	106.0661574	296.2670166	102.71
A.P. Reynolds	Aluminum	AA7050	101.3537555	194.1828693	65.01
A.P. Reynolds	Aluminum	AA7050	85.56303957	139.993547	49.23
A.P. Reynolds	Aluminum	AA7050	73.81569813	97.9196393	28.25
A.P. Reynolds	Aluminum	AA7050	62.80619328	84.4871087	29.65
A.P. Reynolds	Aluminum	AA7050	54.81374197	64.74966544	16.65
T. Long	Aluminum	AA7050	305	701.2442803	83.25
T. Long	Aluminum	AA7050	275	494.9959626	58.77
T. Long	Aluminum	AA7050	205	382.4968802	62.37
T. Long	Aluminum	AA7050	155	290.170047	62.70
T. Long	Aluminum	AA7050	130	233.7480934	58.77
T. Long	Aluminum	AA7050	90	195.6960782	77.67
T. Long	Aluminum	AA7050	75	168.2986273	80.82
T. Long	Aluminum	AA7050	70	145.0850235	72.88
T. Long	Aluminum	AA7050	60	105.1866421	56.13
T. Long	Aluminum	AA7050	55	80.91280158	38.60
T. Long	Aluminum	AA7050	50	76.49937604	42.52
P.A. Colgrove	Aluminum	AA7075	199.2071804	345.1865125	54.97
P.A. Colgrove	Aluminum	AA7075	221.3413116	362.3755171	49.29

Table C.5: Error for the torque accounting for surface heat losses.

Error for torque accounting for surface heat losses part 2					
Author	Material	Especification	M	$\widehat{M}$	Error %
P.A. Colgrove	Aluminum	AA7075	245.0564521	383.9385717	44.89
P.A. Colgrove	Aluminum	AA7075	224.4084698	401.4199536	58.15
P.A. Colgrove	Aluminum	AA7075	250.4724322	416.9087475	50.95
P.A. Colgrove	Aluminum	AA7075	270.5634033	435.0762357	47.50
P.A. Colgrove	Aluminum	AA7075	292.2084755	457.5318372	44.83
P.A. Colgrove	Aluminum	AA7075	342.2142352	488.9016348	35.67
P.A. Colgrove	Aluminum	AA7075	343.7746771	508.5808214	39.16
P.A. Colgrove	Aluminum	AA7075	356.2755744	531.3154806	39.95
P.A. Colgrove	Aluminum	AA7075	384.8149494	560.4522484	37.59
P.A. Colgrove	Aluminum	AA7075	311.4754379	552.8016543	57.36
P.A. Colgrove	Aluminum	AA7075	95.49714498	122.2614205	24.70
P.A. Colgrove	Aluminum	AA7075	119.4267993	135.8048752	12.85
P.A. Colgrove	Aluminum	AA7075	129.7056234	143.385776	10.02
T.J. Lienert	Aluminum	AA7075	58.64	21.88737625	-98.55
T.J. Lienert	Steel	SAE1018	55	102.3474284	62.10
R. Nandan	Steel	SAE1018	68.8	127.6207443	61.78
R. Nandan	Steel	SAE1018	70.9	127.6536017	58.80
R. Nandan	Steel	SAE1018	72.6	127.7193163	56.48
R. Nandan	Steel	SAE1018	75.5	127.8178879	52.64
R. Nandan	Steel	SAE1018	55.2	99.26057889	58.67
R. Nandan	Steel	SAE1018	58	99.28613465	53.75
R. Nandan	Steel	SAE1018	59.2	99.33724604	51.75
R. Nandan	Steel	SAE1018	61.1	99.41391283	48.67
R. Nandan	Steel	SAE1018	45.6	81.21320091	57.71
R. Nandan	Steel	SAE1018	48.4	81.23411017	51.78
R. Nandan	Steel	SAE1018	49.8	81.27592858	48.98
R. Nandan	Steel	SAE1018	51	81.33865595	46.67
R. Nandan	Steel	SAE1018	38.9	68.71886231	56.90
R. Nandan	Steel	SAE1018	41.3	68.73655476	50.94
R. Nandan	Steel	SAE1018	42.8	68.77193957	47.42
R. Nandan	Steel	SAE1018	43.7	68.82501657	45.42

Table C.6: Error for the shear layer thickness accounting for surface heat losses.

Error for the shear layer thickness accounting for surface heat losses					
Author	Material	Especification	δ	$\widehat{\delta}$	Error %
H.N.B. Schmidt	Aluminum	AA2024	0.0006	1.66853E-07	-818.75
R.W. Fondaa	Aluminum	AA2195	0.001109	0.003664153	119.51
Judy Schneider	Aluminum	AA2195	0.000702	0.002332932	120.09
Z.W. Chen	Aluminum	AA5083	0.000278	0.000438025	45.46
M. Song	Aluminum	AA6061	0.000811	0.001148057	34.75
M. Guerra	Aluminum	AA6061	0.000811	7.2468E-05	-241.51
Shaowen Xu	Aluminum	AA6061	0.00066	3.15091E-06	-534.45
Shaowen Xu	Aluminum	AA6061	0.00063	2.96965E-06	-535.72
Shaowen Xu	Aluminum	AA6061	0.000263	2.74433E-06	-456.26
Shaowen Xu	Aluminum	AA6061	0.00047	6.73038E-06	-424.61
Shaowen Xu	Aluminum	AA6061	0.000655	1.33906E-05	-389.00
Shaowen Xu	Aluminum	AA6061	0.00184	2.57074E-05	-427.07
Shaowen Xu	Aluminum	AA6061	0.001	2.42286E-05	-372.02
Shaowen Xu	Aluminum	AA6061	0.00021	2.23902E-05	-223.84
Shaowen Xu	Aluminum	AA6061	0.002735	0.00034319	-207.56
Shaowen Xu	Aluminum	AA6061	0.00334	0.000541211	-181.99
H. Atharifar	Aluminum	AA6061	0.000277	1.80131E-06	-503.55
H. Atharifar	Aluminum	AA6061	0.000168	1.76564E-06	-455.54
H. Atharifar	Aluminum	AA6061	0.000185	1.69744E-06	-469.12
H. Atharifar	Aluminum	AA6061	0.000116	1.60236E-06	-428.21
P.A. Colgrove	Aluminum	AA7075	0.00118	0.001219836	3.32
Bangcheng Yang	Aluminum	AA2024	0.000075	3.60824E-06	-303.42
Bangcheng Yang	Aluminum	AA2024	0.000375	4.16822E-06	-449.94

Annexed D

Summary of data compiled of θ and ϕ.

Table D.1: ϕ and θ for the data that fulfilled the assumptions when the Bessel function is calculated with Pe.

Bessel equation with Pe				
Author	Material	Specification	ϕ	θ
H. Schmidt	Aluminum	AA2024	0.270241	0.826569
Khandkar	Aluminum	AA6061	0.135559	0.693968
G.G. Roy	Aluminum	AA6061	0.462504	0.736932
G.G. Roy	Aluminum	AA6061	0.450225	0.806069
R. Nandan	Aluminum	AA6061	0.464301	0.729426
R. Nandan	Aluminum	AA6061	0.399446	0.797802
R. Nandan	Aluminum	AA6061	0.313151	0.726725
R. Nandan	Aluminum	AA6061	0.389932	0.734075
R. Nandan	Aluminum	AA6061	0.450225	0.729764
Khandkar	Aluminum	AA6061	0.134517	0.660749
A.P. Reynolds	Aluminum	AA7050	0.092216	0.684662
A.P. Reynolds	Aluminum	AA7050	0.122674	0.795337
A.P. Reynolds	Aluminum	AA7050	0.137524	0.825345
A.P. Reynolds	Aluminum	AA7050	0.091062	0.691552
A.P. Reynolds	Aluminum	AA7050	0.094436	0.763722
G.G. Roy	Steel	304SS	1.286229	0.831435
G.G. Roy	Steel	304SS	1.267001	0.896937
G.G. Roy	Steel	SAE1018	0.150656	0.740672
G.G. Roy	Steel	SAE1018	0.139871	0.735113
G.G. Roy	Steel	SAE1018	0.158664	0.725509
G.G. Roy	Steel	SAE1018	0.233714	0.704176
G.G. Roy	Steel	SAE1018	0.310163	0.676518
G.G. Roy	Steel	SAE1018	0.228247	0.738516
G.G. Roy	Steel	SAE1018	0.30622	0.714203
G.G. Roy	Steel	SAE1018	0.220371	0.756043
G.G. Roy	Steel	SAE1018	0.300386	0.742507
G.G. Roy	Steel	SAE1018	0.158664	0.673046
Bangcheng Yang	Aluminum	AA2024	0.254216	1.073367
Bangcheng Yang	Aluminum	AA2024	0.21905	1.002049
Bangcheng Yang	Aluminum	AA2024	0.161317	0.674171
C.M. Chen	Aluminum	AA6061	0.390827	0.671682
H. Schmidt and J. Hattel	Aluminum	AA2024	0.270241	1.046987
H. Schmidt & J. Hattel	Aluminum	AA2024	0.270241	0.903715
R. Nandan	Steel	SAE1018	0.160933	0.806419

Table D.2: ϕ and θ for the data that fulfilled the assumptions when the Bessel function is calculated with ξ.

Bessel equation with ξ				
Author	Material	Specification	ϕ	θ
H. Schmidt	Aluminium	AA2024	0.78358	0.835203
Khandkar	Aluminium	AA6061	0.32541	0.730363
G.G. Roy	Aluminium	AA6061	0.037374	0.862386
G.G. Roy	Aluminium	AA6061	1.105457	0.844534
G.G. Roy	Aluminium	AA6061	1.109946	0.833133
G.G. Roy	Aluminium	AA6061	1.117392	0.819835
R. Nandan	Aluminium	AA6061	1.119973	0.73663
R. Nandan	Aluminium	AA6061	1.109568	0.927791
R. Nandan	Aluminium	AA6061	1.105457	0.765026
R. Nandan	Aluminium	AA6061	1.109946	0.754004
R. Nandan	Aluminium	AA6061	1.117392	0.742226
Khandkar	Aluminium	AA6061	0.325195	0.696211
A.P. Reynolds	Aluminium	AA7050	0.287474	0.686709
A.P. Reynolds	Aluminium	AA7050	0.284658	0.802299
A.P. Reynolds	Aluminium	AA7050	0.288618	0.860811
A.P. Reynolds	Aluminium	AA7050	0.281752	0.693788
A.P. Reynolds	Aluminium	AA7050	0.282706	0.879821
G.G. Roy	Steel	304SS	5.23275	0.842136
G.G. Roy	Steel	304SS	5.230043	0.921791
G.G. Roy	Steel	SAE1018	0.734968	0.823156
G.G. Roy	Steel	SAE1018	0.732977	0.877592
G.G. Roy	Steel	SAE1018	0.736277	0.766972
G.G. Roy	Steel	SAE1018	0.764475	0.72111
G.G. Roy	Steel	SAE1018	0.811528	0.684769
G.G. Roy	Steel	SAE1018	0.763229	0.773128
G.G. Roy	Steel	SAE1018	0.810376	0.731182
G.G. Roy	Steel	SAE1018	0.761333	0.817727
G.G. Roy	Steel	SAE1018	0.808623	0.773245
G.G. Roy	Steel	SAE1018	0.736277	0.71151
Bangcheng Yang	Aluminium	AA2024	0.478325	1.090651
Bangcheng Yang	Aluminium	AA2024	0.467345	1.034916
Bangcheng Yang	Aluminium	AA2024	0.456246	0.679303
C.M. Chen	Aluminium	AA6061	0.837204	0.675554
H. Schmidt and J. Hattel	Aluminium	AA2024	0.78358	1.057924
H. Schmidt & J. Hattel	Aluminium	AA2024	0.78358	0.913155
R. Nandan	Aluminium	SAE1018	0.729768	0.850169